Methodological investigations on quantifications of in situ X-ray diffraction for a reliable characterization of the reaction kinetics of calcined clays during early hydration

Sebastian Scherb

Vollständiger Abdruck an der Fakultät für Bauingenieurwesen und Umweltwissenschaften der Universität der Bundeswehr München zur Erlangung des akademischen Grades eines

Doktors der Naturwissenschaften (Dr. rer. nat.)

genehmigten Dissertation.

Gutachter/Gutachterin:

1. Univ.-Prof. Dr.-Ing. Karl-Christian Thienel
2. Prof. Dr. rer. nat. Bernhard Middendorf
3. Prof. Dr. rer. nat. Jürgen Neubauer

Die Dissertation wurde am 28.04.2021 bei der Universität der Bundeswehr München eingereicht und durch die Fakultät für Bauingenieurwesen und Umweltwissenschaften am 19.07.2021 angenommen. Die mündliche Prüfung fand am 29.07.2021 statt.

Danksagung

Ich danke Herrn Professor Dr.-Ing. Christian Thienel für die Möglichkeit als Mineraloge am Institut für Werkstoffe des Bauwesens eine Promotion schreiben zu dürfen. Seine Offenheit für neue Ideen und sein Einsatz sie umsetzen zu können sind im besonderen Maße bemerkenswert. Zudem bereicherten zahlreiche (morgendliche) Diskussionen, bei denen viele Ideen entwickelt wurden, diese Arbeit sehr.

Ebenso danke ich der Laborleiterin Dr.-Ing. Nancy Beuntner für den riesengroßen und ununterbrochenen Einsatz für das ganze Institut. Ihre fachliche Expertise hat in vielen Diskussionen zum Gelingen der Arbeit beigetragen.

Herrn Professor Dr. Jürgen Neubauer danke ich ebenfalls für die Betreuung, Beratung und Anregungen zum Gelingen der einzelnen Veröffentlichungen und der gesamten Arbeit.

Meinen lieben Kolleginnen und Kollegen Ricarda Sposito, Carola Chucholowski, Matthias Maier, Dr. Mathias Köberl und Timo Haller danke ich für die zahlreichen Gespräche und Diskussionen. Vor allem macht es aber auch dank euch immer Spaß zur Arbeit zu gehen.

Frau Karola Feldmann, Herrn Andreas Krammer, Herrn Wolfgang Saur und auch allen anderen Kolleginnen und Kollegen des aktuellen und ehemaligen Teams danke ich für die Unterstützung bei der Durchführung verschiedenster Untersuchungen.

Den studentischen Hilfskräften der letzten Jahre danke ich für ihren Fleiß und Einsatz und die Bereicherung der Kaffeerunden am Institut.

Stellvertretend für das Laborteam des Instituts für Siedlungswasserwirtschaft danke ich Professor Dr. Steffen Krause für die Möglichkeit der Nutzung und Durchführung einiger analytischer Methoden.

Bei meiner ehemaligen Laborleitung Frau Professor Dr.-Ing. Andrea Kustermann und meiner ehemaligen Kollegin Kerstin Anneser möchte ich mich ebenfalls für die Unterstützung bedanken.

Ganz besonders bedanken möchte ich mich bei meiner Familie und Freunden für ihre Geduld und Unterstützung. Ich weiß, dass ich mich immer auf euch verlassen kann! Vor allem meinen Eltern Resi und Bruno gilt ein ganz besonderer Dank, sowie meinen Geschwistern Johanna, Tobias und Diana mit Anhang und natürlich meiner Frau Châu und Tochter Xíu!

Abstract

In this thesis, the influence of calcined phyllosilicates (meta-phyllosilicates) during early hydration is investigated. Preliminary methodological investigations on the influence of free, not chemically bound water on a diffractogram and on the quantification of metakaolin (MK) allowed a reliable analysis of hydrating systems by in situ X-ray diffraction (XRD) using the "partial or no known crystal structures" (PONKCS) method.

XRD analyses on powder samples with different water contents as well as in situ XRD analyses on a hydrating system show a clear correlation between the consistency of the sample and the scattering contribution in the diffractogram caused by the free water. A direct proportionality to the scattering contribution of the free water and thus quantifiability is given only for a pasty consistency. Even if the quantifiability of the free water is limited, its adaptation is necessary when using the PONKCS method, due to strong overlaps with other X-ray amorphous or poorly crystalline phases such as the meta-phyllosilicates.

The systematic investigation of MK, as a representative of the meta-phyllosilicates, before and after treatment in different alkaline solutions shows that the alkaline solutions cause changes in the X-ray amorphous structure of MK. These structural changes do not cause any change in the position of the X-ray amorphous hump in the diffractogram since the silicon to aluminum ratio remains constant and the dissolution of the MK particles is thus congruent. Therefore, it is possible to use a single hkl-phase model for the quantification of MK and its dissolution is reflected in the decreasing X-ray amorphous hump. However, calculations of reaction degrees show significant differences between the methods used. This is due to the uptake of alkalis as well as the accuracy of the quantifications using the PONKCS method.

The clarification of the methodological issues allows the investigation of the meta-phyllosilicates metakaolin (MK), metaillite (MI) and metamuscovite (MM) during early hydration. XRD quantifications in clinker-free systems with and without sulfate carrier show that all three meta-phyllosilicates can independently form both silicate and aluminate hydrate phases. Al solubility is only sufficient for MK to form the maximum ettringite content. In MI, the content of hydrate phases formed correlates very well with the solubility of Si and Al ions and is about 30 wt.% of the content of MK. However, differences between the dissolution of portlandite (CH) and the sulfate carrier to the water bound in hydrate phases indicate adsorption of calcium ions and calcium sulfate ion complexes on the negatively charged surfaces of the calcined clay particles. Here, the granulometry of the calcined clays seems to play a less important role than the BET surface area. Thus, when assessing the influence of calcined clays on early hydration, both the chemical influence due to the dissolved ions and the complex surface properties of calcined clays must be considered in addition to the physical effects. Initial qualitative investigations in cementitious systems confirm the findings obtained from clinker-free systems. Thereby, the influence of the pure meta-phyllosilicates on the early hydration is significantly stronger compared to a calcined common clay (CC). This is due to the high content of accompanying minerals in the CC.

Kurzfassung

In dieser Arbeit wird der Einfluss calcinierter Schichtsilikate (Meta-Schichtsilikate) während der frühen Hydratation untersucht. Vorangestellte methodische Untersuchungen zum Einfluss des freien, chemisch nicht gebundenen Wassers bei der Röntgenanalyse und zur Quantifizierung des Metakaolins (MK) ermöglichten eine zuverlässige Analyse hydratisierender Systeme mittels in situ Röntgenbeugung (XRD) unter Verwendung der „partiell oder nicht bekannte Kristallstrukturen“ (PONKCS) Methode.

XRD Analysen an Pulverproben mit verschiedenen Wassergehalten sowie in situ XRD Analysen an einem hydratisierenden System zeigen einen klaren Zusammenhang zwischen der Konsistenz der Probe und des durch das freie Wasser verursachten Streubeitrags im Diffraktogramm. Eine direkte Proportionalität zum Streubeitrag als Voraussetzung für die Quantifizierbarkeit des freien Wassers ist lediglich für eine pastöse Konsistenz gegeben. Auch wenn die Quantifizierbarkeit des freien Wassers limitiert ist, ist dessen Anpassung bei Verwendung der PONKCS Methode, aufgrund starker Überlagerungen mit anderen röntgenamorphen bzw. schlecht kristallinen Phasen wie den Meta-Schichtsilikaten, unbedingt erforderlich.

Die systematische Untersuchung von MK, als Vertreter der Meta-Schichtsilikate, vor und nach Behandlung in verschiedenen alkalischen Lösungen zeigt, dass die alkalischen Lösungen Veränderungen der röntgenamorphen Struktur des MK verursachen. Diese strukturellen Veränderungen verursachen jedoch keine Änderung der Position des röntgenamorphen Buckels im Diffraktogramm, da das Silizium zu Aluminium Verhältnis (Si/Al) konstant bleibt und die Auflösung der MK-Partikel somit kongruent ist. Daher ist es möglich, ein einziges hkl-Phasenmodell für die Quantifizierung von MK zu verwenden. Dessen Auflösung spiegelt sich in einem abnehmenden röntgenamorphen Buckel wider. Jedoch zeigen Berechnungen von Reaktionsgraden deutliche Unterschiede zwischen den verwendeten Methoden. Dies liegt zum einen an der Aufnahme von Alkalien als auch an der Genauigkeit der Quantifizierungen mit der PONKCS Methode.

Die Klärung der methodischen Fragestellungen ermöglicht Untersuchungen zum Reaktionsbeitrag der Meta-Schichtsilikate Metakaolin (MK), Metaillit (MI) und Metamuskovit (MM) während der frühen Hydratation. Die XRD Quantifizierungen und Thermogravimetrie in klinkerfreien Systemen mit und ohne Sulfatträger zeigen, dass alle drei Meta-Schichtsilikate eigenständig sowohl Silikat- als auch Aluminathydratphasen bilden können. Die Al Löslichkeit ist lediglich bei MK ausreichend, um den maximalen Ettringitgehalt zu bilden. Bei MI korreliert der Gehalt an gebildeten Hydratphasen sehr gut mit der Löslichkeit von Si und Al Ionen und beträgt circa 30 M.% der Reaktivität von MK. Jedoch deuten Unterschiede zwischen der Auflösung von Portlandit (CH) und des Sulfatträgers zu dem in Hydratphasen gebundenen Wassers auf eine Adsorption von Calciumionen und Calcium-Sulfationenkomplexen auf den negativ geladenen Oberflächen der calcinierten Tonpartikel hin. Hierbei scheint weniger die Granulometrie als die BET Oberfläche der calcinierten Tone eine wichtige Rolle zu spielen. Somit müssen, neben den physikalischen Effekten, sowohl der chemische Einfluss durch die gelösten Ionen als auch die komplexen Oberflächeneigenschaften calcinierter Tone berücksichtigt werden. Erste qualitative Untersuchungen in zementären Systemen bestätigen die aus den klinkerfreien Systemen gewonnenen Erkenntnisse. Dabei ist der Einfluss der reinen Meta-Schichtsilikate auf die frühe Hydratation deutlich stärker im Vergleich zu einem calcinierten, gewöhnlichen Ton (CC). Dies ist auf den hohen Gehalt an Begleitmineralen im CC zurückzuführen.

Content

List of general abbreviations

AFm-Hc	Hemicarboaluminate
AFm-Mc	Monocarboaluminate
AFm-Ms	Monosulfoaluminate
AFt	Ettringite
ATR-FTIR	Attenuated total reflection – Fourier transformed infrared spectroscopy
BET	Brunauer-Emmett-Teller
C-(A)-S-H	Calcium-(aluminate)-silicate-hydrate
CH	Portlandite
FWHM	Full width at half maximum
hkl	Miller indices
ICP-OES	Inductively coupled plasma – optical emission spectroscopy
KOH	potassium hydroxide
NaOH	sodium hydroxide
OPC	Ordinary Portland cement
PONKCS	Partial or no known crystal structures
QPXRD	Quantitative Powder X-ray diffraction
SCM	Supplementary cementitious material
SEM / EDX	Scanning electron microscope / energy dispersive X-ray spectroscopy
TG	Thermogravimetry
XRD	X-ray diffraction

List of self-assigned abbreviations

AFt_{max}	Maximum AFt content
CC	Calcined common clay
FA	Fly ash
LS	Limestone powder
MI	Metaillite
MK	Metakaolin
MK_{Am}	X-ray amorphous content of the metakaolin sample
MM	Metamuscovite
MOH	Mixed alkaline solution of NaOH and KOH
R_{MKAm}	Degree of reaction calculated from the XRD quantifications of MK_{Am}
R_{Quarz}	Degree of reaction calculated from the XRD quantifications of Quartz
$R_{Si/Al}$	Degree of reaction calculated from the Si and Al ions dissolved
R_{weight}	Degree of reaction calculated from the weight

List of Figures

1 Introduction

Calcined clays are currently subject of numerous research projects and attract more and more scientific attention as supplementary cementitious material (SCM) [1]. Their use as SCM could be a major component to achieve the goal of more ecological concretes since the partial replacement of cement by SCM offers one of the greatest opportunities to reduce CO_2 emission in the production of concrete. Calcined common clays (CC) contain, in addition to kaolinite, other phyllosilicates and secondary components and are particularly interesting for the cement industry for the future due to possible higher replacement levels [2].

One of the major challenges regarding establishing calcined clays as SCM is the mineralogical complexity of common raw clays on the one hand and significant mineralogical differences between individual clay pits on the other [3]. The enormous number of reactive and non-reactive phases in CC as well as differences in physical parameters make predicting their influence on the reaction kinetics of early hydration extremely difficult at the current state of knowledge. Previous work focused mainly on metakaolin (MK), which can be used for high-performance concrete [4]. Its high price due to competition with other industries and its high water demand make MK unsuitable as SCM when aiming at replacement levels higher than 10 wt.%. Consequently, low grade kaolinitic clays and illitic clays with a high content of 2:1 phyllosilicates have moved further into the focus of research in recent years [5, 6]. An application of calcined clays in their existing variety requires a fundamental understanding of the influences of the individual phyllosilicates on early hydration. This work shall provide an important contribution to this aspect and shall promote to the future large-scale use of calcined clays in cementitious systems.

While fly ashes primarily offer silicon (Si) ions for the hydration process, calcined clays also provide a substantial quantity of aluminum (Al) ions [7]. This leads to significant differences in the resulting hydration products. In order to understand the complex pozzolanic reaction behavior of CC, it is thus necessary to understand the pozzolanic contribution of the individual reactive phyllosilicates present in these common clays in interaction with modern cements.

This aim requires a methodologically challenging approach, which is part of the present work. Overall, in situ X-ray diffraction (in situ XRD) is a powerful tool to investigate the hydration reaction. In this context, methodological progress allows the quantification of poorly crystalline and X-ray amorphous phases [8]. Nevertheless, some methodological questions remain unanswered. Therefore, the work focuses on the role and influence of free, not chemically bound water on the diffractogram and on the quantification of cement pastes, as well as the dissolution behavior of phyllosilicates in alkaline solution and its influence on the scattering contribution in the diffractogram.

These methodological issues need to be clarified in order to reliably analyze the reaction contribution and reaction mechanisms of calcined phyllosilicates (meta-phyllosilicates) and to demonstrate their effect on early hydration.

2 Scope of the thesis

The idea of this work has its origin in the thesis of Beuntner [9], in which the influence of a CC on the hydration of cements was investigated. CC was shown to contribute significantly to the reaction even during early hydration (< 2 days). This represents a clear difference to common SCM such as fly ash. Current literature mainly focuses on the calcined 1:1 phyllosilicate MK to explain the reaction contribution of calcined clays. The 2:1 phyllosilicates like illite and muscovite, which are further reactive components of CC, are largely ignored thus far. Neißer-Deiters et al. [10] and Maier et al. [3] have substantiated that neither the physical influence nor the chemical reaction contribution of 2:1 phyllosilicates can be neglected.

In order to achieve reliable information about the reaction mechanisms during early hydration, it is important to know the reaction contributions and mechanisms of the individual meta-phyllosilicates that occur when using calcined common clays. As mentioned above, the mineralogical complexity of clays currently makes general predictions difficult about their influence on early hydration. This is the starting point of the present work, in which three individual meta-phyllosilicates (MK, metaillite (MI) and metamuscovite (MM)) are investigated in clinker free model systems (section 5.3, 8.3 and 8.4). In addition to thermogravimetric (TG) and calorimetric measurements, in situ XRD investigations will provide information on the behavior of the individual meta-phyllosilicate during early hydration. The partial or unknown crystal structures (PONKCS) method [8] will be used for the quantification of the in situ XRD measurements, which allows the quantification of crystalline as well as poorly crystalline or X-ray amorphous phases (more details are given in section 3).

Despite major progress in the quantification of cement pastes, like the possibility of quantifying calcium silicate hydrates (C-S-H) [11], some questions remain unanswered in literature. The relationship between the amount of water in the sample and the scattering contribution caused by the free, not chemically bound water in the diffractogram has not yet been investigated. Thus far, no results are available on the possibilities of quantifying the free water in cement pastes during in situ XRD. Understanding the behavior of free, not chemically bound water will provide an important contribution to the progress of quantifying in situ XRD measurements of cement pastes and will be a part of this work (section 5.1 and 8.1).

Furthermore, the following not conclusively clarified questions concern the reaction behavior of the X-ray amorphous phase of the meta-phyllosilicates (section 5.2 and 8.2):

- Is there a correlation between the amount of Si and Al ions in alkaline solution derived from dissolution tests and the quantification of the metaphase with the PONKCS method?
- Is the dissolution process of the metaphase congruent or incongruent?
- And how does the dissolution process of MK affect its X-ray amorphous hump in the diffractogram?

In case of incongruent dissolution, the relationship between the content of reacted phyllosilicate and the decrease in the X-ray amorphous hump of the meta-phyllosilicate would be in doubt, and thus their quantifiability. The present work is intended to make a decisive contribution to clarifying these methodological issues and enabling reliable quantification.

Finally, the investigation of the meta-phyllosilicates in hydrating systems intends to answer questions about differences of the reaction behavior between the meta-phyllosilicates used and the influence of the sulfate carrier on the reaction behavior and mechanisms (section 5.3, 8.3, 8.4 and 8.5). This understanding of the contribution and influence on the reaction

mechanisms can improve future predictions based on the mineralogical composition of common clays on the reaction mechanisms in hydrating cement systems.

3 State of knowledge

3.1 Quantification of hydrating systems using in situ X-ray diffraction

The quantification of hydrating cement pastes using in situ XRD measurements is a very challenging task despite great progress within the last decade. The challenges in this context are mainly the high number of phases present in cement pastes. Hydrating systems are composed of the cement as reactant, free, not chemically bound water as reaction partner and hydrate phases as reaction products.

A Rietveld analysis [12, 13], in which crystalline phases are normalized to 100 wt.%, is only an inadequate evaluation for cement pastes due to large proportions of X-ray amorphous phases, such as free water and the hydration product C-S-H. The internal [14, 15] as well as the external standard method [16] with the calibration factor G [17] are common approaches for quantitative phase analysis with XRD samples containing X-ray amorphous phases. For hydrating systems, the approach with external standard offers the possibility of analysis without influencing the reaction by an internal standard. The X-ray amorphous components are determined in their entirety for both, the internal as well as the external standard method. In order to separate the X-ray amorphous phases, various publications have already dealt with their quantification using the PONKCS method [8]. For this purpose, X-ray amorphous components were modelled and quantified with so called “hkl – or peaks phases” [18-26]. The modelling of phases with the PONKCS method requires X-ray amorphous phases that can be represented by a series of peaks via Pawley [27] or Le Bail [28] fit and that they are available in pure form or as a main phase with known quantity for calibration. The combination of these two methods allows both the quantification of crystalline phases as well as of the individual X-ray amorphous phases with very small domain sizes as demonstrated by Bergold et al. [11].

As already mentioned, cement pastes are multiphase mixtures. In addition to the cement clinker and the sulfate carrier as setting regulator, modern cements usually contain additionally SCM such as fly ash, limestone powder or calcined clays [29, 30]. While limestone powder usually contains only crystalline phases, most other SCM consist of large proportions of X-ray amorphous phase. Thus, modern binder pastes often consist of at least three X-ray amorphous phases (SCM, free water and C-S-H), which can be quantified with the PONKCS method, but exhibit considerable overlap in the diffractogram [18, 19]. Latest research confirms the possibility of quantifying the reacted SCM during in situ XRD measurements of hydrating systems [31]. Other researchers verify that the calculation of the degree of reaction can lead to major deviations resulting from error propagation. This depends largely on the replacement level of the SCM and the degree of reaction [18, 21, 26]. Nevertheless, a detailed description and modeling of the individual X-ray amorphous phases is indispensable in order to be able to separate and quantify them accurately.

Modelling and quantification of free water has received little attention in previous publications since it was to a great extent removed beforehand by stopping hydration with isopropanol, acetone or by vacuum drying [18, 21, 32-34]. However, the common stopping mechanisms do interfere with the hydration reaction, can damage reaction products and lead to deviating results depending on the type and duration of the stopping process [35-38]. Especially for early hydration, it is better to perform in situ XRD measurements directly on the reacting system without stopping the hydration. In this case, the free water and changes related to it during hydration have to be taken into account and must be modelled with a hkl-phase. Although free water has already been modelled as hkl-phase [23, 24] and the scaling factor has been refined

[11, 25], there is no quantification nor a closer examination of the free, not chemically bound water. The question about a correlation between the scattering contribution of the free water and the quantity of water in the sample is therefore still unanswered.

3.2 Challenges in quantifying SCM with XRD analysis

Even though fly ashes and calcined clays consist mainly of X-ray amorphous phases in addition to crystalline phases, there are clear differences when considering them. Due to the high temperatures (1100 – 1700 °C) and fast cooling involved in the formation of fly ash, large proportions of the particles are vitreous. The calcination of clays takes place at significantly lower temperatures (600 – 900 °C). Even if crystalline clay minerals are transformed into X-ray amorphous "metaphases", their habitus and layer structure remain intact (pseudo morphosis). According to Brindley and Nakahira [39], a pseudohexagonal skeleton of [SiO_4]-tetrahedra in the metakaolin is preserved at calcination temperatures of 600 °C. In contrast to fly ash, in which the Si release takes place via a solution process of the vitreous particles in alkaline environment [40], the mechanism of ion release of calcined clays is not finally investigated. Granizo et al. [41] describe the leaching kinetics of the alumosilicate metakaolin in 5M and 8M NaOH solution as a three stage process. According to their hypothesis the dissolution process is initially incongruent for a short time, followed by a longer period of congruent dissolution behavior and finally becomes incongruent again. Garg and Skibsted [42] show that crystallographic defects accelerate dissolution in alkaline solution during the first hours, followed by a period, where the rate of reaction is constant. They conclude that the dissolution process of metakaolin, calcined at 500 °C, is congruent and becomes increasingly incongruent with increasing calcination temperature. The exact influence of the dissolution behavior of the metakaolin on the scattering contribution in the diffractogram has not yet been investigated. Snellings [43] describes a shift of the X-ray amorphous hump towards lower angles 2Θ depending on the SiO_2 content of synthesized calcium aluminosilicate glasses. Therefore, incongruent or selective dissolution of ions in the aluminosilicate structure of metakaolin could lead to a shift of the X-ray amorphous hump in the diffractogram and thus to problems during quantification.

3.3 Calcined clays as supplementary cementitious material

Common clays consist of phyllosilicates (e.g. kaolinite, illite, montmorillonite, mica) and accompanying minerals (e.g. quartz, feldspar, calcite). The type and amount of phyllosilicates and accompanying minerals depend on the genesis of the corresponding deposit and can vary significantly. Phyllosilicates can be divided into two-, three-, and four-layer structures. Two-layer structures consist of a tetrahedral layer which is linked by shared oxygens with an octahedral layer (1:1 phyllosilicate, e.g. kaolinite). Three-layer structures consist of two outer tetrahedral layers and an inner octahedral layer (2:1 phyllosilicates, e.g. illite, muscovite). The four-layer structures (2:1:1 phyllosilicates, e.g. chlorite) play rather a minor role. For all phyllosilicates the tetrahedral sites are predominantly occupied by Si and the octahedral sites by Al or Mg. The hydroxyl group is always connected with the octahedron layer. [44, 45]

Currently, three different categories of clays are in focus: Clays with high kaolinite content (kaolinitic clay), with a moderate kaolinite content (low grade kaolinitic clay) in the raw clay and, additionally, illitic clays, whose composition is dominated by the 2:1 phyllosilicate illite. Low grade kaolinitic and illitic clays have in common that they both contain other phyllosilicates and a larger proportion of accompanying minerals. These two categories offer the greatest

potential to reduce CO_2 emissions caused by the cement industry [46] by permitting high replacement levels due to their worldwide and local availability.

3.3.1 Reactivity of calcined clays

Thermal activation (calcination) of clays in the temperature range between 600 and 900 °C is required to achieve pozzolanic reactivity. In this process, the clays are dehydroxylated by splitting off the bound hydroxide ions [47-51]. Due to the freely accessible hydroxide ions, 1:1 phyllosilicates require a lower calcination temperature for activation than 2:1 phyllosilicates. The pozzolanic reactivity is caused by the availability of Si and Al ions from the phyllosilicates and depends on the calcination temperature [48]. The different Si/Al ratio in the chemical formula of the phyllosilicates is also reflected in the Si/Al ratio of the dissolved ions. 1:1 phyllosilicates have a Si/Al ratio of about 1, while 2:1 phyllosilicates have a Si/Al ratio ranging from 1.5 to 2.0 [47-49]. Overall, the pozzolanic activity, primarily the amount and solubility rate of Al and Si from calcined clays is influenced by the type and amount of the individual phyllosilicates, their structural order especially the degree of dehydroxylation after calcination and additional physical factors [52, 53].

Various scientists have investigated the question of a test method suitable for assessing the pozzolanic reactivity of different SCM directly from the respective SCM [54-58]. Another approach is the determination of the reactivity of SCM in cementitious systems [21, 59-64]. Different parameters such as the reactive silica content, the CaO or $Ca(OH)_2$ consumption, the relative strength index or the content of soluble Si and Al ions in alkaline solution are common to assess the pozzolanic reactivity. Different wet chemical, analytical and empirical methods such as TG analysis, isothermal calorimetry, quantitative X-ray diffraction (QXRD) or compressive strength are used for the different approaches.

For calcined clays, comparison of the test methods revealed a considerable variation in the suitability of individual methods, even if they work very well in some other cases, e.g., for fly ash or slag [21, 56]. The test methods only cover a part of the reactivity and do not consider the dissolved Al ions. Other test methods, such as the solubility of Si and Al ions in alkaline solution [65] or the cumulative heat release using the R^3 test [66] yield a better characterization of the reactivity for calcined clays. On the one hand, a direct dependence of the reactivity on the kaolinite content of the clays [66, 67] and on the other hand a gradation of the reactivity of individual meta-phyllosilicates (metamica < metaillite < metamontmorillonite < metakaolin) [68-70], is laid down in the literature.

These investigations, using the ion solubility or the R^3 test, have in common that they focus exclusively on the reactivity of the SCM, which largely depends on the calcination temperature. Neißer-Deiters et al. [10] highlight that the optimal calcination temperature should not be chosen exclusively aiming at the highest reactivity. Physical-hygroscopic properties must also be considered in order to achieve an optimum in the interaction between water demand, workability and reactivity.

The amount of ions released during early time points indicate an early reaction contribution of the calcined clays in contrast to fly ash. Nevertheless, the described reactivity tests do not give information on the influence of calcined clays on the hydration of cement clinker nor on changes of hydrate phase formation over time. These aspects, however, are important for predicting the influence on the reaction mechanisms of calcined clays during early hydration.

Various investigations on the pozzolanic reaction behavior of MK in clinker-free systems have already been published [71-75]. Murat [74] describes in the MK-CH-H_2O system a dependence

of hydrate phase formation on the CH content and the time frame. In addition to C-S-H, different calcium aluminate hydrates (C_4AH_{13} or C_3AH_6) or strätlingite (C_2ASH_8) are formed in the absence of sulfate carriers and calcite after 28 days. Studies on various meta-phyllosilicates (metakaolinite, metaillite, metasmectite/metamontmorillonite, metamica) also prove the formation of C-S-H and C_4AH_X. Strätlingite or hydrogarnet is only detected for Al-rich clays at 40 °C after 7 or 150 days respectively [48]. Beuntner et al. [7] showed that the monophase (AFm) formation is favored after 2 days for MK in comparison to CC. This is attributed to the higher availability of Al in MK. Furthermore, a clear dependence of the hydrate phase formation from the model pore solution used is shown.

Overall, it can be noted that there is a strong dependence of the hydrate phases formed depending on the phyllosilicate used [48], the availability of CH [72, 76, 77], the model pore solution [7, 76, 78] and the temperature [71, 79].

3.3.2 Influence of calcined clays on the hydration reaction

Generally, during the main reaction of early cement hydration, a distinction is made between the silicate reaction and the aluminate reaction [80]. The influence of SCM on the two reactions can be divided into physical and chemical mechanisms [81-84].

The filler effect as physical mechanism is achieved by the availability of additional surfaces, which serve as further nucleation sites for hydration products [85-87]. These additional surfaces are strongly related to a finer particle size distribution of calcined clays in comparison to cements [82, 83] which leads to an acceleration of the silicate reaction [31, 88]. Additionally, dilution by replacing cement leads to relatively more space for the growth of hydrate phases [89, 90].

The adsorption of ions from the pore solution on calcined clay particles can be described as a chemical surface effect [91]. Zunino and Scrivener [88] found an influence of the sulfate balance in blended cements caused by the surface area, whereas higher surface area leads to an increased sulfate requirement due to the adsorption of sulfate ions onto C-S-H. Investigations of the zeta potential prove the adsorption of Ca^{2+} on the surfaces of raw clay [92] as well as calcined clay particles [93]. The negatively charged surfaces of calcined clays [94] could thus also influence the sulfate balance by adsorption of ions from the pore solution. Furthermore, adsorption of Ca^{2+} from the pore solution could affect nucleation and growth of C-S-H phases, as shown for quartz and calcite [91]. Jansen et al. [95] confirm with their "complete mass balance approach" that understanding the mechanism of adsorbed ions provides a major contribution to the knowledge of hydration reactions.

The chemical mechanism is determined by the amount of released Si and Al ions. According to the traditional definition of the pozzolanic reaction, Si ions react to form strength-building C-S-H phases by consuming CH from the silicate reaction [96]. For calcined clays, this traditional approach must be extended by the incorporation of Al into the C-S-H phases and an increased AFm or ettringite (AFt) formation [7, 97]. An influence is conceivable due to the additional amount of Al ions released from the SCM on the sulfate balance. Furthermore, it is important to note that the composition of C-S-H can vary significantly [98, 99]. The additional presence of Al originating from the SCM causes its incorporation into the C-S-H structure on the bridging sites and leads to the formation of C-A-S-H phases. The C-S-H and C-A-S-H phases generally show a tendency towards lower Ca/Si ratios when using SCM compared to C-S-H phases resulting from pure cement hydration [78, 100, 101].

The availability of sulfate and carbonate ions in the pore solution plays a crucial role concerning the aluminate reaction and leads to the formation of AFt or to sulfate or carbonate containing AFm phases [66]. Thermodynamic models in cementitious systems by Lothenbach and Zajak [102] describe the formation of AFt and AFm phases in the presence of sulfate and carbonate. The thermodynamic stability of the forming aluminate hydrate phases (AFt, monosulfoaluminate (AFm-Ms), hemicarboaluminate (AFm-Hc) and monocarboaluminate (AFm-Mc)) depends significantly on the content of sulfate and carbonate [103]. The additional Al available from calcined clays promotes the thermodynamic stability of the hydrate phases. Experimental studies by Tironi et al. [30, 104] and Danner et al. [105] confirm the thermodynamic modeling. They observe the formation of monophases taking place after the complete consumption of the sulfate carrier.

Overall, a clear impact of calcined clays during early hydration can be observed. Both, the high BET surface of the calcined clays and the released Si and Al ions lead to physical and chemical interactions and influence the silicate and aluminate reactions.

4 Summary of the methods applied

Ion solubility in alkaline solution

The determination of the ion solubility was carried out according to [65, 106]. One gram (section 5.3 and 8.4) or five grams (section 5.2 and 8.2) of the corresponding sample was shaken each in 400 ml alkaline solution on an interval agitator. Afterwards, the suspensions were filtered and the filtrates were acidified with concentrated HCl to a pH of 1 and subsequently filled up to 500 ml in a volumetric flask with distilled water. The concentration of the dissolved ions was determined using inductively coupled plasma – optical emission spectroscopy (ICP-OES).

Inductively coupled plasma – optical emission spectroscopy (ICP-OES)

The ICP-OES measurements were performed with a Varian 720 ES spectrometer (Agilent Technologies) and evaluated with the software 1.1 supplied with the instrument. The measuring range for the respective element was adapted using a multi-point calibration with an external standard. The measurements and their evaluation were conducted according to [107].

Attenuated total reflection – Fourier transformed infrared spectroscopy (ATR-FTIR)

The ATR-FTIR analyses were performed on a ThermoFisher Scientific Nicolet iS10 FTIR spectrometer equipped with an EverGlo TM MIR radiation source (λ = 15,798 cm^{-1}) and dTGS detector. The spectra were measured in the wavenumber range from 400–4000 cm^{-1} with diamond as ATR crystal, collecting a series of 16 scans at a resolution of 4 cm^{-1}. The evaluation of the data was carried out with Omnic 9.3 (ThermoFisher Scientific).

Isothermal calorimetry

Isothermal calorimetry experiments were performed with TA instruments TAM Air calorimeter at 25 °C for 50 h with 2 g of quartz sand in the reference chamber. The equilibrated sample was stirred manually with a spatula for 60 s and immediately transferred into a calorimeter crucible. The measured heat flow was normalized to 1 g of the paste. Data analysis was done with Origin 2018b (OriginLab Corporation).

Thermogravimetry (TG)

Thermogravimetric investigations were carried out with Netzsch STA 449 F3 with a sample quantity of 250 mg in Al_2O_3 crucibles and a heating rate of 2 K min^{-1}. The samples were stopped with acetone after 6, 30 and 48 h of hydration according to [9]. Netzsch Proteus Thermal Analysis 6.1.0 was used to analyze the data.

The bound water was calculated considering the mass loss in the temperature interval from 20 to 400 °C and is referred to weight percent of the paste for direct comparability with the in situ XRD measurements. The CH content was calculated from the mass loss in the temperature interval between 450 and 550 °C using the tangent method according to Marsh and Day [96].

Scanning electron microscopy (SEM) – energy dispersive X-ray spectroscopy (EDX)

The analyses were performed on a Zeiss Evo LS 15 equipped with an Oxford X-MaxN 50 EDX detector at 20 kV and a working distance of 8.5 mm. The EDX analyses were measured against a kaolinite standard (Micro-Analysis Consultants Ltd.) of known composition. For the SEM/EDX analyses, the dried samples were embedded in epoxy resin, ground and polished with isopropanol after hardening, and finally coated with carbon. Since the habitus of the particles is not easily recognizable on embedded samples, a second set of samples was prepared by scattering the powder on two-component adhesives, followed by coating with gold.

X-ray diffraction (XRD)

XRD measurements were performed with an Empyrean diffractometer equipped with a primary Bragg-Brentano^{HD} monochromator and a PIXcel^{1D} linear detector (Malvern Panalytical). A diffractogram was taken from 4° to 42° 2Θ (powder sample) and 200 scans within 50 h from 6° to 40° 2Θ (in situ XRD). For in situ XRD the sample holder of the diffractometer was connected to a temperature-controlling device that allowed in situ XRD measurements at the same temperature as the calorimetric measurements and thus ensuring good comparability between both methods. The use of a Kapton film (DuPont) avoids the evaporation of water and the ingress of CO_2. All measurements were performed in continuous scan mode with a step size of 0.013° 2Θ and a counting time of 25.5 s per step at 40 kV and 40 mA with CuKα radiation (λ = 1.54 Å). Measurements were analyzed with the software HighScore 4.7 (Malvern Panalytical). The quantifications were performed using Rietveld refinement [12, 13] with a combination of external standard [16, 17] and PONKCS method [8] according to Bergold et al. [11].

5 Main results

This part provides a short overview of the main results of this thesis that are presented in three peer reviewed scientific publications and two conference papers.

The first publication (section 8.1) deals with the role of free, not chemically bound water concerning the quantification of w/s mixtures and its quantification during in situ XRD measurements of hydrating systems. The free water content was calculated using a combination of the external standard method [16] using the G-factor [17] and the PONKCS method [8].

The second publication (section 8.2) investigates the reactivity of MK in different alkaline solutions. Since the hydration of cementitious systems takes place in alkaline environment, it is important to know the reaction behavior of metakaolin in this environment. Systematic investigations of the filtrate and the filter residue provided this information. In addition, the publication reveals correlations between results from dissolution experiments in different alkaline solutions and XRD quantifications by calculating the degree of reaction.

In the first conference paper (section 8.3) and a third peer-reviewed journal publication (section 8.4) the reaction mechanisms of three preferably pure meta-phyllosilicates (MK/MI/MM) were investigated. These investigations in clinker-free systems should give a deeper insight into the extent to which the meta-phyllosilicates contribute to the pozzolanic reaction and form hydrate phases independently. Finally, the second conference contribution (section 8.5) provides a first qualitative insight into the influence of the individual phyllosilicates and CC on the hydration of an ordinary Portland cement (OPC).

5.1 Role of free, not chemically bound water during XRD quantifications

The scattering contribution of free, not chemically bound water was evaluated in a first step by solid-water mixtures using limestone powder (LS), fly ash (FA), metakaolin (MK) and metamuscovite (MM) in different water to solid (w/s) ratios. As second step, an in situ XRD measurement was performed. The sample consists of equal parts of MK and portlandite (CH). An alkaline solution (MOH) with 100 mmol l^{-1} sodium hydroxide (NaOH) and 500 mmol l^{-1} potassium hydroxide (KOH) was adapted as model pore solution. The w/s ratio was 1.0. (section 8.1)

5.1.1 Influence of free, not chemically bound water on the diffractogram

LS and FA (section 8.1, Figure 3a) show a comparable behavior when water is added. An increase in the w/s ratio from 0.2 via 0.4 to 0.6 leads to an increase in the scattering contribution of water starting from 20° 2Θ. A correlation between the increase of water and the increase of the scattering contribution can be observed. In contrast, the meta-phyllosilicates exhibit a different behavior. Analogous to LS and FA, a first addition of water leads to a scattering contribution in the diffractogram, while a further addition of water does cause no further scattering contribution by the free, not chemically bound water. Figure 1a displays the diffractograms of MK dry and at different w/s values. It is clearly visible that the scattering contribution of water does not change at w/s ratios between 0.4 and 0.8. Thus, the correlation between water content and scattering contribution of the free water is not given in this range. Following the large area of stagnation, the scattering contribution of the water increases again with further addition of water (w/s = 1.0). Observations during homogenization and preparation of the water-solid mixtures also reveal a deviating behavior of LS and FA compared to the meta-phyllosilicates. While LS and FA can be homogenized to a paste when water is added,

even at low contents, the meta-phyllosilicates initially remain in an earth-moist state. For the meta-phyllosilicates, the transition from the earth-moist state to a paste-like consistency occurs at significantly higher water contents. However, if the water content is too high, a segregation of water on the sample surface occurs. This leads to a drastically increased scattering contribution in the diffractogram as illustrated in Figure 1b. It is important to note that both the transition between earth-moist state and paste as well as the water content at which segregation occurs on the sample surface strongly depend on the material and can differ significantly from one to another.

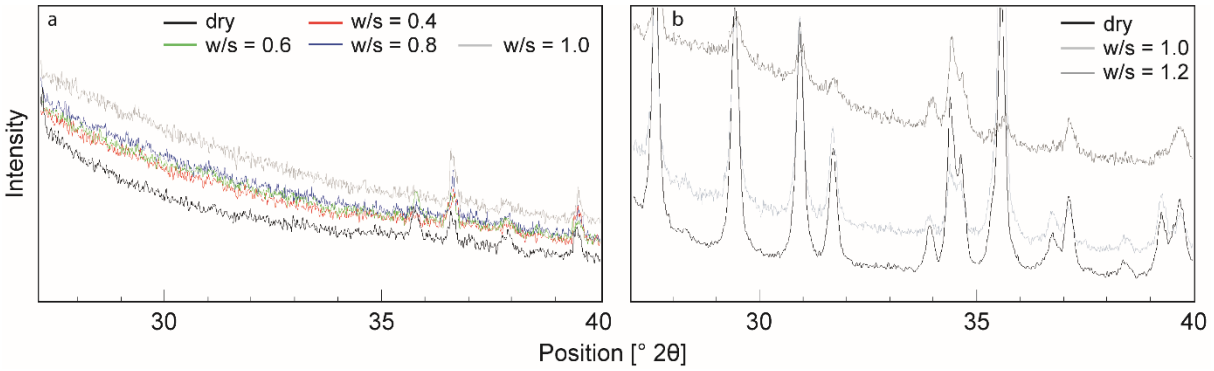

Figure 1 Diffractograms of MK (a) and MM (b) as dry powder and at different w/s ratios. The effect that the scattering contribution does not change over a wide range of water addition (a) and the segregation of water at the sample surface (b) is illustrated.

5.1.2 Modelling and calibration of hkl-phases

The XRD quantification of poorly crystalline or X-ray amorphous phases with the combined PONKCS - G-factor method [8, 11, 16, 17] using hkl-phases requires on the one hand a precise description of the device-specific background and on the other hand an exact modelling and calibration of the hkl-phases. In order to minimize water loss through evaporation and to avoid carbonation, it is state of the art to use a Kapton film for in situ XRD measurements [108, 109]. The preparation of the Kapton film on a single crystal permits the aggregation of the constant scattering contribution of the Kapton film and the device specific background by a constant hkl-phase (Figure 2, grey color). This is an advantage for Rietveld refinement since only a small contribution of the background must be adapted and calculated via a polynomial. In the next step, the hkl-phase model of the water can be created and calibrated on ZnO-water mixtures (Figure 2). It is important to consider not only the scattering contribution of the water but also the lowering of the scattering contribution at small angles. The scattering contribution of both hkl-phases (Kapton film and water) was simulated with Pawley fits and the profile parameters were refined iteratively according to Stetsko et al. [19]. The stepwise modeling of the Kapton film and the free, not chemically bound water is necessary to consider both the reduction at small angles (5 - 15° 2Θ) and the increase of the scattering rate above 20° 2Θ. Furthermore, the hkl-phase model of the free water should be calibrated directly on the system to be investigated, since its scattering contribution depends on the sample and not on the absolute water content.

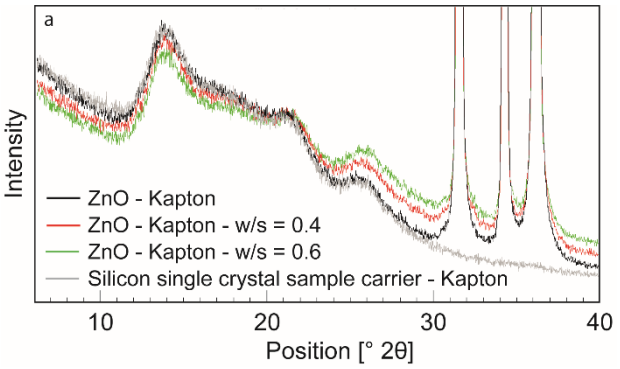

Figure 2 XRD measurements used for modlling the Kapton film and for modelling and calibration of the free, not chemically bound water.

For quantification using the PONKCS method, the X-ray amorphous content of the solids (FA, MK and MM) must also be modelled as an hkl-phase. The modelling was performed on pure samples covered with Kapton film. The scattering contribution of the hkl-phases was simulated with Pawley fits. All calibrations of hkl-phases were performed with ZnO as internal standard.

5.1.3 Quantification of free, not chemically bound water

The quantification of the water content in the ZnO-water mixtures shows only slight deviations from its weighed content (section 8.1). A correlation between calibration and quantification can be determined. The more the content at which calibration was performed differs from the content to be quantified, the greater becomes the error of quantification. The calibration of the ZnO - water mixture at a w/s value of 0.4 was selected to quantify the solid - water mixtures.

While the quantifications of LS- and FA-water mixtures yield good agreement with the theoretically weighed water content, the quantifications of the meta-phyllosilicate-water mixtures (MK and MM) differ significantly from their theoretical values. This is consistent with the observation that the scattering contribution of water in the systems with meta-phyllosilicates does not change over a wide range of water addition.

The quantification of water during in situ XRD measurements of hydrating systems provides a good correlation with TG measurements after 6 and 30 h on samples stopped with acetone. However, it is necessary to calibrate the hkl-phase of the water at the water content of the investigated system at the beginning of the measurement (50 wt.%) to avoid systematic errors, since calibration with ZnO does not match the measurements with meta-phyllosilicates. In the further reaction progress, the quantified water content remains constant in the in situ XRD measurement in contrast to TG, which can be explained by a constant background (Figure 3, constant color in the upper graph after about 30 h). The time from which the background remains constant correlates very well with the maximum heat flow of the main reaction of the calorimetric measurement (Figure 3). This leads to the conclusion that hydrating systems have an inverse effect to the meta-phyllosilicate - water mixtures. In the course of the hydration reaction the paste stiffens up to a point where it behaves like the earth-moist phyllosilicate - water mixture. Transferring the observations to cementitious systems, it can be assumed for in situ measurements with cement pastes that the free water content can only be quantified up to the time of maximum heat flow of the main reaction. Analogously to the measurement in the MK–CH system, the consistency of the paste changes, and thus the reaction behavior changes from solution controlled to diffusion controlled [80]. It is assumed that, because of the progressing hydration process and the associated increase in surface area due to the resulting

hydrate phases, the remaining free water on the surfaces is already coordinated in such a way that further hydration does not provide any additional change in its scattering contribution.

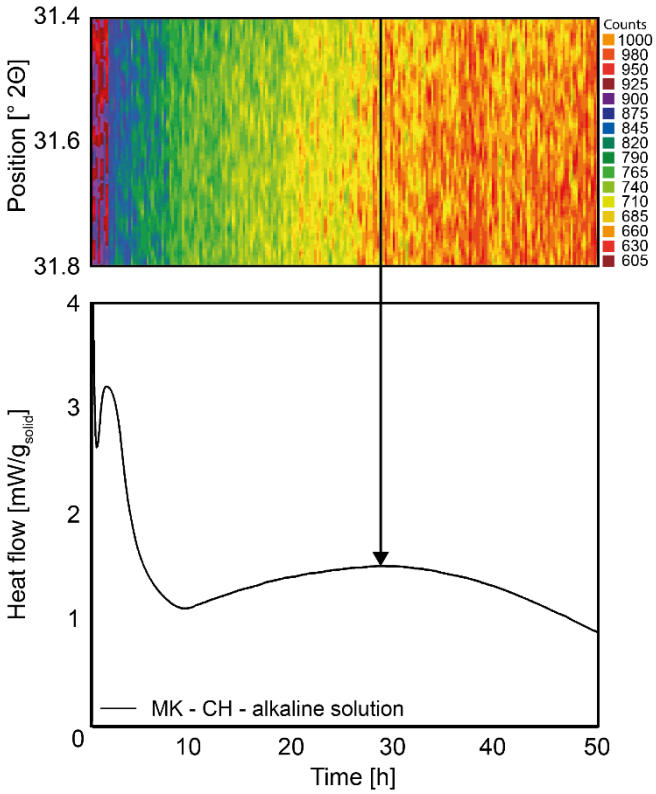

Figure 3 Comparison of the background of the in situ XRD measurement from 31.4 to 31.8° 2Θ with the calorimetric measurement. After the second maximum of the calorimeter curve (black arrow) has been reached, there is no further decrease of the background in the following 20 hours (constant count and thus same color in the upper graph).

It can be summarized from the observations and quantifications that the scattering contribution of free, not chemically bound water depends on the consistency of the sample. A constant consistency leads to a constant scattering contribution of the free water. Figure 4 illustrates and describes the relationship between the consistency of the sample and the scattering contribution of free water. With increasing water content from left to right, the meta-phyllosilicate samples pass through several stages from dry to earth-moist sample to paste and finally to a sample with segregated water on the sample surface. LA and FA have a paste-like consistency even at low water solid ratios and skip the second stage of an earth-moist sample. Thus, not all materials have to run through all stages. For hydrating systems, the graph must be read from right to left with the starting point at stage four (cement paste) and progressing towards step two as the sample stiffens. Stage five just occurs for unstable pastes or for strong sedimentation effects. In these cases, in situ XRD measurements are not quantifiable. Overall, it can be stated that a direct correlation between the scattering contribution of the free water and the water content in the sample is only present in step 4 and thus the free water can only be quantified in this phase. The quantifiability does not depend on the absolute content of water in the sample.

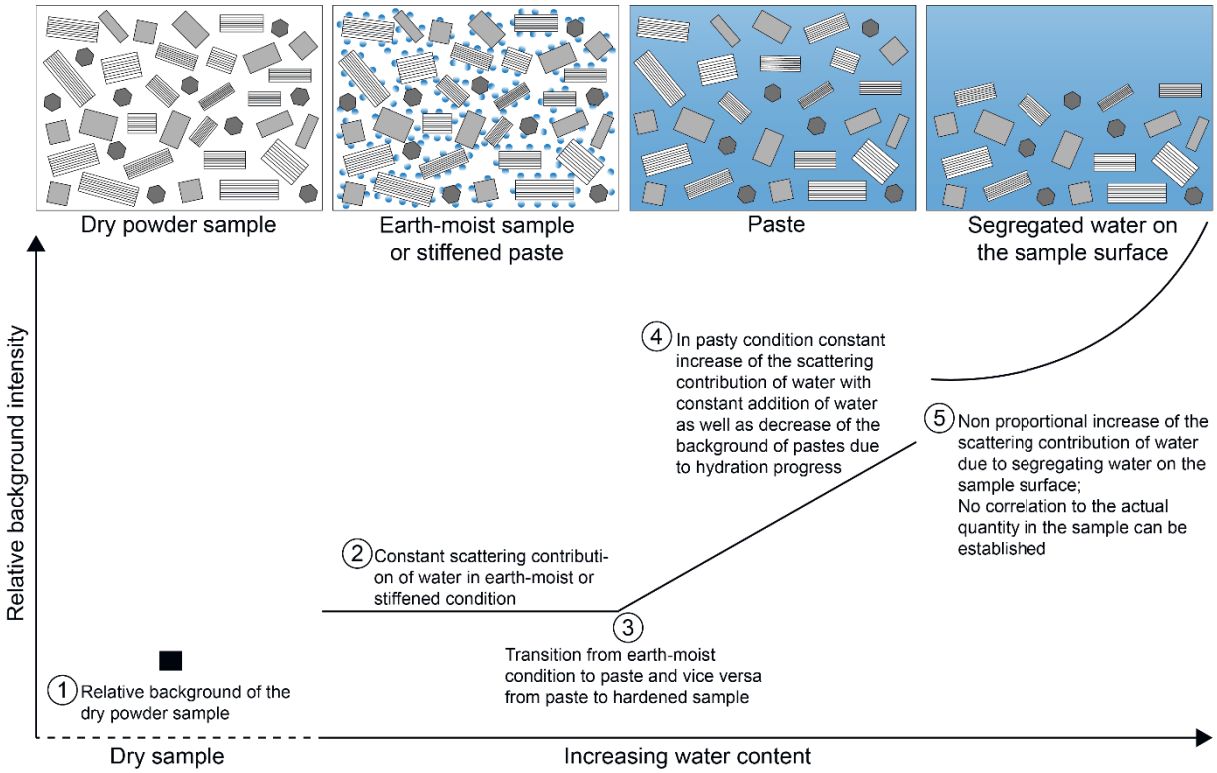

Figure 4 Illustration of the relationship of the scattering contribution of free, not chemically bound water and the consistency of the sample. A quantification of the free water is just possible in stage 4 of the illustration.

Thus, for the first time, a clear relationship between sample consistency and the scattering contribution of free, not chemically bound water in the diffractogram could be shown, which provides an important contribution for reliable quantifications of in situ XRD measurements. In addition, a very important finding is that the scattering contribution is not proportional to the absolute content of water in the sample over the entire range and can differ significantly for varying materials. Although the quantification of free water is limited to a pasty condition of the sample, it is essential for in situ XRD quantifications using the PONKCS method to model its scattering contribution in the diffractogram, owing their complexity and the strong overlap with the hkl-phases of many SCM and C-S-H. Overall, these findings can contribute across disciplines to better handling of XRD data containing free, not chemically bound water.

5.2 Reactivity of metakaolin in alkaline environment

For these experiments (section 8.2), the solids were treated in deionized water, a 10 wt.% NaOH, a 10 wt.% KOH and a model pore solution (MOH, section 5.1). Besides the crystalline phases quartz, anatase and phengite, 93 wt.% of MK is X-ray amorphous, representing the dehydroxylated kaolinite, hereinafter referred to as MK_{Am}. The designation of the samples is composed of MK for the whole sample or MK_{Am} for the X-ray amorphous part and the solution used (e.g. MK-H_2O and MK_{Am}-H_2O).

5.2.1 Implications from the chemical and FTIR analyses

While the chemical analysis of MK_{Am}-H_2O after elution shows hardly any difference to the original sample, the measurements after treatment with the alkaline solutions yield a decrease of the SiO_2 and Al_2O_3 content as well as an enrichment of TiO_2 and Fe_2O_3 in the filter residue. These effects are most pronounced in the NaOH solution. The molar ratio of SiO_2/Al_2O_3 remains almost constant for all investigated samples. Furthermore, an uptake of alkalis can be

detected, depending on the alkaline solution used. The chemical analysis of the dissolved ions in the filtrate reveals an increasing content of dissolved Si and Al ions from MK-H_2O via MK-MOH and MK-KOH to MK-NaOH, the latter having the highest content of dissolved ions. The content of dissolved titanium (Ti) and iron (Fe) ions is very low for all investigated systems and shows hardly any differences. This explains the enrichment of TiO_2 and Fe_2O_3 during the chemical analysis of the filter residue. Overall, the chemical analyses correlate very well with the results of weighing the filter residue, whereat MK-NaOH yields by far the lowest weight.

Scanning electron microscope (SEM) investigations visualize a dissolution of the particles. Areas enriched with Ti and Fe are hardly or not at all dissolved. As a result, especially for MK-NaOH a disintegration of the particles is indicated.

FTIR measurements of MK and MK-H_2O do not differ, which is consistent with the chemical analyses. Both a broadening and a shift to smaller wave numbers of the Si-O vibration between 900 and 1200 cm^{-1} can be determined for samples treated in alkaline solutions. This indicates a significant structural change in MK_{Am}. Figure 5a displays the correlation of the SiO_2 content with the wave number (left y-axis). A lower Si content can be observed in the alumosilicate structure of MK_{Am} leading to a shift towards smaller wave numbers, which is in line with literature [110, 111]. In addition, the change of the chemical environment of the Si-O band due to the enrichment of Fe_2O_3 and TiO_2, as well as the uptake of alkalis might influence the shift of the wave number. This environmental impact is expressed by the molar ratio of $SiO_2/(Al_2O_3 + Fe_2O_3 + TiO_2 + Na_2O + K_2O)$ (Figure 5b). The broadening of the band, represented by the full width at half maximum (FWHM) (Figure 5, right y-axis), can be interpreted as additional defects in the X-ray amorphous structure of the MK_{Am} [110]. It is assumed that the significantly larger ion radii of the alkalis in contrast to Al and Si cause the additional disorder.

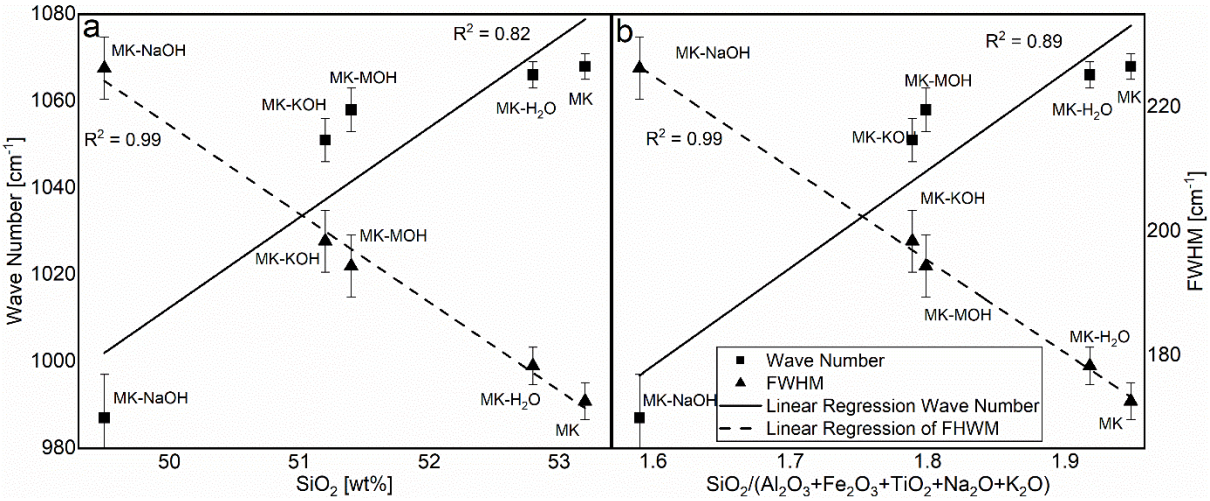

Figure 5 Correlation of the SiO_2 content (a) and the molar ratio of $SiO_2/(Al_2O_3 + Fe_2O_3 + TiO_2 + Na_2O + K_2O)$ (b) in the alumosilicate structure with the wave number and FWHM

5.2.2 Implications from the XRD analyses

The XRD quantification of the filter residues provides a decrease of MK_{Am} and an enrichment of the crystalline phases quartz, anatase and phengite. The effects can be observed directly in the diffractogram as decrease of the X-ray amorphous hump and as increase of the peaks of crystalline phases (Figure 6). This allows the inference that the crystalline phases do hardly dissolve. The quantification of MK-NaOH (MK_{Am} = 83.4 wt.%) is plausible, because the quantified content of MK_{Am} is analogous to the scattering contribution in the diffractogram very close to the measurement with 10 wt.% ZnO (MK_{Am} = 83.7 wt.%) as internal standard

(Figure 6). Nevertheless, based on the content of dissolved Si and Al ions, the MK_{Am} content of MK-NaOH should be lower. Here, the uptake of alkalis seems to have a direct influence on the diffractogram by increasing the scattering contribution. This effect is pronounced for the tested highly alkaline solutions. For cementitious systems in which the content of alkalis in the pore solution is significantly lower [112], the influence on the quantification of MK_{Am} should be minor.

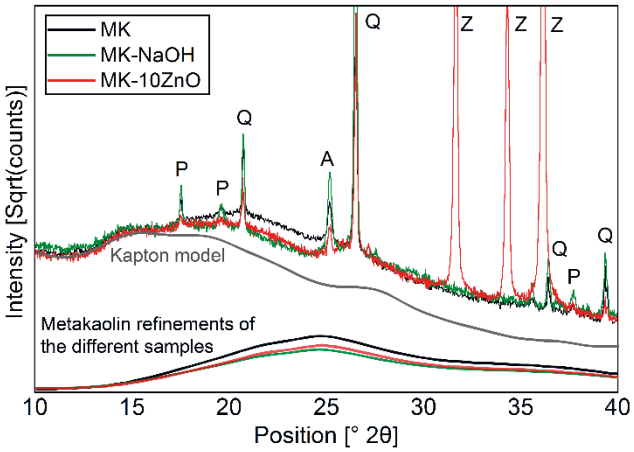

Q: Quartz; P: Phengite; A: Anatase; Z: Zincite

Figure 6 Comparison of dffractograms of MK-NaOH and a MK sample mixed with 10 wt.% ZnO (MK-10ZnO) as internal standard. The scattering contribution of MK_{Am} and of the Kapton film to the diffractogram of the different samples is shown.

Since the SiO_2/Al_2O_3 molar ratio stays almost constant in all systems investigated, the dissolution process of Si and Al ions can be regarded as congruent. Thus, the dissolution of MK_{Am} is reflected in the decreasing X-ray amorphous hump in the diffractogram. A change of the SiO_2/Al_2O_3 ratio to higher SiO_2 contents could cause a shift of the X-ray amorphous hump to smaller angles 2Θ, as described by [43] for synthesized calcium aluminosilicate glasses. An incongruent dissolution process for calcination temperatures above 900 °C [42] leads to changes of the SiO_2/Al_2O_3 molar ratio. Consequently, the X-ray amorphous hump of MK_{AM} might be shifted and MK_{Am} could not be quantified with one hkl-phase. In case of congruent dissolution, the same hkl-phase model of MK_{Am} can be applied for quantification before and after treatment in alkaline solutions thus enabling a reliable quantification during cement hydration.

5.2.3 Implications from calculating the degree of reaction

Calculating the degree of reaction discloses an increase from MK-MOH via MK-KOH to MK-NaOH (Figure 7). Especially for the XRD quantifications (R_{Quartz} and R_{MKAm}), the calculations of the degree of reaction reveals a large error, which becomes larger the lower the reaction rate is. Since only small changes of the MK_{Am} are observed in the analysis, quantification with an accuracy of 1 wt.% leads to large errors due to error propagation. This effect is also reported when calculating the degree of reaction from XRD quantifications with the PONKCS method for low reaction rates or low SCM contents [18, 26]. A comparison of the degrees of reaction within an alkaline solution depicts the highest degree of reaction for $R_{Si/Al}$ for all systems. The lower degrees of reaction from the weighing of the filter residue (R_{weight}) and from the XRD quantifications (R_{Quartz} and R_{MKAm}) are in line with each other and are attributable to the uptake of alkalis. The additional alkalis lead to a higher weight of the filter residue than calculated from the dissolved Si and Al ions and cause an additional slight increase of the X-ray amorphous hump, which leads to the differences in the degrees of reaction. This is also in line with the

observation that a higher amount of alkalis leads to a higher difference between $R_{Si/Al}$ and R_{weight}.

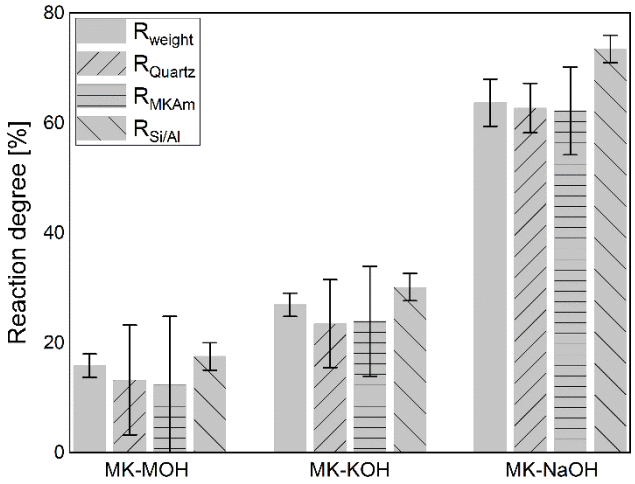

Figure 7 Degree of reaction calculated from the weight (R_{weight}), from the XRD quantifications of Quartz (R_{Quartz}) and MK_{Am} (R_{MKAm}) of the filter residue and of the Si and Al ions dissolved inside the filtrate ($R_{Si/Al}$)

Overall, the resulting trends appear to be consistent. The comparisons of XRD quantifications performed before and after a dissolution process of MK in alkaline solution are important to evaluate and confirm the reliability of the PONKCS quantifications in reacting systems. It was demonstrated for the first time that MK can be reliably quantified with the PONKCS method using a single hkl-phase model. Thus, a congruent dissolution process can be assumed for the reaction of MK in cementitious systems. Nevertheless, the degrees of reaction in highly alkaline solutions determined here do not allow straightforward conclusions about the degree of reaction of calcined clays in cementitious systems. Beyond the latter, the results will be of great interest for research on geopolymers using MK as a precursor in highly alkaline solutions.

5.3 Early hydration of calcined clay

The hydration kinetics of meta-phyllosilicates were analyzed in clinker-free model systems (section 8.3 and 8.4). The composition of the first series contained one meta-phyllosilicate each, calcium hydroxide in powder form and an alkaline solution with the ratio of 1:1:2 (MK/MI/MM-CH). The second measurement series were conducted with a substitution of 10 wt.% of the solid material by anhydrite (MK/MI/MM-CH-C$). Isothermal calorimetry, in situ XRD, TG (on samples stopped with acetone [9] after 6 and 48 hours of hydration respectively) and SEM investigations (prepared after 48 h of hydration) were performed.

Finally, the three meta-phyllosilicates and a CC were tested in cementitious systems. Therefore, an OPC (CEM I 42.5 R) was used at a water-binder-ratio (w/b) of 0.6 as reference system. The measurements including the calcined clays were carried out with a substitution rate of 20 % by mass.

5.3.1 Quantitative analyses of early hydration in clinker-free model systems

The quantification of the in situ XRD measurements as well as the heat flow of the systems with MK and MI are presented in Figure 8. Some crystalline phases (anatase, phengite and quartz for MK and calcite and lime for MI) are not shown which do not change within the error range during the 50 h test duration.

While the systems with MK show pronounced heat flow maxima during the main reaction (Q^{+1}, Q^{+2} and Q^{+1}, Q^{+2}, Q^{+3} in Figure 8A and 8C respectively), the systems with MI yield a slight heat flow maximum only during the measurements with C$ (Q^{+1} in Figure 8D). All systems exhibit a pronounced initial heat flow, which can be assessed only qualitatively due to external stirring of the samples outside the calorimeter. Nevertheless, the pronounced initial heat flow correlates with the XRD quantifications, where a significant decrease of portlandite and meta-phyllosilicate content can be observed at the beginning of the measurements. Subsequently, the CH and meta-phyllosilicate dissolution in the MI systems proceed continuously until the end of the measurement. In the MK systems, an accelerated dissolution takes place in the region of the maxima Q^{+2} (Figure 8A and 8C). A formation of C-S-H can be detected in all four systems, which ranges from 2.9 to 10.6 wt.%. When comparing the sulfate-free systems with the systems with C$, it is noticeable that the formation of C-S-H in the sulfate-free systems starts earlier in both MK and MI. However, the onset of first C-S-H precipitation remains unclear according to Bergold et al. [11]. These authors describe the formation of C-S-H during alite hydration in two steps. During the first hours, short-range ordered C-S-H originate from alite, which cannot be detected nor quantified using the hkl-phase model. Subsequently, both alite and short-range ordered C-S-H react to form long-range ordered C-S-H (C-S-H_{lro}), which can be quantified with the C-S-H model. Thus, it cannot be said with certainty that C-S-H generally forms earlier in systems without C$, but only C-S-$H_{lro}$. Additionally, discrepancies between the quantifications could be caused by the incorporation of Al into the C-S-H structure and by different Ca/Si ratios between the sulfate-free and sulfate-containing systems. The formation of crystalline aluminate hydrates can be observed only in the sulfate-containing systems. The AFt formation initiates after 2 hours in MK-CH-C$ and after 13 hours in MI-CH-C$. When considering the total sulfate content, the maximum AFt content (AFt_{max}) calculated according to Hesse et al. [80] is attained for MK-CH-C$. When reaching AFt_{max} after 20 h, neither AFm-Ms, nor AFm-Hc nor AFm-Mc are formed. This indicates an incorporation of the released Al into C-(A)-S-H following AFt_{max}. It is assumed that the release rate and the released quantity of Al is insufficient to form AFm-Ms at early ages of hydration. Another reason could be a low concentration of hydroxide ions, which inhibits the formation of AFm-Ms as described in [103, 113]. Matschei et al. [103, 114] additionally describe a stabilization of AFt by formation of AFm-Hc or AFm-Mc in the presence of calcite. Thermodynamic modelling of hydrated cements by Lothenbach and Zajac [102] confirm the occurrence of AFm-Hc or AFm-Mc depending on the calcite content already at early times of hydration. In the present study, AFm-Hc or AFm-Mc could not be detected during the first 50 h in any of the investigated clinker-free systems. For the MK systems the calcite content (<1 wt.%) seems to be insufficient to form AFm-Hc or AFm-Mc during early hydration. For the systems containing MI, AFt_{max} has not yet been reached and it can be assumed that sulfate in the pore solution prevents the formation of AFm-Hc or AFm-Mc despite higher calcite contents. The availability of Al in MI-CH-C$ seems to be insufficient to form more AFt.

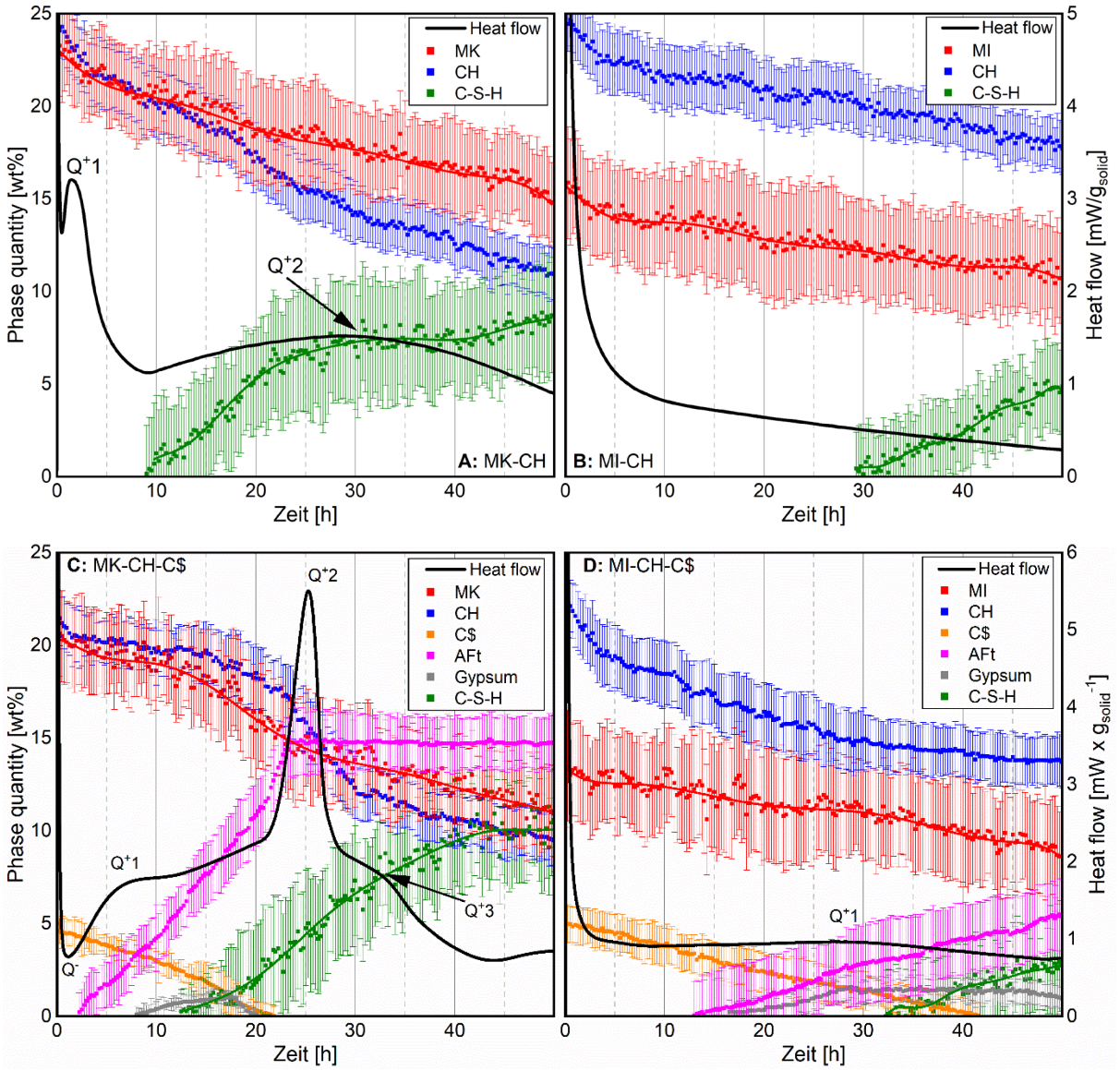

Figure 8 XRD quantification (left y-axis) and heat flow (right y-axis) of MK-CH (A), MI-CH (B), MK-CH-C$ (C) and MI-CH-C$ (D). The start values of the initial phases are marked with a cross on the y-axis. The error bars are calculated by multiple determination of the systems.

Analyses of the TG measurements validate a higher CH dissolution and more bound water in the MK systems compared to MI systems after 48 h. Sulfate-containing systems yield significantly more bound water compared to sulfate-free systems due to the formation of AFt. The XRD quantifications and TG measurements after 6 h of MI systems highlight a strong CH dissolution during the first hours of reaction, while the content of bound water is comparatively lower. This could be explained by the significantly higher BET surface area of MI (82.4 $m^2\ g^{-1}$) compared to MK (14.1 $m^2\ g^{-1}$) and leads to the hypothesis that Ca^{2+} ions adsorb onto the negatively charged surfaces of the calcined clays [93, 94] thus enabling a further dissolution process, even if only small amounts of hydrate phases are formed in relation to the dissolved ions. The continuous dissolution process of the C$ also supports this hypothesis. Especially the measurement of the 2:1 meta-phyllosilicate MI identifies a significant amount of dissolved C$ before AFt is formed. Myers et al. [115, 116] describe the adsorption of calcium – sulfate ions pair complexes onto the negative surfaces of Al-rich leached layers of tricalcium aluminate. This complex formation could also occur on the negatively charged surfaces of the calcined clays and explain the continuous dissolution process of C$. Due to the small amount

of C-S-H in clinker-free systems during early hydration, adsorption must take place on the calcined clay surfaces in addition to adsorption effects on the C-S-H surfaces, as observed by Zunino and Scrivener [88]. The lower amount of bound water after 6 h as well as after 48 h in the MI compared to the MK systems can be attributed to the lower Si and Al ion solubility. MI provides an insufficient amount of Si and Al ions to form more hydration products.

The reactivity of MM-CH and MM-CH-C$ can be regarded as very low. In situ XRD analyses disclose no C-S-H_{lro} formation in both systems. However, TG measurements also indicate the formation of C-S-H in MM systems. Crystalline aluminate hydrate phases can be detected in the sulfate-containing system only. AFt formation begins after 12 h. After about 17 h, the AFt content is 1 wt.% and remains constant until the end of the measurement. Instead of a further AFt formation, gypsum and AFm-Ms form simultaneously after 17 h. The amount of both phases increases continuously until the end of the measurement.

5.3.2 Visualization of clinker-free model systems

Figure 9 shows the SEM image of MI-CH after 50 h. The image displays particles of the corresponding meta-phyllosilicate (MI), CH crystals and poorly crystalline C-S-H. The C-S-H seems to grow out of the CH crystals (center of the image) as well as on the surfaces of the meta-phyllosilicate particles (named C-S-H inside the images).

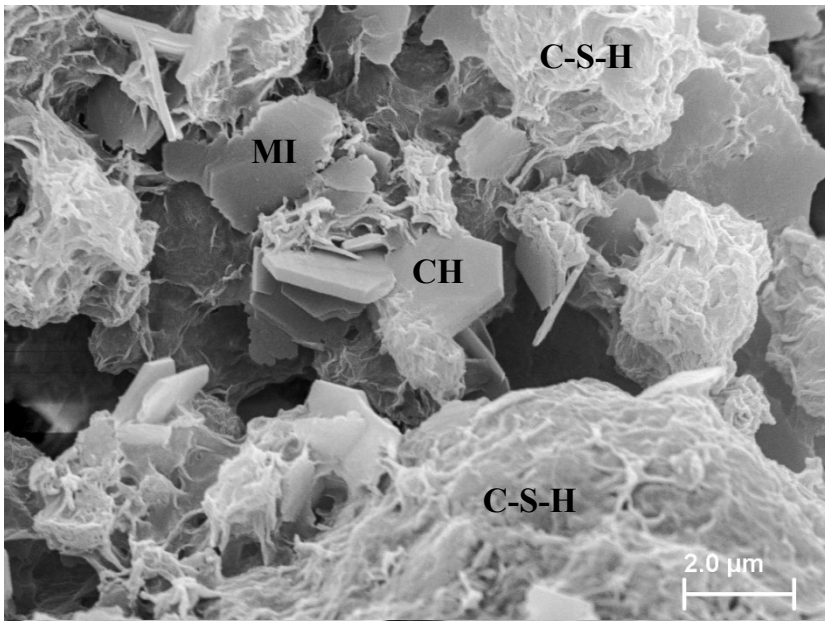

Figure 9 SEM image of MI-CH after 50 h

The SEM images of MK-CH-C$ (Figure 10) presents partly idiomorphic and partly less idiomorphic grown AFt crystals, which dominate the optical impression. The large number and size of the AFt crystals hinders the proper identification of the other phases. AFt crystals and poorly crystalline C-S-H cover most surfaces of the particles. Still, some MK particles can be detected.

Overall, the visual impression from SEM images shows AFt as dominant phase in MK-CH-C$, which is consistent with the analytical investigations and can explain the high amount of bound water.

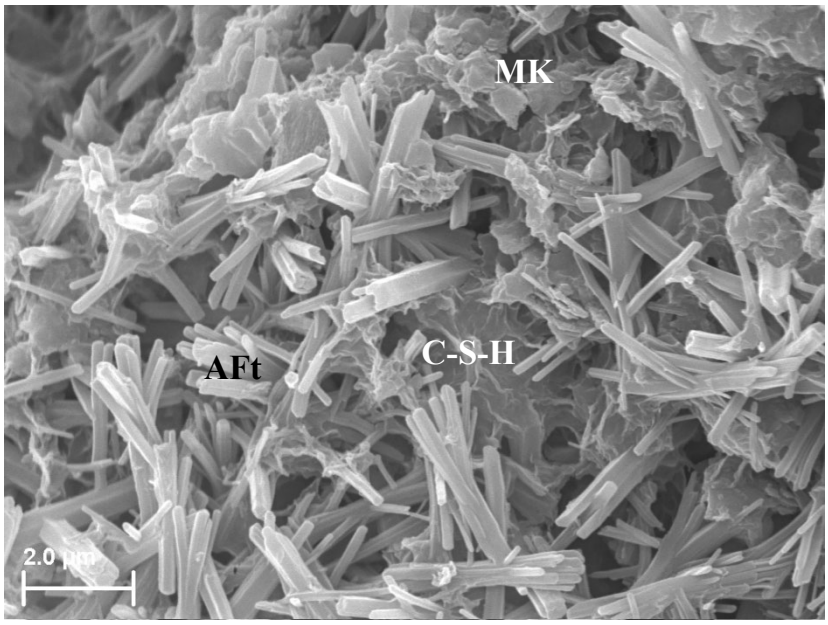

Figure 10 SEM image of MK-CH-C$ after 50 h

5.3.3 Implications from early hydration in clinker-free model systems

Figure 11 displays the CH dissolution and the bound water until 400 °C as well as the C-S-H content for the sulfate-free and C-S-H + AFt for the sulfate-containing systems after 48 h. The content of MK was set at 100 %. Since no C-S-H was detected in the measurements with MM, there is no value for the XRD quantification of MM-CH and MM-CH-C$ represents AFt only. Altogether, the reactivity of MM can be regarded as very low, reaching between 3.9 and 16.3 % of the values of MK. For cementitious systems it can be assumed therefore that the influence of the MM on the reaction mechanisms is less due to the chemical contribution than caused by physical hygroscopic properties, as already described by Neißer-Deiters et al. [10]. A more differentiated picture arises for MI. For MI-CH, all values are within a narrow range between 56.6 and 61.3 % compared to MK-CH. For MI-CH-C$, the individual values are much more divergent. While the CH dissolution yields 53 % of the value of MK-CH-C$, the bound water up to 400 °C and C-S-H + AFt reach only 36.8 % and 32.3 %, respectively. The values of bound water and hydrate phase formation correlate very well with the Si and Al solubility (MI has 30.9 % of the Si and Al solubility compared to MK). However, considerably less water is bound and less hydrate phases are formed than the CH dissolution suggests in comparison to MK. This strongly indicates adsorption effects of calcium – sulfate ion pair complexes on the calcined clay surfaces as mentioned above. Overall, it can be concluded that MI contributes not only physically but clearly also chemically to the early hydration in a clinker-free model system. Physical properties such as BET surface area appear to influence the composition of the pore solution by adsorption of ions or ions pair complexes additionally and thus affect the dissolution and reaction behavior.

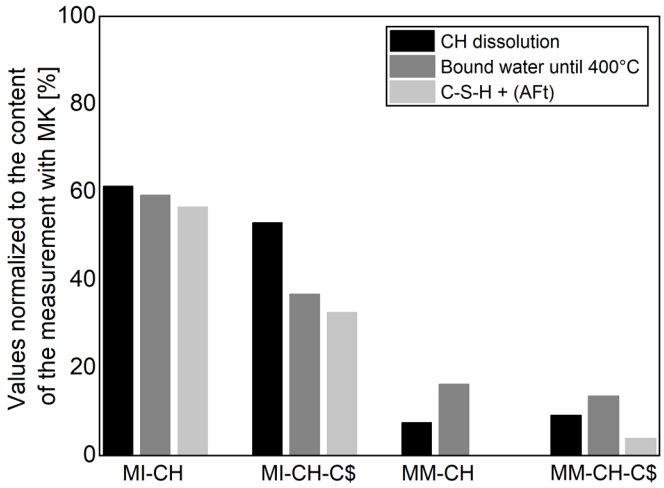

Figure 11 CH dissolution and bound water until 400 °C determined by TG and C-S-H + (AFt) determined by XRD after 48 h of the MI and MM systems. The values are normalized to the content of the measurements with MK and given in %.

Figure 12 summarizes schematically the general results from the sulfate-free and sulfate-containing systems with MK and MI. An increased Si/Al ratio and a decreasing absolute amount of Si and Al ions from the left to the right side of the graph are reflected in the amount of bound water as well as in the composition and quantity of hydrate phases. While for sulfate-free systems it is limited to the silicate reaction to C-(A)-S-H formation (lower, orange part of the graph), the entire graph must be considered for sulfate-containing systems (C-(A)-S-H + AFt). The brighter orange and blue areas indicate differences of bound water and hydrate phase quantity, as well as they reflect uncertainties in quantification.

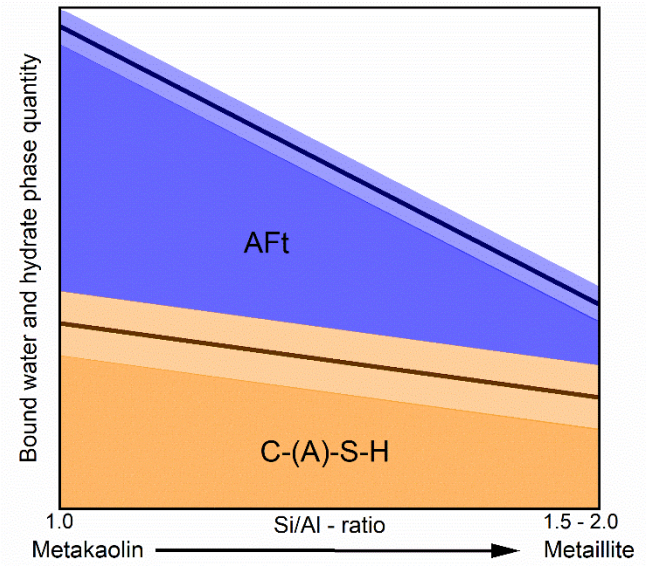

Figure 12 Schematic model to predict reactivity and hydrate phase formation during early hydration after 48 h of kaolinitic and illitic clays.

Overall, it was shown that all three meta-phyllosilicates MK, MI and MM can form both silicate and aluminate hydrate phases independently already during early hydration. Thus, for the first time, quantitative in situ XRD analyses have confirmed that, in addition to physical influences, the chemical contribution from the pozzolanic reaction of calcined clays during early hydration must be considered as well. Due to the slower and lower absolute solubility of Al from MI (about 30 % of that of MK), sulfate consumption in MI-CH-C$ takes place much slower and to a lesser

extent. Therefore, it is crucial to distinguish between kaolinitic and illitic clays regarding the sulfate balance of a composite cement containing calcined clays.

5.3.4 Qualitative implications from calcined clays in cementitious systems

Isothermal calorimetry of calcined clays (20 % by mass of the cement) in cementitious systems (OPC) disclose a significant influence of the meta-phyllosilicates (MK/MI/MM) on early hydration (section 8.5). Both, the dormant period and the main reaction are affected. Conversely, the measurement with CC shows hardly any difference during the dormant period compared to the reference. The high contents of accompanying minerals in the CC (mainly quartz, feldspar), which do not contribute to the reaction and have a low BET surface area, lead to significantly lower differences of the reaction kinetics compared to the reference system as holds for the pure meta-phyllosilicates. The silicate as well as the aluminate reaction is accelerated in all systems, however in the meta-phyllosilicate systems considerably stronger compared to CC. This is in line with literature [9, 113] and might be an advantage for CC when aiming at high replacement levels.

Figure 13 displays the level plot of the investigated systems from 8.5 to 18.5° 2θ. The times are given of the dissolution of the gypsum (G), AFt_{max} and the formation of AFm-Hc. The other reflexes were designated with the respective phase and the corresponding hkl. The in situ XRD investigations confirm the acceleration of the aluminate reaction due to the addition of calcined clays. The dissolution of gypsum accelerates significantly in all systems investigated. While in the reference only a slight formation of AFm-Hc occurs after 42 h, its formation initiates significantly earlier (after 12 to 14 h) with the addition of the meta-phyllosilicates. With CC, the AFm-Hc formation starts at 22 h. The time of maximum AFt formation correlates well with the heat flow maximum. The clinker phase C_3A is dissolved completely at that time for all calcined clays, while undissolved C_3A is still present in the reference system at the end of the measurement after 48 h. The influence on the silicate reaction is more difficult to determine from qualitative in situ XRD measurements. Nevertheless, an acceleration is clearly visible from calorimetry.

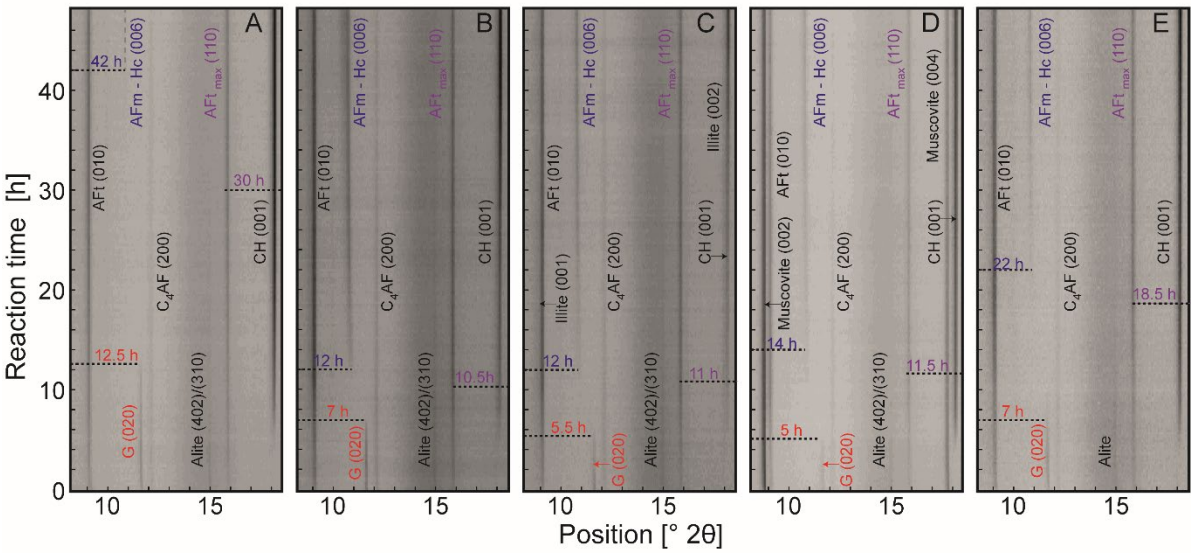

Figure 13 Levelplots from 8.5 to 18.5° 2Θ for 48 h of OPC as Reference (A), MK (B), MI (C), MM (D) and CC (E). The measurements including the calcined clays were carried out with a substitution rate of 20 % by mass. G ≙ Gypsum

The investigations indicate for cements with addition of calcined clays that the early hydration in the first 48 h is chemically controlled by the available ions and the surface chemistry of the

respective calcined clay. The faster reaching of AFt_{max}, the significantly earlier formation of AFm-Hc as well as the determination of the bound water from TG measurements show that the formation of aluminate hydrate phases is favored when calcined clays are added. This is in line with experimental results [7, 9, 104, 105] and thermodynamic modelling [102, 103] and can be explained with a pozzolanic contribution of calcined clays during early hydration according the results of clinker-free model systems in section 5.3.1 and 5.3.3.

The accelerated silicate reaction can be attributed to the filler effect due to a finer particle size distribution of the calcined clays in comparison to the cement [83, 88]. In addition to an accelerated adsorption of sulfate on the earlier formed C-S-H, as described in [88], the transfer of results from the clinker-free systems suggests that there may also be adsorption of calcium ions or calcium-sulfate ion complexes on the negatively charged surfaces of the calcined clay particles. These adsorption effects are related to the high BET surface area of the calcined clays and cause an acceleration of the aluminate reaction.

Overall, it can be stated that the effect described in [83, 90] and the influence of the granulometry of SCM on early hydration must be supplemented by considering the very special surface properties of meta-phyllosilicates and by considering the chemical contribution of the calcined clays.

6 Conclusion and outlook

The mineralogical complexity of CC makes predictions about their reaction mechanisms in cementitious systems very difficult. Studies on pure meta-phyllosilicates, which are the reactive components of CC, contributed to the fundamental understanding of the influence of calcined clays on early hydration. To analyze the reaction mechanism of hydrating systems, in situ XRD analyses are a suitable method. Here, the free, not chemically bound water, as well as the quantification of calcined clays, which are both largely present as X-ray amorphous phases, posed the greatest challenges and required more detailed investigations to reliably quantify in situ XRD analyses.

The quantifications of free, not chemically bound water with an hkl-phase (PONKCS method) were shown to be limited as the scattering contribution depends on the consistency of the sample. It is therefore not the absolute content of free water that is decisive for the feasibility of the quantification. The quantifiable range requires a pasty consistency and can vary greatly from sample to sample. Thus, the free water should be calibrated on the system under investigation. In the case of in situ XRD measurements of hydrating systems, the quantification of the free water is just possible until the maximum reaction rate of the main hydration. Owing to the complex background caused by the addition of water, its adaptation is particularly important for correct quantification. One must consider not only the scattering contribution of the water but also the lowering of the scattering contribution at small angles.

In addition to the role of free water during XRD quantifications, it was necessary to address issues related to the dissolution behavior of the metakaolin particles. By systematic correlation of dissolved silicon and aluminum from dissolution experiments with XRD quantification on MK after treatment in alkaline solutions, it was shown by means of ATR-FTIR that changes occur in the binding condition of MK owing to the treatment in alkali solutions. The enrichment of iron and titanium as well as the uptake of alkalis in the MK structure apparently cause a shift in the Si-O band to smaller wave numbers and a broadening of the bands. There seems to be an inhomogeneous distribution of the cations in the particles. Iron- and titanium-rich areas in the particles seemingly do not dissolve. These observations affect the intensity of the scattering contribution of the MK_{Am} in the diffractogram. However, these structural changes do not cause any change in the position of the X-ray amorphous hump as the dissolution of the MK particles is congruent. Therefore, it is reasonable to use a single hkl-phase model for the quantification of MK calcined at its optimum temperature between 500 and 800 °C.

Consequently, the results of the thesis show that the PONKCS method is a suitable method for investigating the quantity and reaction mechanisms of the X-ray amorphous SCM involved in the hydration of cements. The strong effect of error propagation for low degrees of reaction and low substitution rates in cementitious systems remains a problem when calculating the degree of reaction based on quantifications using the PONKCS method.

Clarifying these methodical issues allowed the examination of three different meta-phyllosilicates in clinker free model systems with a combination of in situ XRD quantifications, TG and calorimetry. The quantifications show that the examined meta-phyllosilicates yield an autonomous formation of hydrate phases. While for MK and MI both silicate and aluminate hydrate phases can be verified by XRD, for MM only aluminate hydrate phases are detectable. However, TG measurements also indicate the formation of C-S-H in MM systems. A pronounced reaction can only be determined for the systems with MK. MI and MM systems are characterized by a continuous dissolution and formation process in the clinker-free system

during early hydration and reveal no intense maxima of the heat flow during main reaction. Only MK is able to form the maximum AFt content during early hydration, while the 2:1 meta-phyllosilicates do not release enough aluminum to reach the maximum AFt content. Moreover, dissolution processes of the reactants and formation of hydrate phases do not seem to be directly coupled, which is supported by differences between the CH and C$ dissolution and the amount of bound water. This could be explained by the adsorption of calcium ions and calcium – sulfate ion pair complexes on the negatively charged calcined clay surfaces. The BET surface area has a decisive influence on the adsorption behavior of the meta-phyllosilicates. Thus, these effects cannot be explained solely by granulometric properties but must consider the chemical influence as well as the complex surface properties of calcined clay particles. The lower reactivity and release of Al of 2:1 meta-phyllosilicates compared to MK have to be considered for the sulfation of the systems when using calcined clays and require more detailed investigations. The influence of MM on the hydration kinetics seem to stem less from the chemical contribution than rather from its physical-hygroscopic properties.

First qualitative investigations of calcined clays in cementitious systems reveal an acceleration of the aluminate reaction in all systems. The formation of AFt and AFm-phases is favored when calcined clays are added. The transfer of the results from the clinker-free model systems shows that apart from filler effect, these effects can be traced to the chemical influence by dissolved ions and the adsorption of ions on the surfaces of the clay particles due to their negative charge and high BET surface area. The high content of accompanying minerals in the CC leads to clear differences between the meta-phyllosilicates and CC. The influence on hydration kinetics of CC is significantly lower, which might be positive when aiming at high replacement levels.

The complete quantification of in situ XRD measurements provides an important contribution to the fundamental understanding of the influence of calcined clays on early hydration. On the way to the large-scale use of calcined clays, further questions need to be addressed. Quantitative investigations in model cement systems, both with individual clinker phases and in a model cement, should provide further detailed insights into the influence of calcined clays on the silicate and aluminate reaction during early hydration. Investigations on the solubility and reaction behavior of the calcined clays are an important precondition for thermodynamic modeling. Thus, the present work and further quantitative investigations in model cement systems can improve the predictions of thermodynamic modeling. Despite a reliable quantification of both 1:1 and 2:1 phyllosilicates, questions remain, especially for the latter, about the processes during dehydroxylation and the resulting properties. The transformation or partial transformation in case of 2:1 phyllosilicates to the X-ray amorphous meta-phyllosilicates during calcination leads to modified surface properties of the clay particles and might affect their dissolution behavior. A more in-depth investigation of these effects could provide crucial information for verifying the theory of adsorption of ions on the clay particle surfaces. Furthermore, the liquefaction of concretes with a high content of calcined clays possesses a great challenge in terms of concrete technology due to their high water demand and reduced flowability. Thus, not least the selection and specification of suitable superplasticizers are closely linked to the surface properties and reaction behavior of calcined clays.

7 References

1. Jaskulski, R., D. Jóźwiak-Niedźwiedzka, and Y. Yakymechko, *Calcined Clay as Supplementary Cementitious Material.* Materials, 2020. **13**(21): p. 4734.
2. Thienel, K.-C. and N. Beuntner, *Calcinierte Tone und ihr Potenzial für die moderne Betontechnologie*, in *14. Symposium Baustoffe und Bauwerkserhaltung KIT - Betone der Zukunft - Herausforderungen und Chancen*, U. Nolting, et al., Editors. 2018, KIT Scientific Publishing: Karlsruhe. p. 37-48.
3. Maier, M., N. Beuntner, and K.-C. Thienel, *Mineralogical characterization and reactivity test of common clays suitable as supplementary cementitious material.* Applied Clay Science, 2021. **202**: p. 105990.
4. Poon, C.S., S.C. Kou, and L. Lam, *Compressive strength, chloride diffusivity and pore structure of high performance metakaolin and silica fume concrete.* Construction and Building Materials, 2006. **20**(10): p. 858-865.
5. Lemma, R., E.F. Irassar, and V. Rahhal, *Calcined Illitic Clays as Portland Cement Replacements*, in *Calcined Clays for Sustainable Concrete - Proceedings of the 1st International Conference on Calcined Clays for Sustainable Concrete*, K. Scrivener and A. Favier, Editors. 2015, Springer Netherlands: Lausanne, Switzerland. p. 269-276.
6. Irassar, E.F., et al., *Durability of blended cements containing illitic calcined clays*, in *15th International Congress on the Chemistry of Cement*, J. Gemrich, Editor. 2019, Research Institute of Binding Materials Prague: Prague, Czech Republic. p. 11.
7. Beuntner, N. and K.-C. Thienel, *Solubility and kinetics of calcined clay: study of interaction by pore solution*, in *2nd International Conference on the Chemistry of Construction Materials (ICCCM 2016)*, J. Plank, L. Lei, and T. Echt, Editors. 2016, Gesellschaft Deutscher Chemiker e.V.: Munich, Germany. p. 157-160.
8. Scarlett, N.V.Y. and I.C. Madsen, *Quantification of phases with partial or no known crystal structures.* Powder Diffraction, 2006. **21**(04): p. 278-284.
9. Beuntner, N., *Zur Eignung und Wirkungsweise calcinierter Tone als reaktive Bindemittelkomponente in Zement (On the suitability and mode of action of calcined clays as reactive binder components in cement)*, in *Fakultät für Bauingenieurwesen und Umweltwissenschaften*. 2017, Universität der Bundeswehr München: Neubiberg. p. 207.
10. Neißer-Deiters, A., et al., *Influence of the calcination temperature on the properties of a mica mineral as a suitability study for the use as SCM.* Applied Clay Science, 2019. **179**: p. 105168.
11. Bergold, S.T., F. Goetz-Neunhoeffer, and J. Neubauer, *Quantitative analysis of C–S–H in hydrating alite pastes by in-situ XRD.* Cement and Concrete Research, 2013. **53**(0): p. 119-126.
12. Rietveld, H.M., *An Algol Program for the Refinement of Nuclear and Magnetic Structures by the Profile Method*, in *RCN*. 1969, Reactor Centrum Nederland.
13. Rietveld, H.M., *Line profiles of neutron powder-diffraction peaks for structure refinement.* Acta Crystallographica, 1967. **22**(1): p. 151-152.
14. Scarlett, N.V.Y., et al., *Outcomes of the International Union of Crystallography Commission on Powder Diffraction Round Robin on Quantitative Phase Analysis: samples 2, 3, 4, synthetic bauxite, natural granodiorite and pharmaceuticals.* Journal of Applied Crystallography, 2002. **35**(4): p. 383-400.
15. Madsen, I.C., N.V.Y. Scarlett, and A. Kern, *Description and survey of methodologies for the determination of amorphous content via X-ray powder diffraction.* Zeitschrift für Kristallographie - Crystalline Materials, 2011. **226(12)**: p. 944-955.
16. O´Connor, B.H. and M.D. Raven, *Application of the Rietveld refinement procedure in assaying powdered mixtures.* Powder Diffraction, 1988. **3**: p. 2-6.
17. Jansen, D., et al., *A remastered external standard method applied to the quantification of early OPC hydration.* Cement and Concrete Research, 2011. **41**(6): p. 602-608.

18. Snellings, R., A. Salze, and K.L. Scrivener, *Use of X-ray diffraction to quantify amorphous supplementary cementitious materials in anhydrous and hydrated blended cements.* Cement and Concrete Research, 2014. **64**: p. 89-98.
19. Stetsko, Y.P., et al., *Quantification of supplementary cementitious content in blended Portland cement using an iterative Rietveld-PONKCS technique.* Journal of Applied Crystallography, 2017. **50**(2): p. 498-507.
20. Durdziński, P.T., et al., *Phase assemblage of composite cements.* Cement and Concrete Research, 2017. **99**: p. 172-182.
21. Durdziński, P.T., et al., *Outcomes of the RILEM round robin on degree of reaction of slag and fly ash in blended cements.* Materials and Structures, 2017. **50**(2): p. 135.
22. Kletti, H., et al., *Differenzierte Quantifizierung röntgenamorpher Phasen mittels PONKCS in praxisnahen Labormischungen*, in *19. Internationale Baustofftagung ibausil*, H.-B. Fischer, C. Boden, and M. Neugebauer, Editors. 2015, F.A. Finger – Institut für Baustoffkunde: Weimar. p. 634-640.
23. Adu-Amankwah, S., et al., *Influence of limestone on the hydration of ternary slag cements.* Cement and Concrete Research, 2017. **100**: p. 96-109.
24. Adu-Amankwah, S., et al., *Effect of sulfate additions on hydration and performance of ternary slag-limestone composite cements.* Construction and Building Materials, 2018. **164**: p. 451-462.
25. Dittrich, S., J. Neubauer, and F. Goetz-Neunhoeffer, *The influence of fly ash on the hydration of OPC within the first 44 h—A quantitative in situ XRD and heat flow calorimetry study.* Cement and Concrete Research, 2014. **56**(0): p. 129-138.
26. Avet, F., X. Li, and K. Scrivener, *Determination of the amount of reacted metakaolin in calcined clay blends.* Cement and Concrete Research, 2018. **106**: p. 40-48.
27. Pawley, G., *Unit-cell refinement from powder diffraction scans.* Journal of Applied Crystallography, 1981. **14**(6): p. 357-361.
28. Le Bail, A., H. Duroy, and J.L. Fourquet, *Ab-initio structure determination of LiSbWO6 by X-ray powder diffraction.* Materials Research Bulletin, 1988. **23**(3): p. 447-452.
29. Schöler, A., et al., *Early hydration of SCM-blended Portland cements: A pore solution and isothermal calorimetry study.* Cement and Concrete Research, 2017. **93**: p. 71-82.
30. Tironi, A., et al., *Kaolinitic calcined clays – Portland cement system: Hydration and properties.* Construction and Building Materials, 2014. **64**: p. 215-221.
31. Naber, C., et al., *The PONKCS method applied for time resolved XRD quantification of supplementary cementitious material reactivity in hydrating mixtures with ordinary Portland cement.* Construction and Building Materials, 2019. **214**: p. 449-457.
32. Zhang, J. and G.W. Scherer, *Comparison of methods for arresting hydration of cement.* Cement and Concrete Research, 2011. **41**(10): p. 1024-1036.
33. Snellings, R., et al., *Report of TC 238-SCM: hydration stoppage methods for phase assemblage studies of blended cements—results of a round robin test.* Materials and Structures, 2018. **51**(4): p. 111.
34. Snellings, R., et al., *RILEM TC-238 SCM recommendation on hydration stoppage by solvent exchange for the study of hydrate assemblages.* Materials and Structures, 2018. **51:172**(6).
35. Zhang, L. and F.P. Glasser, *Critical examination of drying damage to cement pastes.* Advances in Cement Research, 2000. **12**(2): p. 79-88.
36. Khoshnazar, R., et al., *Solvent exchange in sulphoaluminate phases. Part I: ettringite.* Advances in Cement Research, 2013. **25**(6): p. 314-321.
37. Khoshnazar, R., et al., *Solvent exchange in sulfoaluminate phases. Part II: monosulfate.* Advances in Cement Research, 2013. **25**(6): p. 322-331.
38. Schöler, A., et al., *Hydration of quaternary Portland cement blends containing blast-furnace slag, siliceous fly ash and limestone powder.* Cement and Concrete Composites, 2015. **55**: p. 374-382.
39. Brindley, G.W. and M. Nakahira, *The Kaolinite-Mullite Reaction Series: II, Metakaolin.* Journal of the American Ceramic Society, 1959. **42**(7): p. 314-318.

40. Halse, Y., et al., *Development of microstructure and other properties in flyash OPC systems.* Cement and Concrete Research, 1984. **14**(4): p. 491-498.
41. Granizo, N., A. Palomo, and A. Fernandez-Jiménez, *Effect of temperature and alkaline concentration on metakaolin leaching kinetics.* Ceramics International, 2014. **40**(7, Part A): p. 8975-8985.
42. Garg, N. and J. Skibsted, *Dissolution kinetics of calcined kaolinite and montmorillonite in alkaline conditions: Evidence for reactive Al(V) sites.* Journal of the American Ceramic Society, 2019. **102**(12): p. 7720-7734.
43. Snellings, R., *Solution-Controlled Dissolution of Supplementary Cementitious Material Glasses at pH 13: The Effect of Solution Composition on Glass Dissolution Rates.* Journal of the American Ceramic Society, 2013. **96**(8): p. 2467-2475.
44. Okrusch, M. and S. Matthes, *Mineralogie - Eine Einführung in die spezielle Mineralogie, Petrologie und Lagestättenkunde*. 8 ed. Springer-Lehrbuch. 2010: Springer Spektrum. XX, 728.
45. Salmang, H. and H. Scholze, *Keramik*. 7. ed. 2007: Springer-Verlag Berlin Heidelberg. 1165.
46. Scrivener, K.L., V.M. John, and E.M. Gartner, *Eco-efficient cements: Potential economically viable solutions for a low-CO_2 cement-based materials industry.* Cement and Concrete Research, 2018. **114**: p. 2-26.
47. He, C., E. Makovicky, and B. Osbæck, *Thermal stability and pozzolanic activity of calcined kaolin.* Applied Clay Science, 1994. **9**(3): p. 165-187.
48. He, C., B. Osbæck, and E. Makovicky, *Pozzolanic reactions of six principal clay minerals: activation, reactivity assessments and technological effects.* Cement and Concrete Research, 1995. **25**(8): p. 1691-1702.
49. He, C., E. Makovicky, and B. Osbæck, *Thermal stability and pozzolanic activity of calcined illite.* Applied Clay Science, 1995. **9**(5): p. 337-354.
50. He, C., E. Makovicky, and B. Osbaeck, *Thermal treatment and pozzolanic activity of Na- and Ca-montmorillonite.* Applied Clay Science, 1996. **10**(5): p. 351-368.
51. He, C., E. Makovicky, and B. Osbæck, *Thermal stability and pozzolanic activity of raw and calcined mixed-layer mica/smectite.* Applied Clay Science, 2000. **17**(3–4): p. 141-161.
52. Sabir, B.B., S. Wild, and J. Bai, *Metakaolin and calcined clays as pozzolans for concrete: a review.* Cement and Concrete Composites, 2001. **23**(6): p. 441-454.
53. Tironi, A., et al., *Kaolinitic calcined clays: Factors affecting its performance as pozzolans.* Construction and Building Materials, 2012. **28**(1): p. 276-281.
54. Raask, E. and M.C. Bhaskar, *Pozzolanic activity of pulverized fuel ash.* Cement and Concrete Research, 1975. **5**(4): p. 363-375.
55. Surana, M.S. and S.N. Joshi, *Spectrophotometric method for estimating the reactivity of pozzolanic materials.* Advances in Cement Research, 1998. **1**(4): p. 238-242.
56. Katyal, N.K., et al., *Development of rapid method for the estimation of reactive silica in fly ash.* Cement and Concrete Research, 2008. **38**(1): p. 104-106.
57. Donatello, S., M. Tyrer, and C.R. Cheeseman, *Comparison of test methods to assess pozzolanic activity.* Cement and Concrete Composites, 2010. **32**(2): p. 121-127.
58. Ferraz, E., et al., *Pozzolanic Activity of Metakaolins by the French Standard of the Modified Chapelle Test: A Direct Methodology.* Acta Geodynamica et Geomaterialia, 2015. **12**(3): p. 289–298.
59. Tashiro, C., K. Ikeda, and Y. Inoue, *Evaluation of pozzolanic activity by the electric resistance measurement method.* Cement and Concrete Research, 1994. **24**(6): p. 1133-1139.
60. Roszczynialski, W., *Determination of pozzolanic activity of materials by thermal analysis.* Journal of Thermal Analysis and Calorimetry, 2002. **70**: p. 387-392.
61. Baert, G., et al., *Reactivity of fly ash in cement paste studied by means of thermogravimetry and isothermal calorimetry.* Journal of Thermal Analysis and Calorimetry, 2008. **94**: p. 485-492.
62. Ben Haha, M., K. De Weerdt, and B. Lothenbach, *Quantification of the degree of reaction of fly ash.* Cement and Concrete Research, 2010. **40**(11): p. 1620-1629.

63. DIN EN 196-1, *Prüfverfahren für Zement - Teil 1: Bestimmung der Festigkeit (Methods of testing cement - Part 1: Determination of strength)*. 2016, Beuth-Verlag: Berlin. p. 31.
64. DIN EN 196-5, *Prüfverfahren für Zement - Teil 5: Prüfung der Puzzolanität von Puzzolanzementen (Methods of testing cement – Part 5: Pozzolanicity test for pozzolanic cement)*. 2011, Beuth-Verlag: Berlin. p. 14.
65. Buchwald, A., et al. *Untersuchung zur Reaktivität von Metakaolinen für die Verwendung in Bindemittelsystemen*. in *Gesellschaft Deutscher Chemiker e.V - Jahrestagung*. 2003. Munich, Germany.
66. Avet, F., et al., *Development of a new rapid, relevant and reliable (R³) test method to evaluate the pozzolanic reactivity of calcined kaolinitic clays.* Cement and Concrete Research, 2016. **85**: p. 1-11.
67. Maier, M., N. Beuntner, and K.-C. Thienel, *An approach for the evaluation of local raw material potential for calcined clay as SCM, based on geological and mineralogical data: Examples from German clay deposits*, in *Calcined Clays for Sustainable Concrete*, S. Bishnoi, Editor. 2020, Springer: Singapore. p. 37-47.
68. Ambroise, J., M. Murat, and J. Pera, *Hydration reaction and hardening of calcined clays and related minerals. IV. Experimental conditions for strength improvement on metakaolinite minicylinders.* Cement and Concrete Research, 1985. **15**(1): p. 83-88.
69. Fernandez, R., F. Martirena, and K.L. Scrivener, *The origin of the pozzolanic activity of calcined clay minerals: a comparison between kaolinite, illite and montmorillonite.* Cement and Concrete Research, 2011. **41**(1): p. 113-122.
70. Hollanders, S., et al., *Pozzolanic reactivity of pure calcined clays.* Applied Clay Science, 2016. **132–133**: p. 552-560.
71. Cabrera, J. and M.F. Rojas, *Mechanism of hydration of the metakaolin–lime–water system.* Cement and Concrete Research, 2001. **31**(2): p. 177-182.
72. De Silva, P.S. and F.P. Glasser, *Phase relations in the system CaO·Al2O3·SiO2·H2O relevant to metakaolin - calcium hydroxide hydration.* Cement and Concrete Research, 1993. **23**(3): p. 627-639.
73. Frías, M. and J. Cabrera, *Influence of MK on the reaction kinetics in MK/lime and MK-blended cement systems at 20°C.* Cement and Concrete Research, 2001. **31**(4): p. 519-527.
74. Murat, M., *Hydration reaction and hardening of calcined clays and related minerals: I. Preliminary investigation on metakaolinite.* Cement and Concrete Research, 1983. **13**(2): p. 259-266.
75. Rojas, M.F. and M.I. Sánchez de Rojas, *The effect of high curing temperature on the reaction kinetics in MK/lime and MK-blended cement matrices at 60 °C.* Cement and Concrete Research, 2003. **33**(5): p. 643-649.
76. De Silva, P.S. and F.P. Glasser, *Hydration of cements based on metakaolin: thermochemistry.* Advances in Cement Research, 1990. **3**(12): p. 167-177.
77. Murat, M., *Hydration reaction and hardening of calcined clays and related minerals: II. Influence of mineralogical properties of the raw-kaolinite on the reactivity of metakaolinite.* Cement and Concrete Research, 1983. **13**(4): p. 511-518.
78. Love, C.A., I.G. Richardson, and A.R. Brough, *Composition and structure of C–S–H in white Portland cement–20% metakaolin pastes hydrated at 25 °C.* Cement and Concrete Research, 2007. **37**(2): p. 109-117.
79. Rojas, M.F. and J. Cabrera, *The effect of temperature on the hydration rate and stability of the hydration phases of metakaolin–lime–water systems.* Cement and Concrete Research, 2002. **32**(1): p. 133-138.
80. Hesse, C., F. Goetz-Neunhoeffer, and J. Neubauer, *A new approach in quantitative in-situ XRD of cement pastes: Correlation of heat flow curves with early hydration reactions.* Cement and Concrete Research, 2011. **41**(1): p. 123-128.
81. Cyr, M., P. Lawrence, and E. Ringot, *Efficiency of mineral admixtures in mortars: Quantification of the physical and chemical effects of fine admixtures in relation with compressive strength.* Cement and Concrete Research, 2006. **36**(2): p. 264-277.

82. Kadri, E.H., et al., *Combined effect of chemical nature and fineness of mineral powders on Portland cement hydration.* Materials and Structures, 2010. **43**(5): p. 665-673.
83. Lothenbach, B., K. Scrivener, and R.D. Hooton, *Supplementary cementitious materials.* Cement and Concrete Research, 2011. **41**(12): p. 1244-1256.
84. Scrivener, K., P. Juilland, and P.J.M. Monteiro, *Advances in understanding hydration of Portland cement.* Cement and Concrete Research, 2015.
85. Gutteridge, W.A. and J.A. Dalziel, *Filler cement: The effect of the secondary component on the hydration of Portland cement: Part I. A fine non-hydraulic filler.* Cement and Concrete Research, 1990. **20**(5): p. 778-782.
86. Garrault-Gauffinet, S. and A. Nonat, *Experimental investigation of calcium silicate hydrate (C-S-H) nucleation.* Journal of Crystal Growth, 1999. **200**(3): p. 565-574.
87. Oey, T., et al., *The Filler Effect: The Influence of Filler Content and Surface Area on Cementitious Reaction Rates.* Journal of the American Ceramic Society, 2013. **96**(6): p. 1978-1990.
88. Zunino, F. and K. Scrivener, *The influence of the filler effect on the sulfate requirement of blended cements.* Cement and Concrete Research, 2019. **126**: p. 105918.
89. Lawrence, P., M. Cyr, and E. Ringot, *Mineral admixtures in mortars: Effect of inert materials on short-term hydration.* Cement and Concrete Research, 2003. **33**: p. 1939-1947.
90. Cyr, M., P. Lawrence, and E. Ringot, *Mineral admixtures in mortars: Quantification of the physical effects of inert materials on short-term hydration.* Cement and Concrete Research, 2005. **35**(4): p. 719-730.
91. Ouyang, X., et al., *Insights into the mechanisms of nucleation and growth of C–S–H on fillers.* Materials and Structures, 2017. **50**(5): p. 213.
92. Lei, L. and J. Plank, *A study on the impact of different clay minerals on the dispersing force of conventional and modified vinyl ether based polycarboxylate superplasticizers.* Cement and Concrete Research, 2014. **60**: p. 1-10.
93. Li, R., et al., *Effectiveness of PCE superplasticizers in calcined clay blended cements.* Cement and Concrete Research, 2021. **141**: p. 106334.
94. Sposito, R., N. Beuntner, and K.-C. Thienel, *Characteristics of components in calcined clays and their influence on the efficiency of superplasticizers.* Cement and Concrete Composites, 2020. **110**: p. 103594.
95. Jansen, D., et al., *The early hydration of OPC investigated by in-situ XRD, heat flow calorimetry, pore water analysis and 1H NMR: Learning about adsorbed ions from a complete mass balance approach.* Cement and Concrete Research, 2018. **109**: p. 230-242.
96. Marsh, B.K. and R.L. Day, *Pozzolanic and cementitious reactions of fly ash in blended cement pastes.* Cement and Concrete Research, 1988. **18**(2): p. 301-310.
97. Scrivener, K.L., et al., *TC 238-SCM: hydration and microstructure of concrete with SCMs.* Materials and Structures, 2015. **48**(4): p. 835-862.
98. Richardson, I.G., *The nature of C-S-H in hardened cements.* Cement and Concrete Research, 1999. **29**(8): p. 1131-1147.
99. Richardson, I.G., *The calcium silicate hydrates.* Cement and Concrete Research, 2008. **38**: p. 137-158.
100. Avet, F., E. Boehm-Courjault, and K. Scrivener, *Investigation of C-A-S-H composition, morphology and density in Limestone Calcined Clay Cement (LC3).* Cement and Concrete Research, 2019. **115**: p. 70-79.
101. Rossen, J.E., *Composition and morphology of C-A-S-H in pastes of alite and cement blended with supplementary cementitious materials*, in *Faculté des Sciences et Techniques de l'Ingénieur, Laboratoire des Matériaux de Construction*. 2014, École Polytechnique Fédérale de Lausanne: Lausanne. p. 154.
102. Lothenbach, B. and M. Zajac, *Application of thermodynamic modelling to hydrated cements.* Cement and Concrete Research, 2019. **123**: p. 105779.

103. Matschei, T., B. Lothenbach, and F.P. Glasser, *The AFm phase in Portland cement.* Cement and Concrete Research, 2007. **37**(2): p. 118-130.
104. Tironi, A., et al., *Thermal analysis to assess pozzolanic activity of calcined kaolinitic clays.* Journal of Thermal Analysis and Calorimetry, 2014. **117**(2): p. 547-556.
105. Danner, T., *Reactivity of Calcined Clays*, in *Faculty of Natural Science and Technology, Department of Natural Sciences and Engineering*. 2013, NTNU: Trondheim. p. 229.
106. Kaps, C. and A. Buchwald. *Property controlling influences on the generation of geopolymeric binders based on clay*. in *Geopolymer 2002 3rd International Conference*. 2002. Melbourne, Australia.
107. DIN EN ISO 11885, *Water quality - Determination of selected elements by inductively coupled plasma optical emission spectrometry (ICP-OES)*. 2009, Beuth-Verlag: Berlin, Germany. p. 37.
108. Hesse, C., et al., *Quantitative in situ X-ray diffraction analysis of early hydration of Portland cement at defined temperatures.* Powder Diffraction, 2009. **24**(2): p. 112-115.
109. Hesse, C., *Der Reaktionsverlauf der frühen Hydratation von Portlandzement in Relation zur Temperatur*, in *Naturwissenschaftliche Fakultät*. 2009, Friedrich-Alexander-Universität Erlangen-Nürnberg.
110. Król, M., J. Minkiewicz, and W. Mozgawa, *IR spectroscopy studies of zeolites in geopolymeric materials derived from kaolinite.* Journal of Molecular Structure, 2016. **1126**: p. 200-206.
111. Kosslick, H. and R. Fricke, *Chemical Analysis of Aluminosilicates, Aluminophosphates and Related Molecular Sieves*, in *Characterization II*, H.G. Karge and J. Weitkamp, Editors. 2007, Springer Berlin Heidelberg: Berlin, Heidelberg. p. 1-66.
112. Vollpracht, A., et al., *The pore solution of blended cements: a review.* Materials and Structures, 2016. **49**(8): p. 3341-3367.
113. Antoni, M., et al., *Cement substitution by a combination of metakaolin and limestone.* Cement and Concrete Research, 2012. **42**(12): p. 1579-1589.
114. Matschei, T., B. Lothenbach, and F.P. Glasser, *The role of calcium carbonate in cement hydration.* Cement and Concrete Research, 2007. **37**(4): p. 551-558.
115. Myers, R.J., et al., *Role of Adsorption Phenomena in Cubic Tricalcium Aluminate Dissolution.* Langmuir, 2017. **33**(1): p. 45-55.
116. Myers, R.J., et al., *Solution chemistry of cubic and orthorhombic tricalcium aluminate hydration.* Cement and Concrete Research, 2017. **100**: p. 176-185.

8 Publications

8.1 Quantitative X-Ray Diffraction of free, not chemically bound water with the PONKCS method

Reprint
Published in the Journal “Journal of Applied Crystallography”
Vol. 51 (2018) p. 1535-1543, doi: 10.1107/S1600576718012888

Authors: S. Scherb, N. Beuntner, K.-Ch. Thienel and J. Neubauer

research papers

JOURNAL OF APPLIED CRYSTALLOGRAPHY

ISSN 1600-5767

Quantitative X-ray diffraction of free, not chemically bound water with the PONKCS method

Sebastian Scherb,[a]* Nancy Beuntner,[a] Karl-Christian Thienel[a] and Jürgen Neubauer[b]

[a]Civil Engineering and Enviromental Science, Bundeswehr University Munich, Neubiberg, 85579, Germany, and [b]Mineralogy GeoZentrum Nordbayern, Friedrich-Alexander Universität Erlangen–Nürnberg, Erlangen, 91054, Germany. *Correspondence e-mail: sebastian.scherb@unibw.de

Received 7 June 2018
Accepted 12 September 2018

Edited by K. Chapman, Stony Brook University, USA

Keywords: free water; X-ray diffraction analysis; PONKCS; calcined clay; supplementary cementitious material.

The free water in calcined phyllosilicate–water mixtures exhibits a distinctly different behaviour in its X-ray amorphous scattering contribution as opposed to fly ash– or limestone powder–water mixtures. While fly ash and limestone powder yield a continuous increase in the scattering contribution when water is added, the scattering contribution stagnates for calcined phyllosilicates over a wide range of water addition. There is a direct correlation between the consistency of the sample and the X-ray amorphous scattering contribution caused by the water. The same correlation can also be found in *in situ* X-ray diffraction measurements of hydrating systems. As long as the sample has a pasty consistency, the scattering contribution of the water decreases with progressive reaction. After the transition from fresh paste to final set, there is no further reduction of the X-ray amorphous scattering contribution caused by the free water, which means that the free water cannot be quantified correctly from this point in time.

1. Introduction

Calcined clays attract more and more scientific attention as supplementary cementitious material (SCM). While fly ash and slag primarily offer silicon ions for the hydration process, calcined clays also provide a substantial quantity of aluminium ions (Beuntner & Thienel, 2016). This leads to significant differences in the resulting hydration products. In order to understand the complex pozzolanic reaction behaviour of clay mixtures it is necessary to understand the pozzolanic contribution of the individual phyllosilicates contained in these mixtures.

In situ X-ray diffraction (XRD) measurements are generally suitable for monitoring and quantifying the hydration reaction in cementitious systems. Rietveld refinement (Rietveld, 1967, 1969) allows the quantification of all identified crystalline phases normalized to 100%. A common approach of quantitative phase analysis with XRD samples containing X-ray amorphous phases is the internal standard method (Madsen *et al.*, 2011; Scarlett *et al.*, 2002). The external standard approach (O'Connor & Raven, 1988) with the calibration factor G (Jansen *et al.*, 2011) allows the quantification of the crystalline phases without influencing hydration by an internal standard. The X-ray amorphous components such as fly ash, metakaolin, free water and the resulting C–S–H phase are determined in their entirety for both the internal and the external standard method. In order to separate the X-ray amorphous phases, various publications have already dealt with their quantification using the PONKCS method (partial

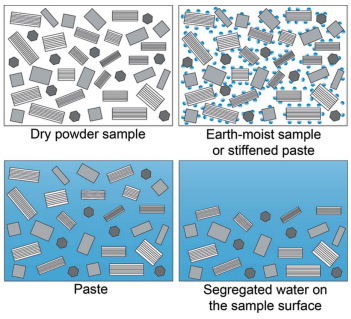

research papers

or no known crystal structure; Scarlett & Madsen, 2006). For this purpose, X-ray amorphous components were modelled and quantified with so-called '*hkl* or peaks phases' (Snellings *et al.*, 2014; Stetsko *et al.*, 2017; Durdziński, Ben Haha, Zajac & Scrivener, 2017; Durdziński, Ben Haha, Bernal *et al.*, 2017; Kletti *et al.*, 2015; Adu-Amankwah *et al.*, 2017, 2018; Dittrich *et al.*, 2014; Avet *et al.*, 2018). The modelling of phases with the PONKCS method requires that X-ray amorphous phases can be represented by a series of peaks *via* Pawley (Pawley, 1981) or Le Bail (Le Bail *et al.*, 1988) fitting and that they are available in pure form or as a main phase with known quantity for calibration. The combination of these two methods allows the quantification of both crystalline phases and the individual X-ray amorphous phases with very small domain sizes as was demonstrated by Bergold *et al.* (2013). The modelling and quantification of free water has received little attention in previous publications since it was to a great extent removed by stopping hydration with 2-propanol or acetone or by vacuum drying (Zhang & Scherer, 2011; Snellings *et al.*, 2014; Durdziński, Ben Haha, Bernal *et al.*, 2017). However, the common stopping mechanisms interfere with the hydration reaction, can damage reaction products, and can lead to deviating results depending on the type and duration of the stopping process (Zhang & Glasser, 2000; Khoshnazar *et al.*, 2013*a*,*b*; Schöler *et al.*, 2015). Especially for early hydration, it is better to perform *in situ* XRD measurements directly on the reacting system without stopping the hydration. In this case, the free water and changes related to it during hydration have to be taken into account and must be modelled with an *hkl* phase. Although previous studies have involved modelling of free water as an *hkl* phase (Adu-Amankwah *et al.*, 2017, 2018) and refinement of the scaling factor (Bergold *et al.*, 2013; Dittrich *et al.*, 2014), there was no quantification and no closer examination of the variation of the scattering contribution due to the water and its influence on the quantification of hydrating pastes. Homogeneity is a prerequisite for a quantification of the water in the samples. Any sedimentation or bleeding of cement paste as reported by various authors (Peng & Jacobsen, 2013; Wheeler, 1966; Wheeler & Chatterji, 1972) leads to a differentiation in the sample and thus to a overdetermined quantification of the free water.

The idea of this paper is to determine to what extent the quantification of free water in XRD measurements with the PONKCS method is possible and which factors influence the quantification.

2. Materials and methods

2.1. Materials and test series

The investigations concentrate on the role and influence of the free water on the quantification of XRD measurements with *hkl* phases of two different calcined phyllosilicates (metakaolin and metamuscovite) and for comparison of a common fly ash from a dry firing coal power plant according to DIN EN 450-1 (DIN, 2012*b*) and limestone powder.

Table 1
Mineralogical composition of metakaolin (MK), metamuscovite (MM), fly ash (FA) and limestone powder (LS).

Phases (wt%)	MK	MM	FA	LS
Quartz	5.0	–	8.0	1.8
Anatase	0.6	–	–	–
Phengite	1.4	–	–	–
Calcite	–	–	–	92.3
Dolomite	–	–	–	5.9
Muscovite	–	76.3	–	–
Mullite	–	–	12.4	–
Hematite	–	–	0.6	–
Magnetite	–	–	0.3	–
X-ray amorphous	93	24	79	–

Table 2
Chemical composition, loss of ignition (LOI), mass attenuation coefficient (MAC), water absorption coefficient (WAC) and BET surface area of MK, MM, FA and LS.

Oxides (wt%)	MK	MM	FA	LS
SiO_2	51.9	47.4	51.9	4.8
Al_2O_3	38.3	32.7	20.9	1.2
Fe_2O_3	1.7	5.1	9.6	0.6
CaO	<0.1	0.2	5.1	47.9
MgO	0.2	<0.1	1.7	1.3
SO_3	<0.1	<0.1	0.7	<0.1
Na_2O	0.3	0.6	0.6	<0.1
K_2O	0.3	12.0	4.1	0.7
TiO_2	1.3	0.9	1.0	<0.1
LOI	1.3	0.9	3.5	43.4
MAC ($cm^2\ g^{-1}$)	36.8	54.6	50,1	68.7
WAC (wt%)	77.0	154.5	37.7	37.4
BET ($m^2\ g^{-1}$)	17.8	10.9	1.0	6.0

In the test series the materials were investigated at different water to solid (w/s) ratios ranging from 0.2 (16.7 wt% H_2O) to 1.0 (50 wt% H_2O). Finally, *in situ* XRD measurements over a period of 50 h were conducted to quantify the unbound water with the developed evaluation routine of a metakaolin–portlandite powder (CH)–alkaline solution mixture with the mass ratio 1:1:2. In order to validate the quantification of *in situ* XRD measurements, additional thermogravimetric analyses (TG) and calorimeter measurements were performed. After weighing, the sample was sealed airtight and equilibrated overnight at 298 K. For all sample preparations, the sample was manually homogenized at room temperature (298 ± 2 K) for one minute after addition of water. The XRD measurements were performed on a temperature-controlled sample holder at 298 K. The calorimetric measurements were also carried out at 298 K.

The flash calcined metakaolin is commercially available and was ready for use, while raw muscovite was calcined in a muffle oven for 30 min at 1073 K. The calcination temperature of muscovite was chosen because of its dehydroxylation temperatures determined by differential thermal gravimetry and Si- and Al-ion solubility in alkaline solution after 20 h. Detailed information is given by Scherb *et al.* (2018) on the particle size distribution as well as on the ion solubility of the phyllosilicates. The composition of the alkaline solution was 100 mmol l^{-1} NaOH and 500 mmol l^{-1} KOH. Table 1 shows

the mineralogical composition of the phyllosilicates together with fly ash and limestone powder. The chemical compositions of all four SCMs (Table 2) were determined by inductively coupled plasma optical emission spectrometry. The mass attenuation coefficients (MACs) of the investigated phases (Table 2) were calculated from the MACs of the single elements given in *International Tables for Crystallography* for Cu $K\alpha$ radiation (Creagh & Hubbel, 2006). For CH the chemical composition given by Merck was used to calculate the MAC (91.1 $cm^2\ g^{-1}$). Furthermore the water absorption capacity was measured (DIN, 2012*a*) (Table 2).

2.2. XRD measurements

The solids and water or an alkali solution were mixed manually with a spatula for 60 s for all sample preparations, transferred into a sample holder, and covered with a Kapton film. XRD measurements were performed with a PANalytical Empyrean diffractometer equipped with a primary Bragg–Brentano^{HD} monochromator and a PIXcel^{1D} linear detector. A diffractogram was taken in 15 min from 6 to 40° 2θ at 40 kV and 40 mA with Cu $K\alpha$ radiation. *In situ* XRD was conducted with the same experimental setup for up to 50 h of hydration. Measurements were analysed with the software *HighScore 4.6* (Degen *et al.*, 2014).

A silicon single crystal also covered with a Kapton film was used to calculate the G factor, which is the calibration factor for the complete experimental setup (Jansen *et al.*, 2011). The PONKCS method was applied to the external standard method according to Bergold *et al.* (2013). Here, the contribution of each *hkl* phase (phase density ρ_j and volume of the unit cell V_j) to the crystal structure needed to be replaced by a calibration factor F in the equation for the external standard method (Bergold *et al.*, 201; Jansen *et al.*, 2011):

$$\rho_j V_j^2 = F = \frac{c_j G}{s_j \mu^*_{\mathrm{SAMPLE}}} \qquad (1)$$

In equation (1), c_j represents the phase content, s_j the scale factor calculated by Rietveld refinement of each phase j and μ^*_{SAMPLE} the MAC of the whole sample which was calculated for the different solid to water ratios with respect to the MAC of water (10.3 $cm^2\ g^{-1}$).

2.3. Development and calibration of *hkl* phases

The scattering contribution of the *hkl* phases was simulated with Pawley fits. For refinement of profile parameters the width and shape were split and refined iteratively (Stetsko *et al.*, 2017). The Caglioti function (Caglioti *et al.*, 1958) served for refining the profile parameters u, v and w. All calibrations were carried out with ZnO as internal standard.

2.3.1. Kapton film and free water model. The modelling of the Kapton film and the free water was carried out in successive steps because of the higher background intensities at small angles 2θ of dry powder samples compared to solid–water mixtures. Fig. 1 shows these differences for ZnO powder and ZnO–water mixtures. The modelling comprises five steps:

(1) A silicon single-crystal sample carrier covered with Kapton film [Fig. 1*a* (1)] was measured to develop the Kapton film model as described in §2.3 with a tetragonal space group. For the refinement, a fixed polynomial 1/(2θ) background was used to consider the higher background at small angles 2θ.

(2) The lattice and profile parameters of ZnO were refined on a pure ZnO sample [Fig. 1*a* (2)] with the structure proposed by Kihara & Donnay (1985) as well as a polynomial 1/(2θ) background.

(3) Dry ZnO samples covered with Kapton film [Fig. 1*a* (3)] were measured subsequently. The Kapton film model and the refined ZnO structure were inserted in the refinement routine and the scale factor of ZnO was refined. For the Kapton film model the same procedure as described in §2.3 was performed to refine the differences between the single-crystal sample carrier and the powder sample. This procedure allows the *hkl* phase to be adjusted without calculating fractions of the crystalline structure in the *hkl* phase. The background was kept fixed and is the same as in step 1.

(4) A ZnO–water mixture (w/s = 0.4) without Kapton film [Fig. 1*a* (4)] was used to model the free water according to §2.3

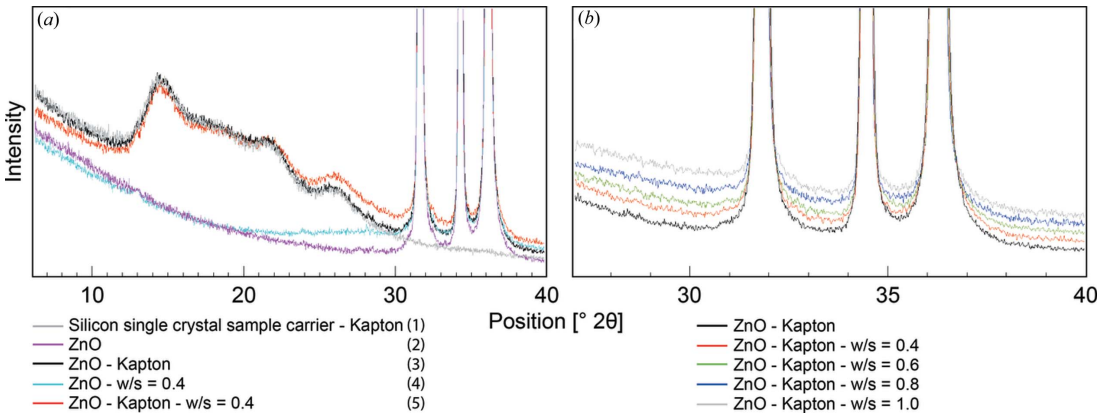

Figure 1
(*a*) XRD measurements used for modelling the Kapton film and free water. The lower intensity of the background at small angles 2θ with the addition of water (4), (5) compared to dry samples (2), (3) can be seen. (*b*) ZnO sample, dry and at different w/s ratios.

research papers

Table 3
ICSD structure data for the Rietveld refinement.

Phase	Author	ICSD-No.
Quartz	Le Page & Donnay (1976)	174
Anatase	Horn *et al.* (1972)	9854
Phengite	Ivaldi *et al.* (2001)	158072
Muscovite	Catti & Ferraris (1989)	68548
Mullite	Balzar & Ledbetter (1993)	74008
Hematite	Blake *et al.* (1966)	15840
Magnetite	Bragg (1915)	29129
Calcite	Sitepu *et al.* (2005)	158257
Dolomite	Reeder & Markgraf (1987)	40971

with a cubic space group. The background remained the same as refined in step 2. This leads to a small misalignment in between 6 and 12° 2θ, but allows a good refinement of the scattering contribution caused by the free water from 20 to 40° 2θ.

(5) Finally the ZnO–water mixture (w/s = 0.4) covered with Kapton film [Fig. 1*a* (5)] was measured and the refined structure of ZnO as well as of the Kapton film and the water model was inserted into the refinement procedure. The fitting mode of the water model was changed to the '*hkl*-file fit' and the scale factor was fixed. The scale factor of ZnO, a polynomial 1/(2θ) background and the Kapton film model according to §2.3 were refined.

The described procedure summarizes the instrumental background and the background caused by the Kapton film and ensures a stable refinement. It takes into account the requirements of the lowering background at small angles 2θ with the addition of water (Fig. 1*a*). The Kapton film model was changed to the '*hkl*-phase fit' mode and kept fixed for all following modelling, calibration and quantification procedures. Fig. 1(*b*) shows the XRD measurements of ZnO in dry conditions and with different w/s ratios. The scattering contribution caused by the free water continuously increases with the addition of water. The calibrations of free water of two ZnO–water mixtures (w/s = 0.4 and w/s = 1.0) were used to quantify the different ZnO–water mixtures. The calibration of free water of ZnO–water mixtures at w/s = 0.4 was used to quantify all MK/MM/FA/LS–water mixtures.

2.3.2. Modelling and calibration of the X-ray amorphous content. Since the limestone powder has no X-ray amorphous content, only the crystalline structures (Table 3) were adapted to a pure measurement covered with Kapton film. For the preparation of the models for MK, MM and FA the respective samples were measured as pure powder. The background was adjusted manually *via* base points and included the X-ray amorphous fraction of the sample. Subsequently the lattice and profile parameters of the crystalline structures were refined. The modelling of the X-ray amorphous fractions of the samples was performed on pure samples covered with Kapton film. Only the scale factor of the adapted crystalline phases and a polynomial 1/(2θ) background were refined. The Kapton film model was inserted into the refinement routine and was kept fixed. The procedure described in §2.3 was used for modelling.

Table 4
Unit-cell parameters of the *hkl* phases.

Phase	Space-group No.	*a* (Å)	*c* (Å)
Kapton film	123	9.72	26.53
Free water	202	8.46	–
FA	225	8.13	–
MK	123	1	499.95
MM	123	1	469.95

The calibrations of the *hkl* phases were performed with ZnO as internal standard. The space-group number and the lattice parameters for all *hkl* phases are summarized in Table 4.

2.3.3. Quantification of the water–solid mixtures. The scale factors of corresponding crystalline phases, the free water model and the 'metaphase' model (except of LS) were refined to quantify the systems investigated. Additionally, the sample displacement and a polynomial 1/(2θ) background were refined. The model of the Kapton film was added to the refinement routine and was kept fixed.

2.4. Thermogravimetric measurements

In order to validate the quantification of the free water in the *in situ* XRD measurements of the MK–CH powder–alkaline solution mixture, the quantity of free water was determined by TG according to equation (2) on samples stopped with acetone (Beuntner, 2017). The measurements were performed with Netzsch STA 449 F3 Jupiter with a sample quantity of 250 mg in Al_2O_3 crucibles and a heating rate of 2 K min^{-1}. For preparation, the sample was stirred manually for 60 s and then transferred into a calorimeter crucible. The sample was purged with nitrogen for 10 s and sealed airtight with a cap and paraffin film. The samples were stored in a conditioning cabinet at 298 K until they were stopped after either 6, 30 or 48 h. For stopping the sample, about 2 g of the sample were carefully ground with a hand mortar and added to 60 ml of acetone, and the mixture was shaken manually. After the powder had precipitated, the excess acetone was removed by suction. This process was repeated three times, and the last time the acetone was removed by suction after a waiting time of 30 min. The samples were then dried at 313 K in a conditioning cabinet for 16 h. Assuming that the free water was completely removed by acetone and that no other decomposition products but water were produced up to 823 K, the mass loss determined from the TG measurement (313–823 K) can be equated with the chemically bound water (w_{bound} [wt%]):

$$w_{free} = \left[\frac{m_{H2O}}{m_{total}} + \frac{m_{CH}}{m_{total}}\frac{M(H_2O)}{M(CH)}\right]100 - w_{bound}, \qquad (2)$$

where w_{free} is the amount of free water [wt%], m_{H2O} the weighed mass of water [g], m_{total} the total weighed mass (powder + water) [g], m_{CH} the weighed mass of CH powder [g], $M(H_2O)$ the molar mass of water [g mol^{-1}] and M(CH) the molar mass of CH [g mol^{-1}].

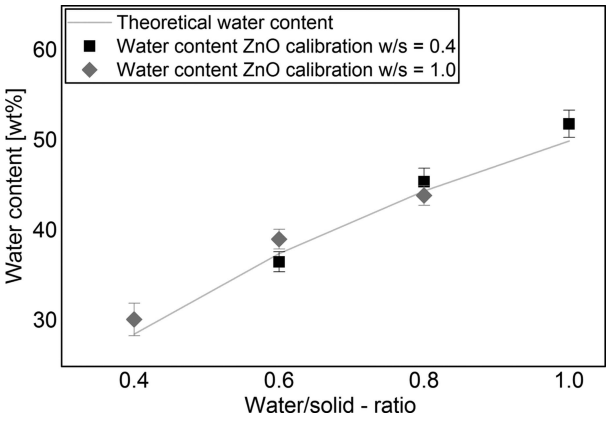

Figure 2
Quantification of the water content by XRD with different calibrations (w/s = 0.4 and w/s = 1.0).

2.5. Calorimetric measurement

Isothermal calorimetry was executed in order to study the relationship between the reaction kinetics of the hardening sample and the background caused by the free water from the *in situ* XRD measurement. The experiments were performed with a TA Instruments TAM Air for 50 h with the MK–CH powder–alkaline solution mixture. Analogously to the preparations in §2.4, the sample was stirred manually for 60 s and subsequently transferred into a calorimeter crucible. The measured heat flow was normalized to 1 g of the solid material.

3. Results and discussion

3.1. Calibration and quantification of ZnO–water mixtures

Fig. 2 shows the quantification of the ZnO–water mixtures with two different calibrations of the *hkl* phase of water. The absolute errors respecting the deviation from theoretically weighed water content are between 0.5 and 1.9 ± 1.8 wt%. The error tends to become larger the further the quantification deviates from the value of the calibration. For the ZnO–water mixtures, homogenization is impossible for w/s ratios lower than 0.4. For this reason, no measurement or calibration was done at w/s = 0.2.

3.2. Quantification of the water–solid mixtures

Fig. 3 shows the results of the XRD measurements of FA (Fig. 3*a*) and MK (Fig. 3*b*) in dry conditions and with different w/s ratios in the range from 27 to 40° 2θ. The contribution of LS and MM to the diffractogram when water is added is comparable to that of FA and MK, respectively. For FA and LS, the consistency of the water–solid mixtures already results in a homogeneous paste at a w/s ratio of 0.2 and the contribution to the diffractogram caused by the water increases continuously with increasing water content. A different picture can be seen for the phyllosilicates. Owing to the high water absorption capacity of the phyllosilicates, the samples are too dry and cannot be homogenized at a w/s of 0.2. Homogenization becomes possible starting with the w/s ratio of 0.4 and leads to earth-moist samples with reproducible diffractograms for MK and MM. The consistency of the mixtures hardly changes with further addition of water (w/s = 0.6; w/s = 0.8) and retains its earth-moist condition. The scattering contribution caused by water hardly increases. In the case of the phyllosilicates, the sample is a paste if the w/s exceeds approximately 1.0 and the X-ray amorphous contribution increases again.

There seems to be a dependency between the consistency of the sample and the X-ray scattering contribution caused by the free water. With further addition of water (w/s = 1.2) the water segregates on the sample surface and thus the contribution of the water significantly increases. This effect is particularly pronounced for MM and is shown in Fig. 4. With LS, the effect of a slight water bleeding can be observed already at a w/s of 0.8.

The results of water quantification of all water–solid mixtures are shown in Fig. 5. It can be observed that the described relationship between the consistency of the sample and the scattering contribution of free water has a direct

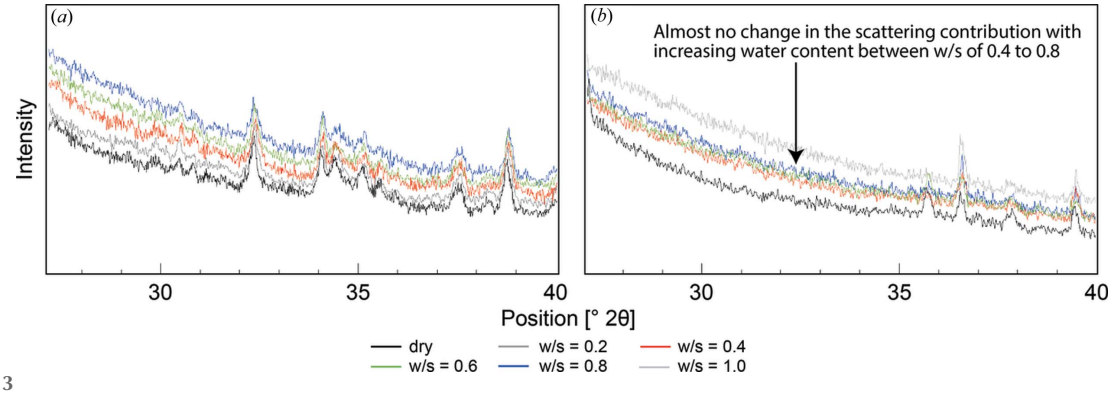

Figure 3
Diffractograms of FA (*a*) and MK (*b*) as dry powder and at different w/s ratios. While for FA the scattering contribution increases continuously with increasing water content, the scattering contribution of MK stagnates over a wide range of w/s ratios.

research papers

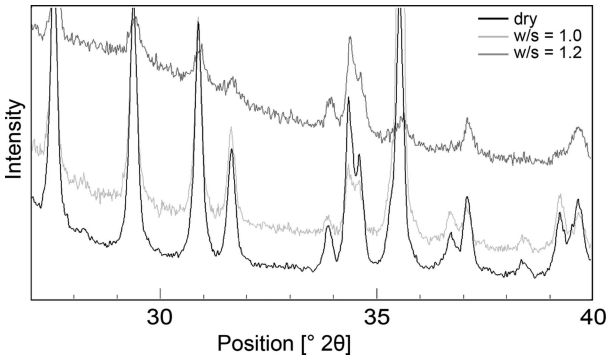

Figure 4
Diffractograms of MM. The addition of a proportionally small amount of water (from w/s = 1.0 to w/s = 1.2) leads to a strong segregation of water at the sample surface and allows no correlation of the scattering contribution to the real water amount in the sample.

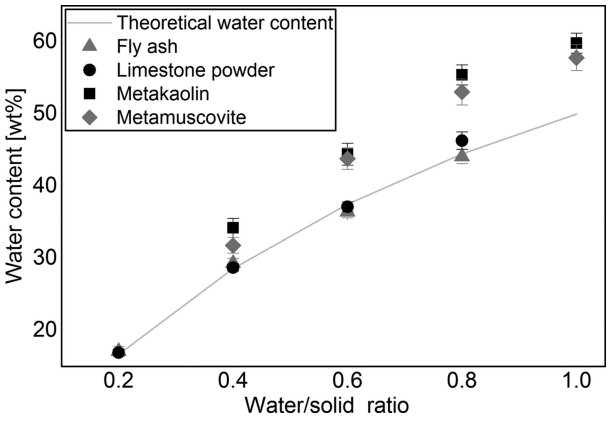

Figure 5
Quantification of the free water content by XRD with ZnO calibration at w/s = 0.4.

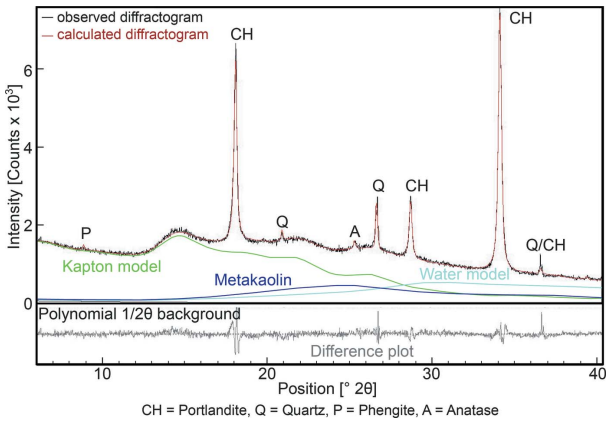

Figure 6
Rietveld refinement of MK–CH–alkaline solution mixture at w/s = 1.0 and 298 K at the beginning of *in situ* XRD measurement (first scan). The *hkl*-phase models used for the Rietveld refinement are shown.

influence on the quantification of the water content in the different systems. The quantifications of FA and LS yield good results and exhibit only a small error. This correlates with the continuous increase of the scattering contribution of free water with increasing water content. A slight water separation can be observed for the LS measurement with a w/s of 0.8, which results in a greater deviation of the quantification from the weighed value. A different picture emerges for the measurements of the temperature-treated phyllosilicates MK and MM. The constant scattering contribution over a wide range of water addition leads to large errors in the quantification. Overall, it seems as if the calibration of the water in the ZnO–water system does not match the measurements with phyllosilicates.

3.3. Quantification of free water content in *in situ* XRD measurements

Fig. 6 shows the diffractogram of the first scan of the *in situ* XRD measurement with the *hkl*-phase models used for refinement of the MK–CH–alkaline solution mixture. The accurate modelling of the instrumental background and the Kapton film with the Kapton model (fixed during refinement) as well as the metakaolin and free water (scale factors refined) allows a good fit and stable refinement over the 50 h of *in situ* XRD measurement. Owing to the overlapping of the scattering contributions of metakaolin and free water, it is important to refine the scaling factor of free water. Modelling the water as a constant background leads to increased errors in the quantification of other *hkl* phases.

The quantification of the free water content during *in situ* XRD is shown in Fig. 7. As described above, the calibration of the water in the ZnO–water system does not match the scattering contribution that the water provides in systems containing phyllosilicates. Consequently, the quantifications of the metakaolin mixtures show a high error (Fig. 5). To avoid the systematic error, the water content of the first scan of the *in situ* XRD measurements (Fig. 6) was calibrated to the

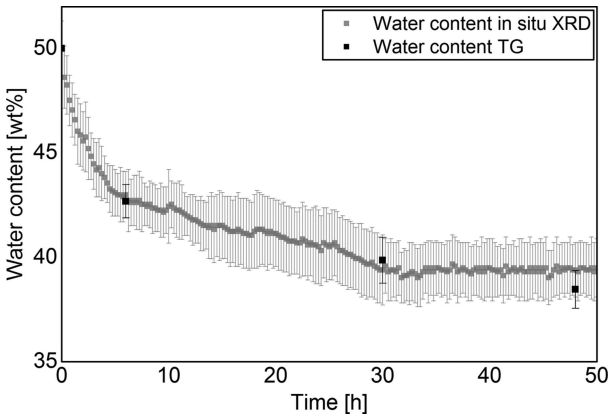

Figure 7
Free water quantification of *in situ* XRD measurement of MK–CH–alkaline solution mixture over 50 h (w/s = 1.0) and the TG quantification after 6, 30 and 48 h.

known content of 50 wt%, which yields very plausible results and a good correlation to the TG measurement after 6 and 30 h. Analogously to Zhang & Scherer (2011), carbonization effects were observed with the solvent exchange method. These effects, which are indicated by carbon dioxide release above 823 K, were neglected for the determination of chemically bound water, which is released at lower temperatures. Furthermore, no reaction products caused by acetone and other organic components were detected after drying the stopped sample. It is noticeable that from 30 h of hydration onwards the quantification of the water content based on *in situ* XRD remains at a constant level until the end of the measurement after 50 h. This leads to an increased deviation between the TG and the XRD quantification after 48 h.

Fig. 8 shows a level plot of the *in situ* XRD measurement from 31.4 to 31.8° 2θ in combination with the result of the accompanying calorimetric measurement. The small angular range was chosen because there is no overlapping of the background and the *hkl* phases with crystalline phases. The *in situ* measurements given in the upper part indicate with a constant colour that after about 30 h of hydration there is no further change in the background intensity. In this reduced system, the constancy of the background can be seen very clearly. In cementitious systems, this clarity is presumably lost because of the large number of reflections caused by the cement clinker phases. This point in time corresponds to the maximum of the main reaction of the calorimetric measurement. It allows the conclusion that, analogously to the phyllosilicate–water mixtures, a connection to the consistency of the sample can be drawn. While for phyllosilicate–water mixtures the scattering contribution of the water does not increase as long as the mixture has an earth-moist condition and the scattering contribution increases only at the transition to paste, the hydration reaction has an inverse effect. At the beginning of the measurement, the MK–CH–alkaline solution is a paste that stiffens as hydration progresses. Hesse *et al.* (2011) showed that the reaction behaviour changes from solution controlled to diffusion controlled at the heat flow maximum of the main reaction of the calorimetric measurement. This seems to be the point at which the paste is hardened to such an extent that its condition can be described as earth moist. As a result, the scattering contribution of free water does not change further and quantification remains at a constant level. This observation is also consistent with the results of a ^{1}H-TD-NMR study (Ectors *et al.*, 2016). The authors found a strong decrease of the relaxation time of the free water until the heat flow maximum of the main reaction, and subsequently only a slight change of the relaxation time occurs in the further progress of the reaction.

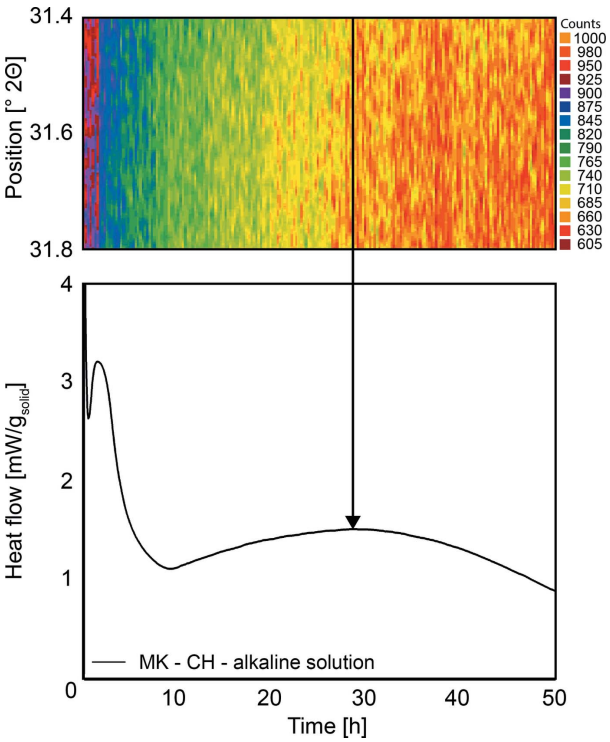

Figure 8
Comparison of the background of the *in situ* XRD measurement from 31.4 to 31.8° 2θ with the calorimetric measurement.

Owing to the correlation between the consistency of the sample and the scattering contribution of the free water, it can be assumed that, for *in situ* measurements with cement pastes, the water content can only be quantified up to the time of maximum heat flow of the main reaction. Analogously to the measurement in the MK–CH system, the consistency of the paste changes, and thus the reaction behaviour changes from solution controlled to diffusion controlled. It is assumed that, because of the progressive hydration process and the associated increase in surface area due to the resulting hydrate phases, the remaining free water on the surfaces is already coordinated in such a way that further hydration does not provide any additional change in the scattering contribution of free water.

Fig. 9 illustrates and describes the relationship between the consistency of the sample and the scattering contribution of free water. The change in the scattering contribution of the free water in both directions, the increase and the decrease of the free water, can be considered.

Besides the described dependence of the scattering contribution of the free water on the water content and the consistency of the sample, the stability of the paste over time plays a role. As long as the sample assumes an earth-moist condition (2 in Fig. 9) at low water contents, no effects are expected. However, as soon as the sample takes the consistency of a paste, sedimentation effects occur. This means that, in the case of unstable pastes, stage 4 in Fig. 9 can be passed through, resulting in segregated water on the surface (5 in Fig. 9) also at a constant water content because of sedimentation as a function of time. Owing to the missing temporal resolution of the XRD measurements, the effect of sedimentation cannot be methodically considered within one individual diffractogram (MK; MM; FA; LS) with different w/s ratios. The situation is different with *in situ* measurements over 48 h, where sedimentation effects can be methodically

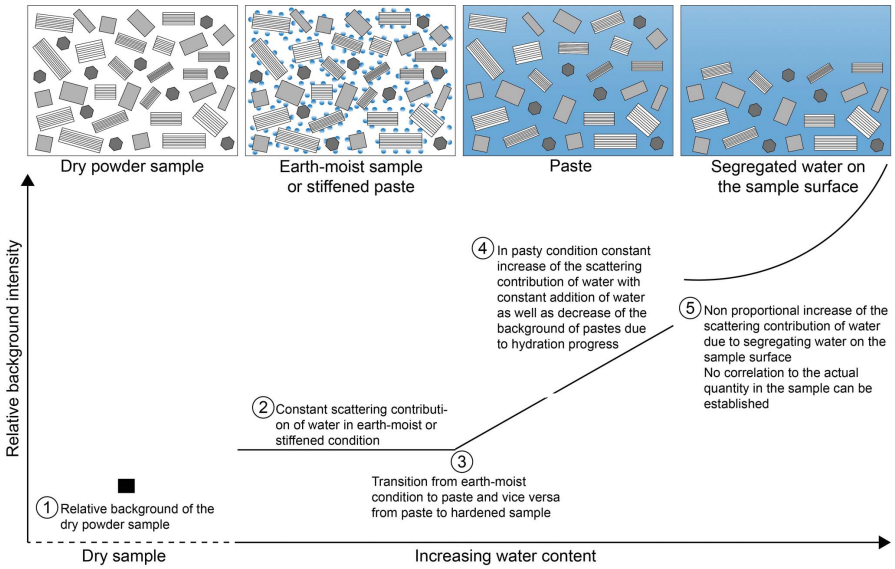

Figure 9
Illustration of the relationship of the scattering contribution of free water and the consistency of the sample. A quantification of the free water is just possible in part 4 of the illustration.

detected owing to slight peak shifts to smaller angles. Because of the parallel reaction and the resulting reaction products in hydrating systems, it is difficult to determine sedimentation. Furthermore, different authors (Winterwerp, 2002; Mietta *et al.*, 2009) describe 'hindered settling' for high concentrations of solid material and thus very low sedimentation velocities. Stoke's law therefore does not apply in this case. Thus, the expected influence of sedimentation can be classified as low and, within the scope of the accuracy of the method, negligible because of the multi-phase nature of cementitious systems and the overlapping of *hkl* phases. However, a water film on the surface of the sample below the Kapton foil as described by Hesse (2009) must be avoided at the beginning of the measurement. For investigations on suspensions with highly crystalline systems or lower particle concentrations, the influence of sedimentation on the scattering contribution of the free water in the diffractogram should be taken into account.

As the RILEM round robin (Durdziński, Ben Haha, Bernal *et al.*, 2017) on stopped samples shows, the reproducibility of the results in different laboratories can be regarded as difficult. The additional *hkl* phase of the water causes a further overlapping of an X-ray amorphous phase and thus its splitting is more complex. Standardized procedures for the adaptation of the background and the generation of the *hkl* phases are necessary.

4. Conclusion

Owing to the complex background caused by the addition of water, its adaptation is particularly important for correct quantification. The effect on both lowering of the background between 6 and 15° 2θ and the scattering contribution between 20 and 40° 2θ have to be taken into account. For the modelling of the Kapton film and the device-specific background, special attention should be paid to the small angular range and the modelling should be carried out in successive steps.

The free water should be calibrated directly on the phyllosilicate system to be investigated. A calibration on other systems as demonstrated by the example of ZnO–water mixtures leads to incorrect quantifications.

The quantification of free water with an *hkl* phase is limited as the scattering contribution depends on the consistency of the sample. It is therefore not the absolute content of free water that is decisive in how far the free water can be quantified. The quantifiable range can vary greatly from sample to sample. In the case of *in situ* XRD measurements of hydrating systems, the quantification of the free water is just possible until the maximum reaction rate of the main hydration.

References

Adu-Amankwah, S., Black, L., Skocek, J., Ben Haha, M. & Zajac, M. (2018). *Constr. Build. Mater.* **164**, 451–462.
Adu-Amankwah, S., Zajac, M., Stabler, C., Lothenbach, B. & Black, L. (2017). *Cem. Concr. Res.* **100**, 96–109.
Avet, F., Li, X. & Scrivener, K. (2018). *Cem. Concr. Res.* **106**, 40–48.
Balzar, D. & Ledbetter, H. (1993). *Am. Mineral.* **78**, 1192–1196.
Bergold, S. T., Goetz-Neunhoeffer, F. & Neubauer, J. (2013). *Cem. Concr. Res.* **53**, 119–126.
Beuntner, N. (2017). Dissertation thesis, Universität der Bundeswehr München, Neubiberg, Germany.
Beuntner, N. & Thienel, K.-C. (2016). *2nd International Conference on the Chemistry of Construction Materials (ICCCM 2016)*, edited by J. Plank, L. Lei & T. Echt, Vol. 50, pp. 157–160. Munich: Gesellschaft Deutscher Chemiker e.V.
Blake, R. L., Hessevick, R. E., Zoltai, T. & Finger, L. W. (1966). *Am. Mineral.* **51**, 123–129.

Bragg, W. H. (1915). *Nature*, **95**, 561.
Caglioti, G., Paoletti, A. & Ricci, F. P. (1958). *Nucl. Instrum.* **3**, 223–228.
Catti, M., Ferraris, G. & Ivaldi, G. (1989). *Eur. J. Mineral.* **1**, 625–632.
Creagh, D. C. & Hubbel, J. H. (2006). *International Tables for Crystallgraphy*, Vol. C *Mathematical, Physical and Chemical Tables*, edited by E. Prince, Table 4.2.4.3, 1st online ed. Chester: International Union of Crystallography.
Degen, T., Sadki, M., Bron, E., König, U. & Nénert, G. (2014). *Powder Diffr.* **29**, S13–S18.
DIN (2012*a*). *Baugrund, Versuche und Versuchsgeräte – Bestimmung des Wasseraufnahmevermögens*, DIN 18132, p. 14. Berlin: Beuth-Verlag.
DIN (2012*b*). *Flugasche für Beton – Teil 1: Definition, Anforderungen und Konformitätskriterien*, DIN EN 450-1. Berlin: Beuth-Verlag.
Dittrich, S., Neubauer, J. & Goetz-Neunhoeffer, F. (2014). *Cem. Concr. Res.* **56**, 129–138.
Durdziński, P. T., Ben Haha, M., Bernal, S. A., De Belie, N., Gruyaert, E., Lothenbach, B., Menéndez Méndez, E., Provis, J. L., Schöler, A., Stabler, C., Tan, Z., Villagrán Zaccardi, Y., Vollpracht, A., Winnefeld, F., Zając, M. & Scrivener, K. L. (2017). *Mater. Struct.* **50**, 135.
Durdziński, P. T., Ben Haha, M., Zajac, M. & Scrivener, K. L. (2017). *Cem. Concr. Res.* **99**, 172–182.
Ectors, D., Goetz-Neunhoeffer, F., Hergeth, W.-D., Dietrich, U. & Neubauer, J. (2016). *Cem. Concr. Res.* **79**, 366–372.
Hesse, C. (2009). Dissertation thesis, Friedrich-Alexander-Universität Erlangen-Nürnberg, Germany.
Hesse, C., Goetz-Neunhoeffer, F. & Neubauer, J. (2011). *Cem. Concr. Res.* **41**, 123–128.
Horn, M., Schwerdtfeger, C. F. & Meagher, E. P. (1972). *Z. Kristallogr.* **136**, 273–281.
Ivaldi, G., Ferraris, G., Curetti, N. & Compagnoni, R. (2001). *Eur. J. Mineral.* **13**, 1025–1034.
Jansen, D., Goetz-Neunhoeffer, F., Stabler, C. & Neubauer, J. (2011). *Cem. Concr. Res.* **41**, 602–608.
Khoshnazar, R., Beaudoin, J., Raki, L. & Alizadeh, R. (2013*a*). *Adv. Cem. Res.* **25**, 314–321.
Khoshnazar, R., Beaudoin, J., Raki, L. & Alizadeh, R. (2013*b*). *Adv. Cem. Res.* **25**, 322–331.
Kihara, K. & Donnay, G. (1985). *Can. Mineral.* **23**, 647–654.
Kletti, H., Isserstedt, A., Eckart, A., Wolf, B. & Ludwig, H.-M. (2015). *19. Internationale Baustofftagung Ibausil*, edited by H.-B. Fischer, C. Boden & M. Neugebauer, pp. 634–640. Weimar: F. A. Finger-Institut für Baustoffkunde.
Le Bail, A., Duroy, H. & Fourquet, J. L. (1988). *Mater. Res. Bull.* **23**, 447–452.
Le Page, Y. & Donnay, G. (1976). *Acta Cryst.* B**32**, 2456–2459.
Madsen, I. C., Scarlett, N. V. Y. & Kern, A. (2011). *Z. Kristallogr. Cryst. Mater.* **226**, 944–955.
Mietta, F., Chassagne, C., Manning, A. J. & Winterwerp, J. C. (2009). *Ocean. Dyn.* **59**, 751–763.
O'Connor, B. H. & Raven, M. D. (1988). *Powder Diffr.* **3**, 2–6.
Pawley, G. S. (1981). *J. Appl. Cryst.* **14**, 357–361.
Peng, Y. & Jacobsen, S. (2013). *Cem. Concr. Res.* **54**, 133–142.
Reeder, R. J. & Markgraf, S. A. (1987). *Am. Mineral.* **72**, 188–193.
Rietveld, H. M. (1967). *Acta Cryst.* **22**, 151–152.
Rietveld, H. M. (1969). Research Report RCN-104. Reactor Centrum Nederland.
Scarlett, N. V. Y. & Madsen, I. C. (2006). *Powder Diffr.* **21**, 278–284.
Scarlett, N. V. Y., Madsen, I. C., Cranswick, L. M. D., Lwin, T., Groleau, E., Stephenson, G., Aylmore, M. & Agron-Olshina, N. (2002). *J. Appl. Cryst.* **35**, 383–400.
Scherb, S., Beuntner, N. & Thienel, K.-C. (2018). *Proceedings of the 2nd International Conference on Calcined Clays for Sustainable Concrete*, edited by F. Martirena, A. Favier & K. Scrivener, pp. 427–433. La Havanna: Springer Nature.
Schöler, A., Lothenbach, B., Winnefeld, F. & Zajac, M. (2015). *Cem. Concr. Compos.* **55**, 374–382.
Sitepu, H., O'Connor, B. H. & Li, D. (2005). *J. Appl. Cryst.* **38**, 158–167.
Snellings, R., Salze, A. & Scrivener, K. L. (2014). *Cem. Concr. Res.* **64**, 89–98.
Stetsko, Y. P., Shanahan, N., Deford, H. & Zayed, A. (2017). *J. Appl. Cryst.* **50**, 498–507.
Wheeler, J. (1966). *Nature*, **212**, 1035–1036.
Wheeler, J. & Chatterji, S. (1972). *J. Am. Ceram. Soc.* **55**, 461–464.
Winterwerp, J. C. (2002). *Continental Shelf Res.* **22**, 1339–1360.
Zhang, J. & Scherer, G. W. (2011). *Cem. Concr. Res.* **41**, 1024–1036.
Zhang, L. & Glasser, F. P. (2000). *Adv. Cem. Res.* **12**, 79–88.

8.2 Reactivity of Metakaolin in Alkaline Environment: Correlation of Results from Dissolution Experiments with XRD Quantifications

Reprint
Published in the Journal “Materials”
Vol. 13-102214 (2020); doi: 10.3390/ma13102214

Authors: S. Scherb, M. Köberl, N. Beuntner, K.-Ch. Thienel and J. Neubauer

materials

MDPI

Article

Reactivity of Metakaolin in Alkaline Environment: Correlation of Results from Dissolution Experiments with XRD Quantifications

Sebastian Scherb [1,*], Mathias Köberl [1], Nancy Beuntner [1], Karl-Christian Thienel [1] and Jürgen Neubauer [2]

[1] Civil Engineering and Environmental Science, Universität der Bundeswehr München, Werner-Heisenberg-Weg 39, 85579 Neubiberg, Germany; mathias.koeberl@unibw.de (M.K.); nancy.beuntner@unibw.de (N.B.); christian.thienel@unibw.de (K.-C.T.)

[2] GeoZentrum Nordbayern, Mineralogy, Friedrich-Alexander Universitaet Erlangen-Nuernberg, Schlossgarten 5a, 91054 Erlangen, Germany; juergen.neubauer@fau.de

* Correspondence: sebastian.scherb@unibw.de

Received: 15 April 2020; Accepted: 11 May 2020; Published: 12 May 2020

check for updates

Abstract: Systematic investigation of filtrates and filter residues resulting from a 24 h treatment of metakaolin in different alkaline solutions were performed. On filtered metakaolin particles, inductively coupled plasma-optical emission spectrometry (ICP-OES) measurements reveal an enrichment of iron and titanium, which suggests an inhomogeneous distribution of these cations. Since the SiO_2/Al_2O_3 ratio remains constant in all filter residues examined, the dissolution of the Si and Al monomers is congruent. Structural differences, identified by attenuated total reflection–Fourier transform infrared spectroscopy (ATR-FTIR) as a consequence of alkali uptake, influence the X-ray scattering contribution of metakaolin, and thus quantifications with the partial or no known crystal structure (PONKCS) method. This leads to deviations between the degree of reaction calculated from Si and Al solubility from filtrate and that quantified by quantitative powder X-ray diffraction (QPXRD) using the filter residue. Nevertheless, the described changes do not cause a shift in the X-ray amorphous hump in case of congruent dissolution, and thus allow the quantification of the metakaolin before and after dissolution with the same hkl-phase model.

Keywords: metakaolin; degree of reaction; PONKCS; calcined clay; supplementary cementitious material; alkaline solution

1. Introduction

In recent years, the pozzolanic reactivity of calcined clays has increasingly moved into the focus of research. Their use as a supplementary cementitious material (SCM) could be a component to achieve the goal of more ecological concretes, since the replacement of cement by SCM offers one of the greatest opportunities to reduce CO_2 emission in the production of concrete. The assessment of pozzolanic reactivity plays a crucial role in determining the possible degree of replacing cement with SCM and is directly linked to concrete strength and durability properties [1–6]. Different SCMs intervene variably in cement hydration by means of physical and chemical parameters and mechanisms [7,8]. Various scientists were investigating the question of a test method suitable for assessing the pozzolanic reactivity of different SCM directly from the respective SCM [9–18]. Another approach is the determination of the reaction degree of SCM in cementitious systems [19–30]. Different parameters such as the reactive silica content, the CaO or $Ca(OH)_2$ consumption, the relative strength index or the content of soluble silicon (Si) and aluminum (Al) ions in alkaline solution are common to assess the pozzolanic reactivity. Different wet chemical, analytical and empirical methods such

as thermogravimetric analysis, isothermal calorimetry, quantitative X-ray diffraction (QXRD) or compressive strength are used for the different approaches.

For calcined clays, which, in addition to silicon, can provide a considerable amount of reactive aluminum, comparison of the test methods revealed a considerable variation in the suitability of individual methods, even if they work very well in some other cases, e.g., for fly ash or slag [13,23,31–34].

The quantification of X-ray amorphous SCM with the partial or no known crystal structure (PONKCS) method [35] is a powerful tool to determine the SCM content in blended cements [36,37]. Quantification of SCM in hydrating systems is a challenging task due to strong overlap of the broad SCM peaks with X-ray amorphous hydrates and the free, not chemically bound, water [36,38]. The latest research confirms the possibility of quantifying the reacted SCM during in situ XRD measurements of hydrating systems [28]. Others show that the calculation of the degree of reaction can lead to major deviations resulting from error propagation. This depends largely on the substitution rate of the SCM and the degree of reaction [23,26,36].

Due to the high temperatures (1100–1700 °C) and fast cooling involved in the formation of fly ash, a large proportion of the particles are vitreous. The calcination of clays takes place at significantly lower temperatures (600–900 °C). Even if crystalline clay minerals are transformed into X-ray amorphous "metaphases", their habitus and layer structure remain intact (pseudomorphosis). According to Brindley and Nakahira [39], a pseudohexagonal skeleton of [SiO_4]-tetrahedra in the metakaolin is preserved at calcination temperatures of 600 °C. Massiot et al. [40] describe effects observed with nuclear magnetic resonance (NMR) between 450 and 850 °C as a newly formed silicon network without structural long-range order. In contrast to fly ash, in which the silicon release takes place via a solution process of the vitreous particles in alkaline environment [41], the mechanism of ion release of calcined clays is not finally investigated. Granizo et al. [42] describe the leaching kinetics of metakaolin in 5 and 8 M NaOH solution as a three-stage process. According to their hypothesis, the dissolution process is initially incongruent for a short time, followed by a longer period of congruent dissolution behavior and, finally, incongruent again. Garg and Skibsted [43] show that crystallographic defects accelerate dissolution in alkaline solution during the first hours, followed by a period where the rate of reaction is constant. They conclude that the dissolution process of metakaolin calcined at 500 °C is congruent and becomes increasingly incongruent with increasing calcination temperature. An incongruent dissolution process of metakaolin could lead to changes in the contribution of metakaolin to the diffractogram and thus falsify the quantifications with the PONKCS method. This is the starting point of this study, which intends to provide an insight into the following questions: Is there a correlation between the amount of Si- and Al-ions in alkaline solution derived from dissolution tests and the quantification of the metakaolin with the PONKCS method? How does the dissolution process of metakaolin affect its X-ray amorphous hump in the diffractogram? Although the reactivity of metakaolin has been described in numerous publications [14,15,17,27] and its content has already been quantified [26,28,36], the previous questions raised have not yet been considered. Therefore, the method of Kaps and Buchwald [11,12] is used to determine the pozzolanic reactivity of metakaolin on the basis of the solubility of Si- and Al-monomers in alkaline solution. A systematic investigation of the filter residue should provide information about the processes taking place during ion release, the impact on the metakaolin and correlations between the ions dissolved and the quantity evaluated with the PONKCS method for the first time. The contribution of this work shows the possibilities and limitations of the established methods. A better understanding contributes directly to improving the quantification with the PONKCS method and the assessment of the results obtained. Thus, the present study contributes to the evaluation of the suitability of calcined clays as SCM.

2. Materials and Methods

2.1. Materials and Test Program

The investigation deals with the solubility behavior of metakaolin (MK) in deionized water and various alkaline solutions. The flash calcined metakaolin is commercially available and was ready for use. The chemical composition was determined by inductively coupled plasma-optical emission spectrometry (ICP-OES) and the mineralogical composition by quantitative powder X-ray diffraction (QPXRD) with 20 wt.% ZnO as an internal standard to determine the X-ray amorphous content (Table 1). The data have already been published by the authors in [38,44].

Table 1. Chemical composition, loss on ignition (LOI) and mineralogical composition of metakaolin (MK) [38,44].

Oxides (wt.%)	MK	Phases (wt.%)	MK
SiO_2	54.5	Quartz	5.0
Al_2O_3	40.2	Anatase	0.6
Fe_2O_3	1.8	Phengite	1.4
CaO	<0.1	X-ray amorphous	93.0
MgO	0.2		
SO_3	<0.1		
Na_2O	0.3		
K_2O	0.3		
TiO_2	1.4		
LOI	1.3		

For the experiments, 5 g MK was shaken in 400 mL solution for 24 h on a vibrating unit. The solutions used were deionized water (H_2O; pH = 5.8) as reference, 10 wt.% sodium hydroxide solution (NaOH; pH = 13,2), 10 wt.% potassium hydroxide solution (KOH; pH = 14.1) and a model pore solution of 100 mmol/L NaOH and 500 mmol/L KOH (MOH; pH = 13.5). The pH of the suspensions was measured after 5 min, 30 min, 6 h, and 24 h. The measurements of the pH were carried out with the digital pH meter WTWmulti 3430 with SenTix 940-3 pH-electrode (WTW, Weilheim, Germany). Two independent preparations were applied for each solution. Subsequently, the samples were filtered through a suction filter with depression. Both the filtrate and the filter residue were used for further analysis. The filter residue was first kept in the filter and washed with distilled water until the measured pH value of the water leaking from the filter was less than 8. This procedure was necessary to prevent the hydroxide solutions from adhering to the particle surfaces and falsifying further analyses of the filter residue. Finally, the filter residue was dried over night at 60 °C in a warming cabinet and carefully crushed in an agate hand mortar the next day. The differences between drying a sample without prior washing and drying a washed sample are shown in Figure 1. Analogous to other studies [45,46], the carbonization of NaOH can be clearly identified.

In addition to weighing the filter residue, following methods were used to analyze the sample:

1. Quantitative Powder X-Ray Diffraction (QPXRD);
2. Scanning Electron Microscopy/Energy Dispersive X-ray analysis (SEM/EDX);
3. Element analysis by Inductively Coupled Plasma Optical Emission Spectrometry (ICP-OES);
4. Attenuated Total Reflection–Fourier Transform Infrared spectroscopy (ATR-FTIR).

The filtrate was acidified with concentrated HCl to a pH of 1 and filled up to 500 mL in a volumetric flask with distilled water, ready for ICP-OES analysis. A schematic summary of the experimental program is shown in Figure 2.

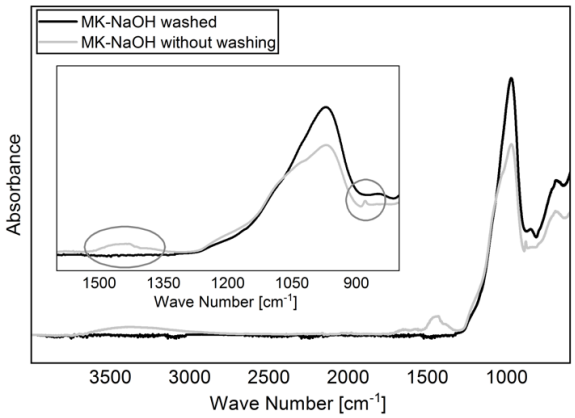

Figure 1. FTIR spectra of dried MK-NaOH after and without prior washing the sample. The carbonization of adhered NaOH to the particle surfaces can be avoided by washing the sample.

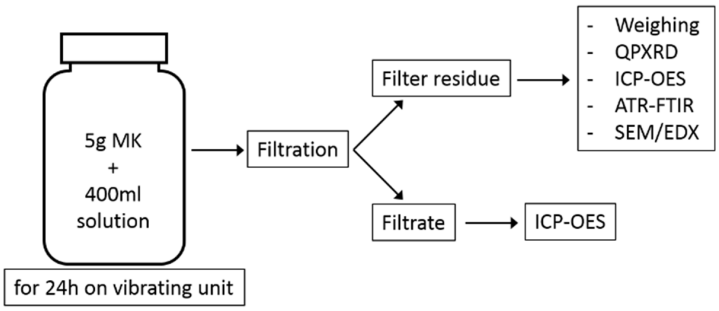

Figure 2. Schematic illustration of the test program.

2.2. QPXRD

XRD measurements were performed with a PANalytical Empyrean diffractometer equipped with a primary Bragg-Brentano^{HD} monochromator and a PIXcel^{1D} linear detector (Malvern Panalytical, Malvern, UK). A diffractogram was taken from 4° to 42° 2Θ in continuous scan mode with a step size of 0.013 and a counting time of 25.5 s per step at 40 kV and 40 mA with CuKα radiation. Measurements were analyzed with the software HighScore 4.7. The sample was prepared with a back-loading tool and covered with a Kapton film (DuPont, Wilmington, DE, USA). The use of the Kapton film allows to summarize the instrumental background and the background caused by the Kapton film and ensures a stable refinement [38]. The quantifications were performed combining external standard [47,48] and PONKCS method [35,49]. Table 2 shows the structures used for Rietveld refinement of the crystalline components of the sample.

Table 2. Inorganic Crystal Structure Database (ICSD) structure data for the Rietveld refinement.

Phase	Author	ICSD-No.
Quartz	Le Page and Donnay [50]	174
Anatase	Horn, et al. [51]	9854
Phengite	Ivaldi, et al. [52]	158072

The calibrations for quantitative analysis of the hkl-phases were performed with ZnO as internal standard. The procedure for creating the hkl-phases, their calibration, as well as the refinement parameters, are described in detail in [38].

2.3. SEM/EDX

For the SEM/EDX analyses, the dried samples were embedded in epoxy resin, ground and polished with isopropanol after hardening, and finally coated with carbon. Since the habitus of the particles is not easily recognizable on embedded samples, a second set of samples was prepared by scattering the powder on two-component adhesives, followed by coating with gold.

The analyses were performed on a Zeiss Evo LS 15 (Zeiss, Oberkochen, Germany) equipped with an Oxford X-Max^N 50 EDX detector (Oxford Instruments, High Wycombe, UK) at 20 kV and a working distance of 8.5 mm. The EDX analyses were measured against a kaolinite standard (Processing Plant, Bugle, Cornwall, UK from Micro-Analysis Consultants Ltd.) of known composition. Each EDX spectrum was collected for 100 live seconds of accumulated count duration. In the EDX analyses, special attention was paid to the metakaolin particles and areas were selected for analysis in which no crystalline phases could be detected on the surface. Thus, the EDX analyses represent the chemical composition of the X-ray amorphous part of the sample (MK_{Am}).

2.4. ICP-OES

The filter residue had to be solved for ICP-OES analysis in nitric acid after melt fusion using lithium metaborate. For this purpose, 0.4 g of the sample was weighed with 1.6 g lithium metaborate and melted at 950 °C in a platinum crucible in a muffle furnace. In the next step, the melted sample was quenched in 200 mL concentrated nitric acid (65 wt.% HNO_3) and dissolved in an ultrasonic bath. Finally, the solution was filled up to 500 mL in a volumetric flask with distilled water.

The ICP-OES measurements were performed with a Varian 720 ES spectrometer (Agilent Technologies, Santa Clara, CA, USA) and evaluated with the software 1.1 supplied with the instrument. The measuring range for the respective element was adapted using a multi-point calibration with an external standard. The measurements and their evaluation were conducted according to [53]. The chemical composition of the X-ray amorphous content (MK_{Am}) was calculated from the total analysis of the MK. The fractions of quartz (SiO_2) and anatase (TiO_2) determined by QPXRD were subtracted from the oxidic composition. For phengite, the individual oxidic components were calculated using an idealized phengite formula ($KAl_{1.5}Fe_{0.5}(Al_{0.5}Si_{3.5}O_{10})(OH)_2$) and subtracted from the total analysis. Finally, the calculated oxides were normalized to 100%. This method provides comparable results to the EDX analysis and was used to cross check the EDX measurements. The deviation of the ICP results from the EDX analyses is ±1 wt.% for the main elements (>10 wt.%) and ±0.5 wt.% for the secondary elements (<10 wt.%).

2.5. ATR-FTIR

The ATR-FTIR analyses were performed on a ThermoFisher Scientific Nicolet iS10 FTIR spectrometer equipped with an EverGlo TM MIR radiation source (λ = 15,798 cm^{-1}) and dTGS detector (Waltham, MA, USA). The spectra were measured in the wavenumber range from 400–4000 cm^{-1} with diamond as ATR crystal, collecting a series of 16 scans at a resolution of 4 cm^{-1}. The evaluation of the data was carried out with Omnic 9.3 (ThermoFisher Scientific, Waltham, MA, USA).

2.6. Calculation of the Degree of Reaction

The degree of reaction was calculated with different approaches using the results from weighing the filter residue,

$$R_{weight}[\%] = \left[1 - \frac{m_{filter} - m_{cry}}{m_{MKAm}}\right] \times 100 \quad (1)$$

the XRD quantification of the quartz,

$$R_{Quartz}[\%] = \left[1 - \frac{m_{Quartz} \times \frac{100}{c_{Quartz}} - m_{cry}}{m_{MKAm}}\right] \times 100 \quad (2)$$

the amorphous content (MK_{Am}) and

$$R_{MKAm}[\%] = \left[1 - \frac{m_{cry} \times \frac{100}{(100-c_{MKAm})} - m_{cry}}{m_{MKAm}}\right] \times 100 \quad (3)$$

from Si- and Al-solubility ($R_{Si/Al}$ [%]).

The calculation of the degree of reaction from weighing the filter residue (m_{filter} [g]) (Equation (1)) is based on the assumption that the absolute amount of crystalline phases of the sample remains constant and does not dissolve during shaking. The mineralogical composition was used to calculate the absolute mass of the crystalline phases (m_{cry} = 0.35 g) and the weight of the MK_{Am} (m_{MKAm} = 4.65 g) in 5 g of the sample.

The calculations from the QPXRD results are also based on the assumption that the crystalline phases do not dissolve during the experiment. For the calculation of the reaction degree from the quartz content (Equation (2)), the absolute mass of quartz (m_{Quartz} = 0.25 g) in 5 g sample was used. The degree of reaction can be calculated directly from its quantification (c_{Quartz}). For the calculation of the degree of reaction from the quantification of MK_{Am} (c_{MKAm}) (Equation (3)), the total crystalline content of the sample (100 - c_{MKAm}) was taken into account.

The degree of reaction from the ion solubility ($R_{Si/Al}$) is calculated from the quotient of the sum of the dissolved Si- and Al-ions and the initial content of Si and Al in MK_{Am}. The chemical composition of the ICP-OES analysis was used to calculate the initial content of Si and Al in MK_{AM} (2.3 g).

3. Results

3.1. Time Dependent pH Values of the Suspensions

Table 3 shows the time-dependent pH-values of the suspension. There are almost no measurable changes during the observation period. Previous investigations show that the measurement of pH values at very high concentrations with a glass electrode is faulty and is underdetermined due to the alkali error [54]. This effect occurs mainly with NaOH. Due to the logarithmic nature of the pH scale, even significant changes in concentration at very high concentrations cause only a slight change in the pH value. Accordingly, no conclusions can be drawn at this point from the results of the pH measurements at such high concentrations of KOH and NaOH.

Table 3. Time dependent pH-values of the different MK suspensions.

	MK-H_2O	**MK-MOH**	**MK-KOH**	**MK-NaOH**
pH after 5 min	5.8	13.5	14.1	13.1
pH after 30 min	6.0	13.5	14.0	13.0
pH after 6 h	6.0	13.4	14.0	12.9
pH after 24 h	6.2	13.5	14.1	13.1

3.2. Weighing the Filter Residue

Table 4 lists the masses of the filter residues determined after 24 h of dissolution, filtration, washing and drying. The given error was determined from the deviation of the mean value of the two individual determinations. As expected, the difference to the initial weight (5 g) is small for MK stored in distilled water. In contrast, the weight loss with the various alkaline solutions is very clear, with MK-NaOH showing by far the highest one, with approximately 3 g. A conventional presentation of the results in wt.% falsifies the results due to the presence of crystalline phases in the sample, which might not dissolve.

Table 4. Results of weighing the filter residue after dissolution of 5 g MK in different solutions in g.

MK-H_2O	MK-MOH	MK-KOH	MK-NaOH
4.93 ± 0.05	4.27 ± 0.10	3.75 ± 0.10	2.04 ± 0.20

3.3. QPXRD

Figure 3 shows the diffractograms of the filter residues. For the sake of a clearer overview, the MK-MOH measurement is not given. The intensity is expressed as a square root of the counts and the peaks of the crystalline phases are partially cut off. This emphasizes the changes in the X-ray amorphous hump. The diffractograms MK and MK-H_2O are almost congruent. Thus, no structural change can be detected when the sample (MK) is treated with distilled water (MK-H_2O). With MK-KOH, a slight decrease in the X-ray amorphous hump and a slightly higher maximum intensity of the peaks in the crystalline phases can be observed. This trend becomes more pronounced with MK-NaOH and leads to clearly discernible differences between MK and MK-NaOH. The increase in the intensity of the peaks of the crystalline phases is clearly visible at the (011)-reflex of the quartz, which is highlighted in the enlarged insert displaying a range from 26–27° 2Θ (Figure 3).

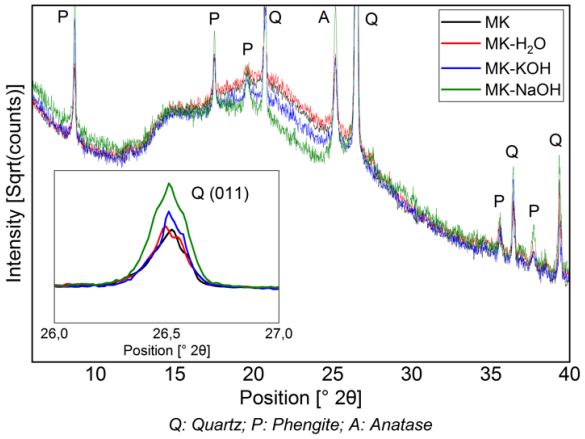

Figure 3. Diffractogram (CuKα) of MK compared to those of insoluble residues of MK treated with different solutions. The decrease in the X-ray amorphous hump and the enrichment of crystalline phases (quartz peak (011) is highlighted in the enlarged range between 26–27° 2Θ) can be seen.

Table 5 summarizes the results of the XRD quantifications. An enrichment of all crystalline phases and a decrease in MK_{Am} from MK-MOH via MK-KOH to MK-NaOH can be observed.

Table 5. Results of QPXRD in wt%. The absolute error is ±0.5 wt.% for the crystalline phases and ±1 wt.% for MK_{AM}.

Phase	MK	MK-H_2O	MK-MOH	MK-KOH	MK-NaOH
Quartz	5.0	5.2	5.6	6.3	12.0
Anatase	0.6	0.6	0.6	0.8	1.1
Phengite	1.4	1.5	1.7	2.1	3.1
MK_{Am}	93.0	92.8	92.1	90.8	83.4

3.4. Chemical Analysis

Table 6 shows the ion content of main elements in the filtrates obtained after the reaction of different solutions with MK. Distilled water treatment (MK-H_2O) results in a low ion content for Si and Al. Here, the values for Fe and Ti are below the detection limit. The dissolved ion content increases

with increasing alkali metal ion content of the alkaline solutions. It is noticeable that the content of Fe and Ti remains very low and changes only slightly with increasing pH, while Si- and Al-ion contents rise drastically.

Table 6. Ion content [mg] of the filtrate measured with ICP-OES (after the experiment of 5 g sample in 400 mL solution).

Elements	MK-H_2O	MK-MOH	MK-KOH	MK-NaOH
Si	24	211	353	866
Al	19	191	341	828
Fe	- *	7	9	15
Ti	- *	3	5	8

* Detection limit is 0.5 mg.

Table 7 gives the results of the ICP-OES analyses of the filter residues. Since the values from the EDX analyses (Section 2.3) show only a small deviation from the ICP-OES results after correction of the crystalline phase content (Section 2.4), they are not shown additionally in the main text. The EDX results are available as supplementary Table S1. Overall, it can be stated that both the SiO_2 and the Al_2O_3 content of MK_{Am} and $MK_{Am\text{-}H2O}$ decreases via $MK_{Am\text{-}MOH}$, $MK_{Am\text{-}KOH}$ and $MK_{Am\text{-}NaOH}$. The values for $MK_{Am\text{-}MOH}$ and $MK_{Am\text{-}KOH}$ are in a similar range, while $MK_{Am\text{-}NaOH}$ shows a further and more pronounced decrease. This correlates with the increasing Si- and Al-ion solubility (Table 6). For Fe_2O_3 and TiO_2, where hardly any ion solubility can be measured (Table 6), the trend is opposite and an enrichment takes place. Furthermore, an uptake of alkalis can be detected, corresponding to the alkalinity of the solution used.

Table 7. Chemical composition [wt.%] of MK_{Am} left after dissolution with different solvents of all samples measured with ICP-OES and the molar ratio of SiO_2/Al_2O_3 and $SiO_2/(Al_2O_3 + Fe_2O_3 + TiO_2 + Na_2O + K_2O)$.

Oxides	MK_{Am}	$MK_{Am\text{-}H2O}$	$MK_{Am\text{-}MOH}$	$MK_{Am\text{-}KOH}$	$MK_{Am\text{-}NaOH}$
SiO_2	53.2	52.8	51.4	51.2	49.5
Al_2O_3	43.7	43.6	42.3	42.2	40.0
CaO	0.1	0.1	0.1	0.1	0.1
Fe_2O_3	1.5	1.8	2.1	2.1	3.1
K_2O	0.0	0.0	2.0	2.7	0.0
MgO	0.2	0.3	0.2	0.1	0.2
Na_2O	0.3	0.4	0.5	0.1	5.1
TiO_2	0.9	0.9	1.5	1.4	2.0
SiO_2/Al_2O_3	2.07	2.05	2.06	2.06	2.10
*	1.95	1.92	1.80	1.79	1.59

* $SiO_2/(Al_2O_3 + Fe_2O_3 + TiO_2 + Na_2O + K_2O)$

3.5. ATR-FTIR

The FTIR spectra of MK and residues analyzed are shown in Figure 4. As reported elsewhere [45,55,56], a broadened band is visible in the region of Si-O vibration (900–1200 cm^{-1}), owing to amorphization of the crystalline kaolinite structure. Special attention will be paid to this band (zoomed region in Figure 4 from 850 to 1300 cm^{-1}). As expected, MK and MK-H_2O behave similarly, and no differences can be found within the range of reproducibility of the measurements. With MK-MOH and MK-KOH, a slight shift in the band to smaller wave numbers and a broadening of the peak can be observed. MK-NaOH leads to a clear shift in the band to smaller wave numbers. Table 8 summarizes the determined wave numbers and the corresponding full width at half maximum (FWHM).

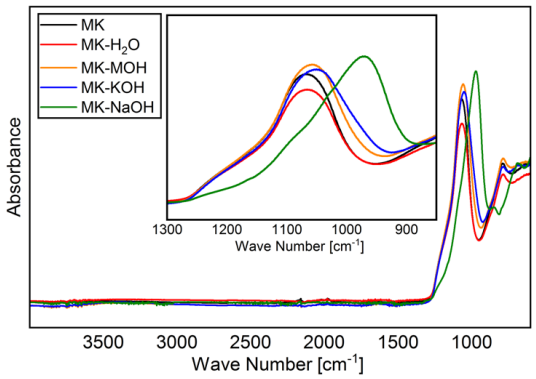

Figure 4. FTIR spectra of all samples analyzed.

Table 8. Summary of the determined wavenumbers and FWHM of the broadened Si-O band.

Sample	Wavenumber [cm^{-1}]	FWHM [cm^{-1}]
MK	1068 ± 3	173 ± 3
MK-H_2O	1066 ± 3	178 ± 3
MK-MOH	1058 ± 3	194 ± 5
MK-KOH	1051 ± 3	198 ± 5
MK-NaOH	982 ± 10	226 ± 5

3.6. SEM Images

Figure 5 A-D display the SEM images of the gold coated samples. Owing to the similarity of MK-MOH and MK-KOH, only MK-KOH is shown. There are no optical differences visible between MK and MK-H_2O. The treatment in distilled water has no effect on the shape, size and habitus of the metakaolin particles. Differences are also very small in comparison to MK-KOH. On closer inspection, a reduction in particle size caused by the dissolution process can be implied. Clear differences become obvious for MK-NaOH. Here, an alteration of the metakaolin particles takes place. The dissolution process has progressed so far that the mean particle size decreases and the morphology of many particles has changed significantly.

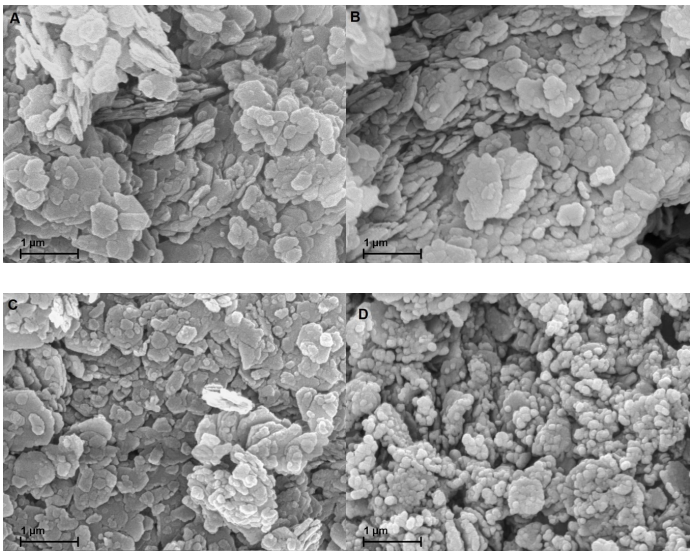

Figure 5. SEM images of the samples coated with gold of (**A**) MK; (**B**) MK-H_2O; (**C**) MK-KOH; (**D**) MK-NaOH.

3.7. Calculations of the Degree of Reaction

Figure 6 displays the results of the calculations of the degree of reaction based on the weighing of the filter residue (Table 4), the QPXRD (Table 5) and the Si/Al-solubility (Table 6). The calculation of the degree of reaction of R_{weight} (Equation (1), Section 2.6) considers the crystalline phases in comparison to the weighing of the filter residue (Table 4). The differences in mass are related exclusively to the X-ray amorphous fraction and thus reflect the mass loss in percent. Since errors in the quantification of one phase do not affect the quantification of another phase when calculating the phase contents following the G-factor method [48,57], the degree of reaction was determined from both the quantification of the quartz and of the MK_{Am}. An increase in the degree of reaction from MK-MOH via MK-KOH to MK-NaOH can be observed. In all systems, the degree of reaction calculated from the Si/Al-solubility is the highest, while the degrees of reaction calculated from XRD quantifications are the lowest. For the calculation of the degree of reaction from the results of the XRD quantifications (R_{Quartz} and R_{MKAM}) a large error in the degrees of reaction occurs. This effect is particularly pronounced with MK-MOH and MK-KOH due to higher error propagation at lower reaction rates. Thus, for MK-NaOH the error in the degree of reaction is significantly lower. This is in line with observations in the literature, which also find a large error in the degree of reaction calculated from XRD quantifications for low reaction rates or low SCM contents [26,36]. Another reason for the large errors in the degree of reaction calculated from the XRD quantifications results from the experimental setup, as the degree of reaction does not reflect the decrease in MK_{AM} in the sample. A degree of reaction of 12.3% (MK-MOH) only leads to a difference in MK_{AM} of 0.9 wt.% and thus to large errors in the calculated degree of reaction based on XRD quantifications of MK_{AM} with an accuracy of ±1 wt.%. Due to the strong error propagation from the XRD quantifications, the data obtained must be interpreted with caution. This is also known from the calculation of the degree of reaction with results of other test methods which exhibit small deviations of the determined contents. Scrivener et al. [58] report, for instance, a possible relative error of ±50%, when calculating the degree of reaction from the CH consumption determined by TG. The absolute differences in the degree of reaction (ΔR) increase with increasing degree of reaction, while the relative differences ($\Delta R/R_{max}$) decrease (Table 9).

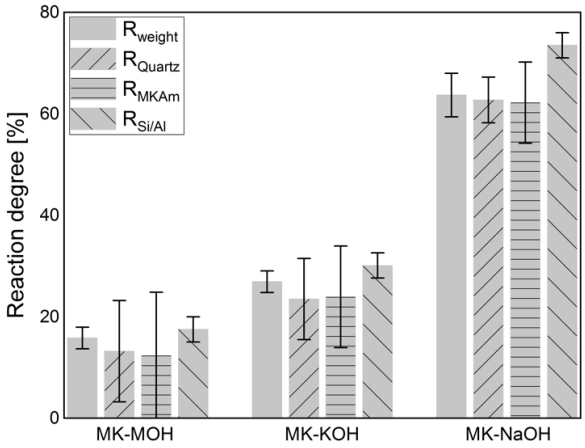

Figure 6. Degree of reaction calculated according to different approaches (Section 2.6).

Table 9. Summary of the minimal (R_{min}) and maximal (R_{max}) degree of reaction, their absolute difference (ΔR) and their relative difference ($\Delta R/R_{max}$).

	R_{min}	R_{max}	Absolute Difference ΔR [%]	Relative Difference $\Delta R/R_{max}$ [%]
MK-MOH	12.3	17.5	5.2	30.0
MK-KOH	23.5	30.1	6.6	22.0
MK-NaOH	62.2	73.5	11.3	15.4

4. Discussion

4.1. Changes of MK_{Am}

The dissolution of MK_{Am} leads to a decrease in the X-ray amorphous hump (Figure 3) and thus a corresponding enrichment of the crystalline phases since these phases are not dissolved. A comparison of the scattering contribution of the X-ray amorphous hump between MK-NaOH and a MK sample mixed with 10 wt.% ZnO as internal standard (MK-10ZnO; MK_{Am} = 83.7 wt.%) confirms this observation. There is only a small difference in the diffractogram between MK-10ZnO and MK-NaOH in the area from 15°–30° 2Θ, where the scattering contribution of metakaolin is visible (Figure 7). Thus, the quantification of MK-NaOH is reliable since the result (83.4 wt.%) corresponds with the MK_{Am} content of MK-10ZnO. Other effects, like, for instance, geopolymerization, can be ruled out. According to Williams [59] geopolymerization would result in a clear shift in the X-ray amorphous hump. No such effect and thus no geopolymer formation can be detected from the XRD data. Additional thermogravimetric analyses show only a small mass loss (<1 wt.%) for all samples. Thus, the high water to solid ratio of 80 is sufficient to avoid condensation of geopolymers. The studies of Kaps et al. [11,60] confirm this. According to Palomo, et al. [61], geopolymers are formed in several stages. The contact of aluminosilicates with high pH solutions leads to the dissolution of Si- and Al-monomers, which in turn interact and form dimers, trimers and so on. If a saturation point is exceeded, geopolymers condense. This saturation point is not reached with the selected high water to solids ratio [33].

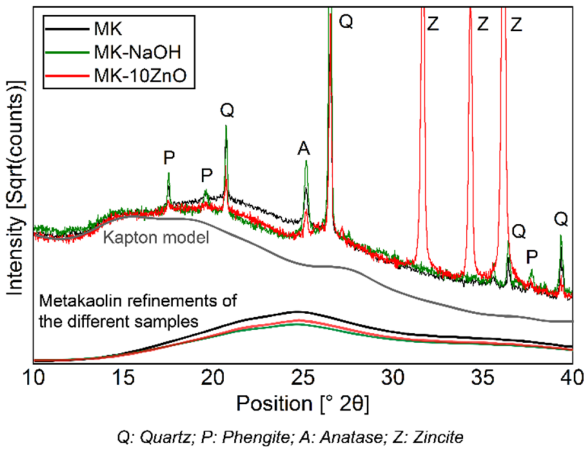

Figure 7. Comparison of diffractograms of MK-NaOH and a MK sample mixed with 10 wt.% ZnO as internal standard. The scattering contribution to the diffractogram of MK_{Am} of the different samples and of the Kapton model is shown.

Based on the results of $R_{Si/Al}$ of MK-NaOH given in Figure 6, the MK_{Am} content in the residue should be 78 wt.%. Here, the uptake of alkalis seems to have a direct influence on the diffractogram, namely increasing the scattering contribution of metakaolin compared to the dissolved Si- and Al-monomers. Pore solution tests on cement paste [62–66] in cementitious systems yield, in comparison, a significantly reduced availability of alkalis (c(Na) ≈ 50 mmol/L, c(K) ≈ 450 mmol/L [64]), and thus the effect should be reduced on the diffractogram which is caused by alkali uptake. As a result, the quantification of metakaolin in cementitious systems is influenced only to a minor extent by alkali uptake. Quantifications of the degree of reaction of metakaolin in cementitious systems with the PONKCS method [28] also confirm this assumption. An accurate modelling and calibration of the X-ray amorphous content as well as a precise description of the background [38] seems to be more important for a reliable quantification with the PONKCS method.

The analysis of the FTIR data reveals a significant structural change in the MK_{Am}. A shift in the position of the Si-O band maximum as well as a broadening of the peak can be observed. The related literature [45,67] reports a shift in this band to smaller wave numbers depending on the silicon content in the aluminosilicate structure. The dependence of the wave number (Table 8) on the silicon content (Table 7) is elaborated in Figure 8a. There is a good correlation between the silicon content and the shift in the band. A similar correlation is given for the molar ration of $SiO_2/(Al_2O_3 + Fe_2O_3 + TiO_2 + Na_2O + K_2O)$ (Figure 8b). The enrichment of Fe_2O_3 and TiO_2, as well as the uptake of alkalis, might influence the chemical environment of the Si-O band. A possible increase in the bond length of the Si-O band might induce the shift to lower wavenumbers. The FWHM can indicate the degree of disorder within a structure. Disordered structures show a broader peak than ordered structures [45,68]. Since parts of the kaolinite structure remain intact during calcination and transformation into metakaolin [39], the broadening of the peak can be interpreted as additional defects in the X-ray amorphous structure after treatment in alkaline solution according to Król et al. [45]. This effect can also be observed here. It is assumed that the ionic radii in 6-fold coordination with oxygen of Na^+ (116 pm) and K^+ (152 pm), which are significantly larger than Si^{4+} (54 pm) and Al^{3+} (53 pm) [69], also affect and additionally disorder the structure of the metakaolin. This highlights the correlation of $SiO_2/(Al_2O_3 + Fe_2O_3 + TiO_2 + Na_2O + K_2O)$ with the FWHM (Figure 8b). The SiO_2 content shows a just as good correlation with the FWHM (Figure 8a). However, it is assumed that the broadening of the peak is less due to the SiO_2 content than the enrichment of Fe_2O_3 and TiO_2, as well as the uptake of alkalis. Garg and Skibsted [43] showed by NMR measurements before and after dissolution in alkaline solution that 5-fold coordinated Al dissolves preferably and conclude a higher structural stability for 4-fold coordinated Al. These modifications have an influence on the binding conditions of the metakaolin structure and thus could influence the position of the FTIR bands.

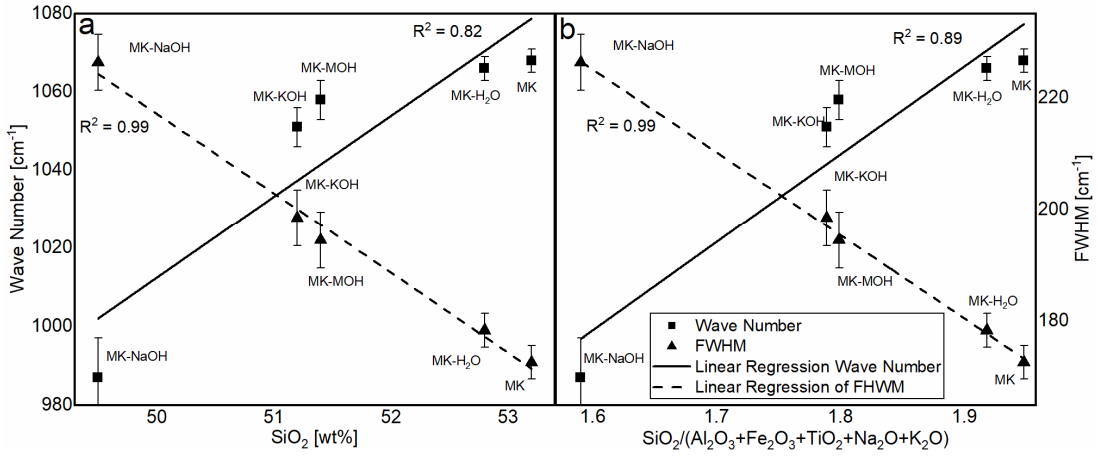

Figure 8. Correlation of the SiO_2 content (**a**) and the molar ratio of $SiO_2/(Al_2O_3 + Fe_2O_3 + TiO_2 + Na_2O + K_2O)$ (**b**) in the aluminosilicate structure with the wavenumber and FWHM.

SEM investigations demonstrate the influence of the dissolution of the Si- and Al-monomers on the shape of the particles. A dissolution process of the particles seems to take place. The enrichment of iron and titanium allows the conclusion that areas enriched with iron and titanium (Table 7) are hardly or not at all dissolved. As a result, metakaolin particles are not evenly dissolved from their edges and the SEM image of MK-NaOH (Figure 5D) could suggest the disintegration of the particles. Further investigations of the metakaolin particles in a transmission electron microscope could provide information about the element distribution within the particles. Inhomogeneous distribution of cations in the metakaolin structure could support the mentioned hypothesis.

Overall, the contribution of metakaolin to the pozzolanic reaction seems to be a congruent dissolution process. The almost constant SiO_2/Al_2O_3 molar-ratio of about 2 (Table 7) in all investigated

samples confirms that all areas are dissolved congruently and that neither Si- nor Al- ions are preferred. Thus, the structural changes seem to only slightly modify the scattering contribution of metakaolin to the diffractogram and the dissolution of metakaolin in alkaline solution, respectively, in cementitious systems is reflected in the decreasing X-ray amorphous hump in the diffractogram. In case of congruent dissolution, the same hkl-phase model of metakaolin can be used for quantification before and after treatment in alkaline solutions and thus enables a reliable quantification during cement hydration. Snellings [70] describes a shift in the X-ray amorphous hump towards lower angles 2Θ depending on the SiO_2 content of synthesized calcium aluminosilicate glasses. In case of an incongruent dissolution process of metakaolin calcined at higher temperatures (>900 °C) [43], an enrichment of or reduction in the SiO_2 content could also cause a shift in the X-ray amorphous hump. Such behavior could not be quantified with one hkl-phase model for metakaolin and would require the use of different hkl-phase models. As already described in the literature [26,28,36,37,58], the PONKCS method offers a powerful opportunity to investigate the influence of X-ray amorphous SCM on the hydration of cements.

4.2. Differences of the Degree of Reactions

The comparison in Figure 6 of R_{weight} and $R_{Si/Al}$ shows a lower degree of reaction for R_{weight}. The difference is due to the uptake of alkalis in MK_{Am}. The additional alkalis lead to a higher weight of the filter residue than calculated from the Si/Al-solubility only, and thus to a lower degree of reaction based on R_{weight} in comparison to $R_{Si/Al}$. Consequently, the deviations between the two degrees of reaction increases with increasing alkali uptake. This relationship is illustrated in Figure 9. MK-H_2O is somewhat out of the range, because, on the one hand, the degree of reactions and thus the measurable effects are very low and, on the other hand, no alkalis are available for uptake in the distilled water. Without MK-H_2O, the correlation fits very well and confirms the aforementioned.

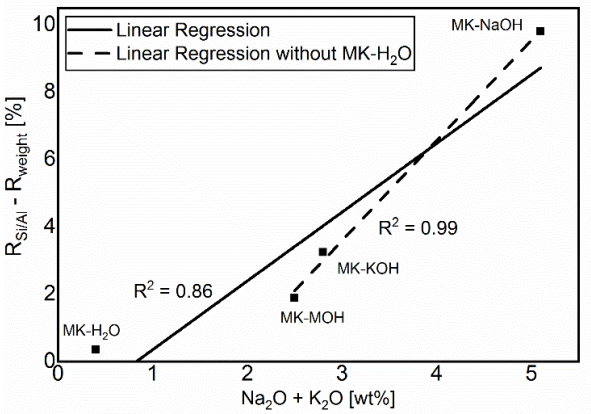

Figure 9. Correlation between the sum of alkalis and the difference of the calculated degrees of reaction.

When comparing the degrees of reaction within an alkaline solution, it is noticeable that $R_{Si/Al}$ is the highest for all investigated systems. From the evaluation of the weight of the filter residue and the QPXRD data, their lower calculated degree of reaction seems to be connected. Both the additional weight and the increased scattering contribution in the diffractogram appear to be related to the uptake of alkalis. This relationship is particularly evident for MK-NaOH. There is only a very small deviation in the calculated degrees of reaction between R_{weight} and R_{Quartz} or R_{MKAm} (Figure 6).

More obvious differences exist between R_{weight} and R_{MKAm} or R_{Quartz} for lower reaction degrees such as for MK-MOH and MK-KOH. A reason for this is the small quantitative difference in the MK_{Am} content between the initial sample and the samples MK-MOH and MK-KOH after the test. Even small deviations in the quantification of the MK_{Am} or quartz content (±1 or ±0.5 wt.%, Table 5) lead to significant errors in the calculation of the degree of reaction due to the experimental setup and error propagation (Figure 6). Avet, Li and Scrivener [26] and Snellings, Salze and Scrivener [36] showed in

their investigations in cementitious systems that errors in the determination of the reacted metakaolin with the PONKCS method could lead to pronounced errors in the determination of the degree of reaction. This effect was also reported for other SCM like fly ash and slag [23]. Due to the resulting large errors, the data must be interpreted with care. Overall, the resulting trends appear to be consistent. The present investigations are not dealing with a hydrating system, but the XRD quantifications are performed before and after a dissolution process of metakaolin in alkaline solution. In contrast to Avet et al. [26], the results of the degree of reaction cannot be determined directly from the decrease of MK_{AM}. Thus, the results represent a comparison between the degree of reaction from the Si- and Al-solubility and the PONKCS quantifications, but the procedure cannot be transferred to hydrating systems. Nevertheless, these comparisons are important to evaluate and confirm the reliability of the PONKCS quantifications in reacting systems, as the reaction of metakaolin in hydrating systems is also a dissolution process.

The degrees of reaction in highly alkaline solutions determined here do not allow straightforward conclusions to be drawn about the degree of reaction of the SCM in cementitious systems. But the significantly higher solubility of Si and Al for MK-NaOH in contrast to MK-KOH leads to the assumption that a higher degree of reaction of metakaolin may be expected in cements with a high sodium content in the pore solution. However, a classification of the reactivity of clays due to Si and Al solubility in NaOH solution with different metakaolin content [12] as well as of calcined clays and different phyllosilicates, seems possible and plausible [43,44,71]. This is in line with Maier, et al. [72], who found that Si- and Al-solubility, such as heat of hydration determined by R^3 reactivity test [17], exhibit both comparable correlation with the total Al_2O_3 content as well as the kaolinite content of the clays.

5. Conclusions

The correlation of dissolved silicon and aluminum from dissolution experiments with XRD quantification on MK after treatment in alkaline solutions offers new insights into the possibilities and limitations of quantifying MK during pozzolanic reaction with the PONKCS method. After systematic investigations of the filtrate and the filter residue, the following conclusions can be drawn.

A change in the binding condition of metakaolin owing to the treatment in alkali solutions can be proven using ATR-FTIR. The enrichment of iron and titanium as well as the uptake of alkalis in the metakaolin structure seem to cause a shift in the Si-O band to smaller wave numbers and a broadening of the bands.

The participation of the metakaolin in the pozzolanic reaction is a congruent dissolution process of the Si- and Al-monomers to a large extent. There seems to be an inhomogeneous distribution of the cations in the particles. Iron- and titanium-rich areas in the particles do not seem to dissolve and thus cause the particles to disintegrate.

These observations affect the intensity of the scattering contribution of the MK_{Am} in the diffractogram. However, these structural changes do not cause any change in the position of the X-ray amorphous hump if the dissolution of the metakaolin particles is congruent. Therefore, it is reasonable to use one hkl-phase model for the quantification of metakaolin calcined at its optimum temperature between 500 and 800 °C before and after dissolution in alkaline solution as well as during the hydration of cementitious systems.

The effect of the uptake of alkalis on the intensity of the X-ray amorphous hump results in a difference in XRD quantifications compared to the expected value calculated from the dissolved Si- and Al-ions. This effect can be measured for highly alkaline solutions on a pure metakaolin sample and leads to differences in the calculation of the degree of reaction. For common substitution rates of metakaolin in cementitious systems, where the content of alkalis in the pore solution is rather low, the effect on the quantification of MK_{Am} with the PONKCS method seems to be negligible or at least below the error of the quantification. Accurate modelling and calibration, as well as a very precise description of the background, is more decisive for the success of the quantification. Consequently, the PONKCS method is a suitable method for investigating the quantity and reaction mechanisms of the X-ray

amorphous SCMs involved in the hydration of cements. The strong effect of error propagation for low degrees of reaction and low substitution rates in cementitious systems remains a problem when calculating the degree of reaction based on quantifications using the PONKCS method.

Supplementary Materials: The following are available online at http://www.mdpi.com/1996-1944/13/10/2214/s1, Table S1: Chemical composition [wt.%] of MK_{Am} left after dissolution with different solvents of all samples measured with EDX and the molar ratio of SiO_2/Al_2O_3 and $SiO_2/(Al_2O_3 + Fe_2O_3 + TiO_2 + Na_2O + K_2O)$.

Author Contributions: Conceptualization, S.S., N.B. and K.-C.T.; methodology, S.S.; validation, S.S. and M.K.; investigation, S.S. and M.K.; data curation, S.S. and M.K.; writing—original draft preparation, S.S.; writing—review and editing, S.S., N.B., K.-C.T. and J.N.; supervision, K.-C.T. and J.N. All authors have read and agreed to the published version of the manuscript.

Funding: This research received no external funding.

Conflicts of Interest: The authors declare no conflict of interest.

References

1. Ramezanianpour, A.M.; Hooton, R.D. A study on hydration, compressive strength, and porosity of Portland-limestone cement mixes containing SCMs. *Cem. Concr. Compos.* **2014**, *51*, 1–13. [CrossRef]
2. Justnes, H. How SCMs Improve Concrete Durability—A Fundamental View. In Proceedings of the Fourth International Conference on Sustainable Construction Materials and Technologies, Las Vegas, NV, USA, 7–11 August 2016.
3. Sabir, B.B.; Wild, S.; Bai, J. Metakaolin and calcined clays as pozzolans for concrete: A review. *Cem. Concr. Compos.* **2001**, *23*, 441–454. [CrossRef]
4. Wang, A.; Kovler, K.; Provis, J.L.; Buchwald, A.; Cyr, M.; Patapy, C.; Kamali-Bernard, S.; Courard, L.; Sideris, K. Metakaolin. In *Properties of Fresh and Hardened Concrete Containing Supplementary Cementitious Materials*; De Belie, N., Soutsos, M., Gruyaert, E., Eds.; Springer International Publishing: Cham, Germany, 2018; pp. 153–179. [CrossRef]
5. Kadri, E.-H.; Kenai, S.; Ezziane, K.; Siddique, R.; De Schutter, G. Influence of metakaolin and silica fume on the heat of hydration and compressive strength development of mortar. *Appl. Clay Sci.* **2011**, *53*, 704–708. [CrossRef]
6. Said-Mansour, M.; Kadri, E.-H.; Kenai, S.; Ghrici, M.; Bennaceur, R. Influence of calcined kaolin on mortar properties. *Constr. Build. Mater.* **2011**, *25*, 2275–2282. [CrossRef]
7. Lothenbach, B.; Scrivener, K.; Hooton, R.D. Supplementary cementitious materials. *Cem. Concr. Res* **2011**, *41*, 1244–1256. [CrossRef]
8. Kadri, E.H.; Aggoun, S.; De Schutter, G.; Ezziane, K. Combined effect of chemical nature and fineness of mineral powders on Portland cement hydration. *Mater. Struct.* **2010**, *43*, 665–673. [CrossRef]
9. Raask, E.; Bhaskar, M.C. Pozzolanic activity of pulverized fuel ash. *Cem. Concr. Res.* **1975**, *5*, 363–375. [CrossRef]
10. Surana, M.S.; Joshi, S.N. Spectrophotometric method for estimating the reactivity of pozzolanic materials. *Adv. Cem. Res.* **1998**, *1*, 238–242. [CrossRef]
11. Kaps, C.; Buchwald, A. Property controlling influences on the generation of geopolymeric binders based on clay. In Proceedings of the Geopolymer 2002 3rd International Conference, Melbourne, Australia, 28–29 October 2002.
12. Buchwald, A.; Kriegel, R.; Kaps, C.; Zellmann, H.-D. Untersuchung zur Reaktivität von Metakaolinen für die Verwendung in Bindemittelsystemen. In Proceedings of the Gesellschaft Deutscher Chemiker e.V -Jahrestagung, Munich, Germany, 9–10 October 2003.
13. Katyal, N.K.; Sharma, J.M.; Dhawan, A.K.; Ali, M.M.; Mohan, K. Development of rapid method for the estimation of reactive silica in fly ash. *Cem. Concr. Res* **2008**, *38*, 104–106. [CrossRef]
14. Donatello, S.; Tyrer, M.; Cheeseman, C.R. Comparison of test methods to assess pozzolanic activity. *Cem. Concr. Compos.* **2010**, *32*, 121–127. [CrossRef]
15. Ferraz, E.; Andrejkovičová, S.; Hajjaji, W.; Velosa, A.L.; Silva, A.S.; Rocha, F. Pozzolanic Activity of Metakaolins by the French Standard of the Modified Chapelle Test: A Direct Methodology. *Acta Geodyn. Geomater.* **2015**, *12*, 289–298. [CrossRef]

16. Quarcioni, V.A.; Chotoli, F.F.; Coelho, A.C.V.; Cincotto, M.A. Indirect and direct Chapelle's methods for the determination of lime consumption in pozzolanic materials. *Rev. Ibracon Estrut. Mater.* **2015**, *8*, 1–7. [CrossRef]
17. Avet, F.; Snellings, R.; Alujas Diaz, A.; Ben Haha, M.; Scrivener, K. Development of a new rapid, relevant and reliable (R^3) test method to evaluate the pozzolanic reactivity of calcined kaolinitic clays. *Cem. Concr. Res.* **2016**, *85*, 1–11. [CrossRef]
18. Li, X.; Snellings, R.; Antoni, M.; Alderete, N.M.; Ben Haha, M.; Bishnoi, S.; Cizer, Ö.; Cyr, M.; De Weerdt, K.; Dhandapani, Y.; et al. Reactivity tests for supplementary cementitious materials: RILEM TC 267-TRM phase 1. *Mater. Struct.* **2018**, *51*, 151. [CrossRef]
19. Tashiro, C.; Ikeda, K.; Inoue, Y. Evaluation of pozzolanic activity by the electric resistance measurement method. *Cem. Concr. Res* **1994**, *24*, 1133–1139. [CrossRef]
20. Roszczynialski, W. Determination of pozzolanic activity of materials by thermal analysis. *J. Anal. Calorim.* **2002**, *70*, 387–392. [CrossRef]
21. Baert, G.; Hoste, S.; De Schutter, G.; De Belie, N. Reactivity of fly ash in cement paste studied by means of thermogravimetry and isothermal calorimetry. *J. Anal. Calorim.* **2008**, *94*, 485–492. [CrossRef]
22. Ben Haha, M.; De Weerdt, K.; Lothenbach, B. Quantification of the degree of reaction of fly ash. *Cem. Concr. Res.* **2010**, *40*, 1620–1629. [CrossRef]
23. Durdziński, P.T.; Ben Haha, M.; Bernal, S.A.; De Belie, N.; Gruyaert, E.; Lothenbach, B.; Menéndez Méndez, E.; Provis, J.L.; Schöler, A.; Stabler, C.; et al. Outcomes of the RILEM round robin on degree of reaction of slag and fly ash in blended cements. *Mater. Struct.* **2017**, *50*, 135. [CrossRef]
24. Bhagath Singh, G.V.P.; Subramaniam, K.V.L. Method for Direct Determination of Glassy Phase Dissolution in Hydrating Fly Ash-Cement System Using X-ray Diffraction. *J. Am. Ceram. Soc.* **2017**, *100*, 403–412. [CrossRef]
25. Villagrán-Zaccardi, Y.A.; Vollpracht, A.; Gruyaert, E.; De Belie, N. Recommendation of RILEM TC 238-SCM: Determination of the degree of reaction of siliceous fly ash and slag in hydrated cement paste by the selective dissolution method. *Mater. Struct.* **2018**, *51*, 27. [CrossRef]
26. Avet, F.; Li, X.; Scrivener, K. Determination of the amount of reacted metakaolin in calcined clay blends. *Cem. Concr. Res.* **2018**, *106*, 40–48. [CrossRef]
27. Ramanathan, S.; Moon, H.; Croly, M.; Chung, C.-W.; Suraneni, P. Predicting the degree of reaction of supplementary cementitious materials in cementitious pastes using a pozzolanic test. *Constr. Build. Mater.* **2019**, *204*, 621–630. [CrossRef]
28. Naber, C.; Stegmeyer, S.; Jansen, D.; Goetz-Neunhoeffer, F.; Neubauer, J. The PONKCS method applied for time resolved XRD quantification of supplementary cementitious material reactivity in hydrating mixtures with ordinary Portland cement. *Constr. Build. Mater.* **2019**, *214*, 449–457. [CrossRef]
29. DIN EN 196-1. *Prüfverfahren für Zement—Teil 1: Bestimmung der Festigkeit (Methods of Testing Cement—Part 1: Determination of Strength)*; Beuth-Verlag: Berlin, Germany, 2016; p. 31.
30. DIN EN 196-5. *Prüfverfahren für Zement—Teil 5: Prüfung der Puzzolanität von Puzzolanzementen (Methods of Testing Cement—Part 5: Pozzolanicity Test for Pozzolanic Cement)*; Beuth-Verlag: Berlin, Germany, 2011; p. 14.
31. Chatterjee, A.K. Pozzolanicity of Calcined Clay. In *1st International Conference Calcined Clays for Sustainable Concrete*; Scrivener, K., Favier, A., Eds.; Springer: Lausanne, The Netherlands, 2015; pp. 83–89. [CrossRef]
32. Antiohos, S.K.; Tsimas, S. Reactive Silica of Fly Ash as an Indicator for the Mechanical Performance of Blended Cements. In *Measuring, Monitoring and Modeling Concrete Properties*; Konsta-Gdoutos, M.S., Ed.; Springer: Dordrecht, The Netherlands, 2006; pp. 403–409. [CrossRef]
33. Snellings, R.; Scrivener, K.L. Rapid screening tests for supplementary cementitious materials: Past and future. *Mater. Struct.* **2016**, *49*, 3265–3279. [CrossRef]
34. Kalina, R.D.; Al-Shmaisani, S.; Ferron, R.D.; Juenger, M.C.G. False Positives in ASTM C618 Specifications for Natural Pozzolans. *ACI Mater. J.* **2019**, *116*, 165–172. [CrossRef]
35. Scarlett, N.V.Y.; Madsen, I.C. Quantification of phases with partial or no known crystal structures. *Powder Diffr.* **2006**, *21*, 278–284. [CrossRef]
36. Snellings, R.; Salze, A.; Scrivener, K.L. Use of X-ray diffraction to quantify amorphous supplementary cementitious materials in anhydrous and hydrated blended cements. *Cem. Concr. Res.* **2014**, *64*, 89–98. [CrossRef]

37. Stetsko, Y.P.; Shanahan, N.; Deford, H.; Zayed, A. Quantification of supplementary cementitious content in blended Portland cement using an iterative Rietveld-PONKCS technique. *J. Appl. Crystallogr.* **2017**, *50*, 498–507. [CrossRef]
38. Scherb, S.; Beuntner, N.; Thienel, K.-C.; Neubauer, J. Quantitative X-ray diffraction of free, not chemically bound water with the PONKCS method. *J. Appl. Crystallogr.* **2018**, *51*, 1535–1543. [CrossRef]
39. Brindley, G.W.; Nakahira, M. The Kaolinite-Mullite Reaction Series: II, Metakaolin. *J. Am. Ceram. Soc.* **1959**, *42*, 314–318. [CrossRef]
40. Massiot, D.; Dion, P.; Alcover, J.F.; Bergaya, F. 27Al and 29Si MAS NMR Study of Kaolinite Thermal Decomposition by Controlled Rate Thermal Analysis. *J. Am. Ceram. Soc.* **1995**, *78*, 2940–2944. [CrossRef]
41. Halse, Y.; Pratt, P.L.; Dalziel, J.A.; Gutteridge, W.A. Development of microstructure and other properties in flyash OPC systems. *Cem. Concr. Res.* **1984**, *14*, 491–498. [CrossRef]
42. Granizo, N.; Palomo, A.; Fernandez-Jiménez, A. Effect of temperature and alkaline concentration on metakaolin leaching kinetics. *Ceram. Int.* **2014**, *40*, 8975–8985. [CrossRef]
43. Garg, N.; Skibsted, J. Dissolution kinetics of calcined kaolinite and montmorillonite in alkaline conditions: Evidence for reactive Al(V) sites. *J. Am. Ceram. Soc.* **2019**, *102*, 7720–7734. [CrossRef]
44. Scherb, S.; Beuntner, N.; Thienel, K.-C. Reaction kinetics of the basic clays present in natural mixed clays. In *Calcined Clays for Sustainable Concrete, Proceedings of the 2nd International Conference on Calcined Clays for Sustainable Concrete, La Havanna, Cuba, 5–7 December 2017*; Springer: Dordrecht, The Netherlands, 2018; pp. 427–433.
45. Król, M.; Minkiewicz, J.; Mozgawa, W. IR spectroscopy studies of zeolites in geopolymeric materials derived from kaolinite. *J. Mol. Struct.* **2016**, *1126*, 200–206. [CrossRef]
46. Król, M.; Rożek, P.; Chlebda, D.; Mozgawa, W. ATR/FT-IR studies of zeolite formation during alkali-activation of metakaolin. *Solid State Sci.* **2019**, *94*, 114–119. [CrossRef]
47. O'Connor, B.H.; Raven, M.D. Application of the Rietveld refinement procedure in assaying powdered mixtures. *Powder Diffr.* **1988**, *3*, 2–6. [CrossRef]
48. Jansen, D.; Goetz-Neunhoeffer, F.; Stabler, C.; Neubauer, J. A remastered external standard method applied to the quantification of early OPC hydration. *Cem. Concr. Res* **2011**, *41*, 602–608. [CrossRef]
49. Bergold, S.T.; Goetz-Neunhoeffer, F.; Neubauer, J. Quantitative analysis of C–S–H in hydrating alite pastes by in-situ XRD. *Cem. Concr. Res* **2013**, *53*, 119–126. [CrossRef]
50. Le Page, Y.; Donnay, G. Refinement of the crystal structure of low-quartz. *Acta Crystallogr. Sect. B Struct. Sci.* **1976**, *32*, 2456–2459. [CrossRef]
51. Horn, M.; Schwerdtfeger, C.F.; Meagher, E.P. Refinement of the structure of anatase at several temperatures. *Zeitschrift Für Kristallographie Cryst. Mater.* **1972**, *136*, 273–281. [CrossRef]
52. Ivaldi, G.; Ferraris, G.; Curetti, N.; Compagnoni, R. Coexisting 3T and 2M1 polytypes of phengite from Cima Pal (Val Savenca, western Alps): Chemical and polytypic zoning and structural characterisation. *Eur. J. Mineral.* **2001**, *13*, 1025–1034. [CrossRef]
53. DIN EN ISO 11885. *Water Quality—Determination of Selected Elements by Inductively Coupled Plasma Optical Emission Spectrometry (ICP-OES)*; Beuth-Verlag: Berlin, Germany, 2009; p. 37.
54. Licht, S. pH Measurement in Concentrated Alkaline Solutions. *Anal. Chem.* **1985**, *57*, 514–519. [CrossRef]
55. Chakchouk, A.; Trifi, L.; Samet, B.; Bouaziz, S. Formulation of blended cement: Effect of process variables on clay pozzolanic activity. *Constr. Build. Mater.* **2009**, *23*, 1365–1373. [CrossRef]
56. Tironi, A.; Trezza, M.A.; Irassar, E.F.; Scian, A.N. Thermal Treatment of Kaolin: Effect on the Pozzolanic Activity. *Procedia Mater. Sci.* **2012**, *1*, 343–350. [CrossRef]
57. Jansen, D.; Stabler, C.; Goetz-Neunhoeffer, F.; Dittrich, S.; Neubauer, J. Does Ordinary Portland Cement contain amorphous phase? A quantitative study using an external standard method. *Powder Diffr.* **2012**, *26*, 31–38. [CrossRef]
58. Scrivener, K.L.; Lothenbach, B.; De Belie, N.; Gruyaert, E.; Skibsted, J.; Snellings, R.; Vollpracht, A. TC 238-SCM: Hydration and microstructure of concrete with SCMs. *Mater. Struct.* **2015**, *48*, 835–862. [CrossRef]
59. Williams, R.P. Quantification of the Extent of Reaction of Metakaolin-Based Geopolymers Using X-Ray Diffraction, Scanning Electron Microscopy, and Energy-Dispersive Spectroscopy. *J. Am. Ceram. Soc.* **2011**, *94*, 2663–2670. [CrossRef]

60. Kaps, C.; Buchwald, A.; Hohmann, M.; Zellmann, H.-D. Untersuchungen zur Bindероptimierung in alumosilikatischen Polymerbindern. In Proceedings of the 15 Internationale Baustofftagung Ibausil, Weimar, Germany, 24–27 September 2003.
61. Palomo, A.; Krivenko, P.; Garcia-Lodeiro, I.; Maltseva, O.; Fernández-Jiménez, A. A review on alkaline activation: New analytical perspectives. *Mater. Constr.* **2014**, *64*. [CrossRef]
62. Andersson, K.; Allard, B.; Bengtsson, M.; Magnusson, B. Chemical composition of cement pore solutions. *Cem. Concr. Res.* **1989**, *19*, 327–332. [CrossRef]
63. Caruso, F.; Mantellato, S.; Palacios, M.; Flatt, R.J. ICP-OES method for the characterization of cement pore solutions and their modification by polycarboxylate-based superplasticizers. *Cem. Concr. Res.* **2017**, *91*, 52–60. [CrossRef]
64. Vollpracht, A.; Lothenbach, B.; Snellings, R.; Haufe, J. The pore solution of blended cements: A review. *Mater. Struct.* **2016**, *49*, 3341–3367. [CrossRef]
65. Schöler, A.; Lothenbach, B.; Winnefeld, F.; Haha, M.B.; Zajac, M.; Ludwig, H.-M. Early hydration of SCM-blended Portland cements: A pore solution and isothermal calorimetry study. *Cem. Concr. Res.* **2017**, *93*, 71–82. [CrossRef]
66. Vollpracht, A.; Lothenbach, B.; Snellings, R.; Haufe, J. Influence of SCM on Pore Solution Composition. In Proceedings of the International RILEM Conference Materials Systems and Structures in Civil Engineering 2016 (MSSCE 2016), Lynby, Denmark, 22–24 August 2016; pp. 309–318.
67. Kosslick, H.; Fricke, R. Chemical Analysis of Aluminosilicates, Aluminophosphates and Related Molecular Sieves. In *Characterization II*; Karge, H.G., Weitkamp, J., Eds.; Springer: Berlin/Heidelberg, Germany, 2007; pp. 1–66. [CrossRef]
68. Król, M.; Mozgawa, W.; Morawska, J.; Pichór, W. Spectroscopic investigation of hydrothermally synthesized zeolites from expanded perlite. *Microporous Mesoporous Mater.* **2014**, *196*, 216–222. [CrossRef]
69. Shannon, R.D.; Prewitt, C.T. Effective ionic radii in oxides and fluorides. *Acta Crystallogr. Sect. B* **1969**, *25*, 925–946. [CrossRef]
70. Snellings, R. Solution-Controlled Dissolution of Supplementary Cementitious Material Glasses at pH 13: The Effect of Solution Composition on Glass Dissolution Rates. *J. Am. Ceram. Soc.* **2013**, *96*, 2467–2475. [CrossRef]
71. Beuntner, N.; Thienel, K.-C. Solubility and kinetics of calcined clay: Study of interaction by pore solution. In Proceedings of the 2nd International Conference on the Chemistry of Construction Materials (ICCCM 2016), Munich, Germany, 10–12 October 2016; pp. 157–160.
72. Maier, M.; Beuntner, N.; Thienel, K.-C. An approach for the evaluation of local raw material potential for calcined clay as SCM, based on geological and mineralogical data: Examples from German clay deposits. In Proceedings of the 3rd International Conference on Calcined Clays for Sustainable Concrete, Delhi, India, 15–17 October 2019.

materials

MDPI

Supplementary

Reactivity of Metakaolin in Alkaline Environment: Correlation of Results from Dissolution Experiments with XRD Quantifications

Sebastian Scherb [1,*], Mathias Köberl [1], Nancy Beuntner [1], Karl-Christian Thienel [1] and Jürgen Neubauer [2]

[1] Civil Engineering and Environmental Science, Univ ersitätder Bundeswehr Mu nich, Werner-Heisenberg-Weg 39, Neubiberg 85579, Germany; ma thias.koeberl@unibw.de (M.K.); nancy.beuntner@un ibw.de (N.B.); christian.thienel@unibw.de (K.-C.T.)

[2] GeoZentrum Nordbayern,Mineralogy, Friedric h-Alexander Universitaet Erlangen-Nuernberg, Schlossgarten 5a, Erlangen 91054, Germany; juergen.neubauer@fau.de

* Correspondence: sebastian.scherb@unibw.de

Received: 15 April 2020; Accepted: 11 May 2020; Published: 12 May 2020

Table S1. Chemical composition [wt.%] of MK_{Am} left after dissolution with different solvents of all samples measured with EDX and the molar ratio of SiO_2/Al_2O_3 and $SiO_2/(Al_2O_3 + Fe_2O_3 + TiO_2 + Na_2O + K_2O)$.

Oxides	MK_{Am}	$MK_{Am\text{-}H2O}$	$MK_{Am\text{-}MOH}$	$MK_{Am\text{-}KOH}$	$MK_{Am\text{-}NaOH}$
SiO_2	53.9	53.6	52.0	51.7	48.7
Al_2O_3	43.2	43.4	41.8	42.0	39.4
CaO	0.1	0.1	0.1	0.1	0.1
Fe_2O_3	1.6	1.4	2.3	1.8	3.6
K_2O	0.0	0.0	2.0	3.1	0.0
MgO	0.1	0.2	0.1	0.1	0.2
Na_2O	0.3	0.3	0.4	0.1	5.5
TiO_2	0.7	1.0	1.3	1.1	2.4
SiO_2/Al_2O_3	2.12	2.10	2.09	2.10	2.11
*	2.00	1.98	1.85	1.82	1.54

* $SiO_2/(Al_2O_3 + Fe_2O_3 + TiO_2 + Na_2O + K_2O)$.

8.3 Reaction Kinetics of Basic Clay Components Present in Natural Mixed Clays

Reprint

Published in Proceedings of the 2nd International Conference on Calcined Clays for Sustainable Concrete, RILEM Bookseries 16, doi: 10.1007/978-94-024-1207-9_69

Authors: S. Scherb, N. Beuntner, K.-Ch. Thienel

Reaction Kinetics of Basic Clay Components Present in Natural Mixed Clays

S. Scherb(✉), N. Beuntner, and K.-C. Thienel

University of the Federal Armed Forces, Munich, Germany

Abstract. The investigation reveals the reaction kinetics of three calcined phyllosilicates (metakaolin, metaillite and metamuscovite) in an alkaline solution which was prepared without the addition of clinker. The phyllosilicates were calcined at their individual optimal calcination temperature. Two test series without and with the addition of anhydrite were investigated. Calcite is present in all measurement series due to the impurity of portlandite. The reaction kinetics were investigated by means of isothermal calorimetry and in-situ x-ray diffraction (XRD). All measurement series show crystalline reaction products after 7 d in the absence of anhydrite. The addition of anhydrite leads to a first formation of ettringite within the first 13 h of reaction with all phyllosilicates tested. The water absorption capacity of phyllosilicates does not correlate with the specific surface area measure as BET-surface. Especially for metamuscovite, the high water absorption leads to a simultaneous formation of monosulfate and gypsum after 17 h. While metakaolin exhibits a significant concentration of dissolved alumina and silicon ions, the influences of metaillite and metamuscovite are less pronounced in that respect and exhibit reaction at a later stage. Nevertheless, it can be concluded that the reactivity of naturally occurring mixed layered clays cannot be reduced their metakaolin content but is due in addition to the contribution originating from other clays present in the mixtures. Metaillite and metamuscovite contribute even to the formation of hydrate phases at early ages of the reaction. Thus, the content and kind of phyllosilicates deserve more attention when used as supplementary cementitious material because of their high water absorption, their contribution to reactivity and their consumption of portlandite.

1 Introduction

Calcined clays represent an interesting perspective as supplementary cementitious materials (SCM). The use of naturally occurring clays as pozzolanic material becomes important due to their low material immanent CO_2 emission during calcination and their high global availability. The pozzolanic activity, primarily the amount and solubility rate of aluminum and silicon from calcined clays is influenced by the type and amount of the individual phyllosilicates, their structural order especially the degree of dehydroxylation after calcination and additional physical factors [1, 2]. Furthermore, the pozzolanic reaction mechanism differs depending on the Si/Al-ion content ratio of the calcined clay and the supply of ions into the pore solution. C-A-S-H and strätlingite are formed in alumina rich clay compositions. In the presence of sulfate and carbonate the

F. Martirena et al. (eds.), *Calcined Clays for Sustainable Concrete*, RILEM Bookseries 16,
https://doi.org/10.1007/978-94-024-1207-9_69

stability of AFm- and AFt-solid solutions are promoted. The availability of portlandite influences the kind and amount of the crystalline hydration products formed [3].

It is important to investigate the contribution of the individual components for a better understanding of the reaction mechanisms of a complex phase mixtures like natural clays. This research work identifies the reaction kinetics in cement free systems with and without sulfate being present.

2 Experimental Procedure

2.1 Characterization of Calcined Phyllosilicates

Three different preferably pure phyllosilicates were used. An industrial flash calcined metakaolin (containing quartz, anatase and phengite as impurities) was ready for use, while illite (containing kaolinite and calcite) and highly pure muscovite were calcined in a muffle oven for 30 min. The optimal calcination temperature of illite at 770 °C and muscovite at 800 °C was chosen due to their dehydroxylation temperatures determined by DTA and Si- and Al-ion solubility in alkaline solution after 20 h. Figure 1 shows the Al- and Si-ion solubility of metaillite and metamuscovite at different calcination temperatures and of metakaolin at 550 °C. The chemical composition was measured by inductively coupled plasma optical emission spectrometry (ICP-OES). Further the particle size distribution [4] (Fig. 2), the BET–specific surface area [5] and the water absorption capacity according to DIN 18132 [6] were measured (Table 2). Note that BET surface and water absorption do not have any correlation.

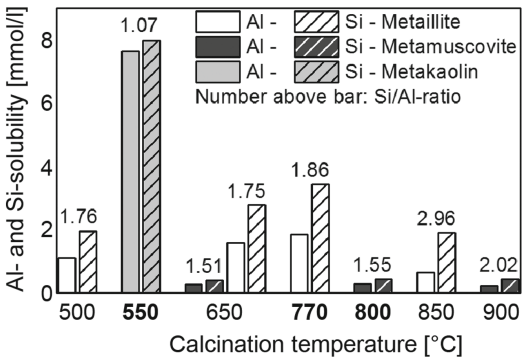

Fig. 1. Solubility of aluminum- and silicon-ions in alkaline solution

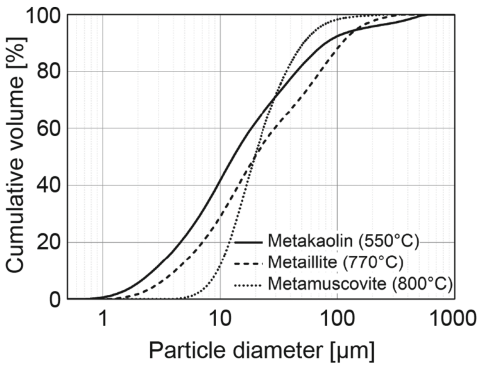

Fig. 2. Particle size distribution of the calcined phyllosilicates

Table 1. BET–specific surface area and water absorption capacity of the calcined phyllosilicates

	Metakaolin	Metaillite	Metamuscovite
BET [m^2/g]	17.76	82,38	10.89
Water absorption capacity [%]	77.0	76.4	154.5

Table 2. Mineralogical compositions (wt%) of the calcined phyllosilicates

Minerals	Metakaolin	Minerals	Metaillite	Minerals	Metamuscovite
Quartz	5.0	Illite	31.3	Muscovite	76.3
Anatase	0.6	Calcite	3.6		
Phengite	1.4	Lime	0.5		
		Portlandite	1.5		
X-ray amorphous	93.0	X-ray amorphous	63.1	X-ray amorphous	23.7

The mineralogical composition of the calcined clays was characterized by means of XRD (Table 2). Therefore, zincite was used as internal standard to quantify the x-ray amorphous content of the samples. While kaolinite lost its crystallinity completely, metaillite and metamuscovite still contain crystalline primary phyllosilicates after calcination procedure. The x-ray amorphous percentages contain the "meta-phases" of the phyllosilicates.

2.2 Equipment and Measurement Parameters

In situ XRD and isothermal calorimetry were used to investigate the reaction kinetics. For both measurements, the samples were stirred manually for one minute and transferred into appropriate sample crucibles which were closed for calorimetry and covered with a KAPTON film for XRD measurements. Isothermal calorimetry was performed with a TAM Air calorimeter at 25 °C for at least 70 h. For a good comparability of calorimetry and XRD the sample holder of the diffractometer was connected to a temperature device that allowed in situ XRD measurements at the same temperature. XRD was performed with a PANalytical Empyrean equipped with a primary Bragg-Brentano^{HD} monochromator and a PIXcel^{1D} linear detector. A diffractogram was taken every 15 min from 6 to 40° 2Θ at 40 kV and 40 mA up to 50 h of hydration. HighScore 4.2 was used as software to analyze the measurements.

Two test series were examined. The composition of the first series contained one calcined phyllosilicate each, calcium hydroxide in powder form and an alkaline solution with the ratio of 1:1:2. The second measurement series were conducted with a substitution of 10% by mass of the solid material by anhydrite. The alkaline solution to solid ratio was 1. The composition of the alkaline solution was 100 mmol/l NaOH and 500 mmol/l KOH. Calcite is due to the impurity of portlandite present in all measurement series.

3 Results and Discussion

3.1 Reaction Kinetics During Early Reaction Time

Figure 3 shows the heat flow of the two measurement series. The initial heat flow was not taken into account because of the external sample preparation for the measurements. While metakaolin and metaillite are homogeneous pastes after stirring the powder and

the alkaline solution for one minute, metamuscovite has an earth-moist consistency because of its high water absorption capacity.

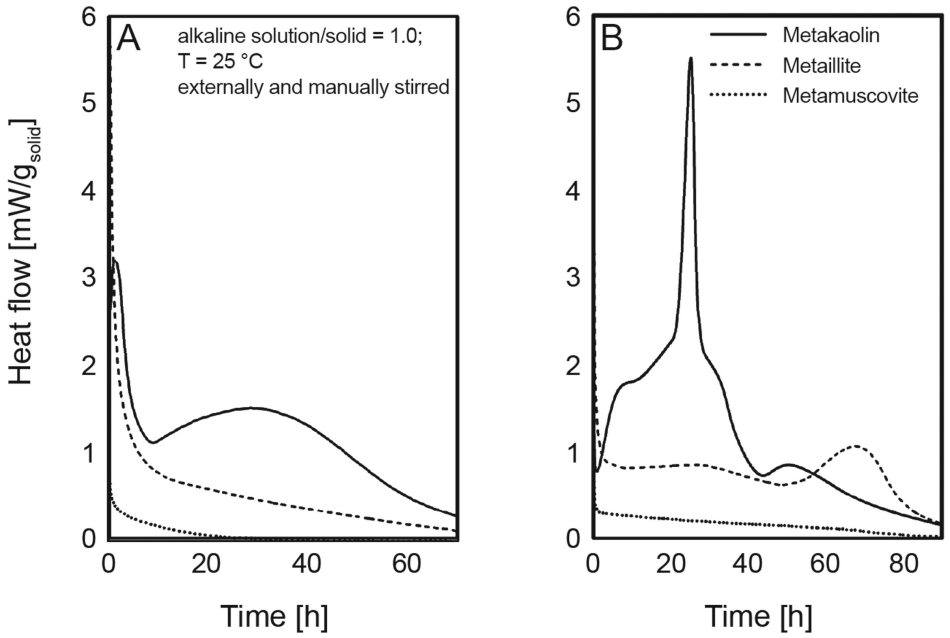

Fig. 3. Calorimetric measurements without anhydrite (A) and with anhydrite (B)

In the absence of anhydrite does Metakaolin cause two maxima at about 1 h (Q_{max} = 3.2 mW/g) and 30 h (Q_{max} = 1.5 mW/g) (Fig. 3A). The corresponding in situ XRD measurement does not show any formation of crystalline reaction products until 50 h (Fig. 5A). Only a dissolution of portlandite can be detected. Without anhydrite metaillite and metamuscovite do not have any maxima except for the initial heat. If anhydrite is added, the formation of ettringite can be detected in all measurements. For metakaolin, a first formation of ettringite can be observed after 3.5 h, for metaillite after 13 h and for metamuscovite after 12 h (Fig. 4). The complete dissolution of sulfates (anhydrite, gypsum) after 20 h leads to an increased ettringite formation in the mix containing metakaolin. The heat flow maximum at 25 h (Q_{max} = 5.5 mW/g) correlates well with the maximum content of ettringite, which remains constant after reaching the maximum. The heat flow of metaillite is relatively constant between 0.6 and 0.8 mW/g for the first 50 h of hydration and has its maximum at 68 h (Q_{max} = 1.1 mW/g). The visible dissolution of anhydrite starts after 3 h and lasts until 46 h. Gypsum can be detected after 15 h and is completely dissolved after 49 h again. Although the in situ XRD measurement just allows following the reaction kinetics until 50 h, it can be assumed that the maximal heat flow at 68 h correlates with the maximum content of ettringite comparable with the reaction of metakaolin. Metamuscovite exhibits a divergent reaction behavior. Following a slight ettringite formation a simultaneous crystallization of monosulfate, pyroaurite and gypsum takes place after 17 h (Fig. 4C). The high water absorption capacity seems to be the reason for a lower availability of water preventing continuously formation of ettringite.

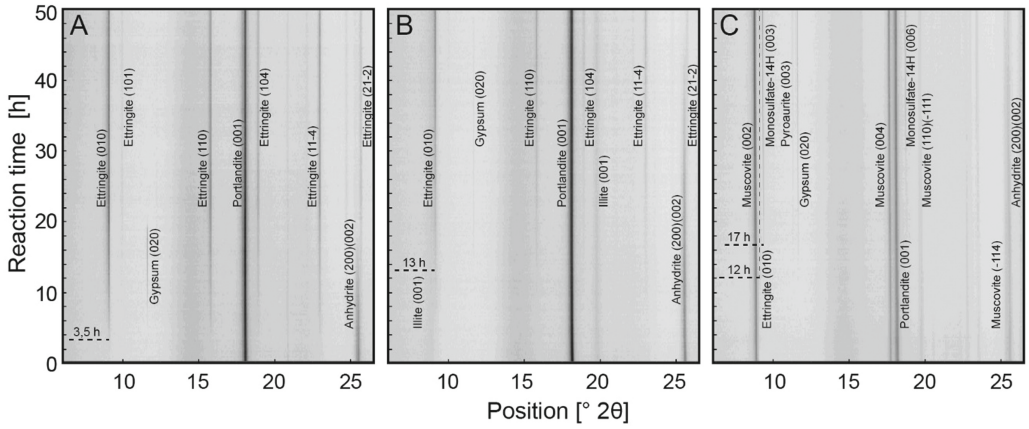

Fig. 4. In situ XRD measurement over 50 h from 6 to 26° 2Θ of metakaolin (A), metaillite (B) and metamuscovite (C) with the addition of anhydrite

3.2 Reaction Kinetics Until 28 Days

The XRD patterns of systems containing metakaolin and metaillite and prepared without the addition of anhydrite until 28 d are shown in Fig. 5. Hemicarboaluminate (AFm-Hc) and monocarboaluminate (AFm-Mc) are formed in both systems after 7 d. While portlandite is completely dissolved at 7 d with metakaolin, the dissolution process of portlandite needs until 28 d for metaillite. The higher calcite content in the measurement with metaillite leads to a preferential formation of AFm-Mc and AFm-Hc disappears after 28 d, while in the system with metakaolin both AFm-phases are still present after

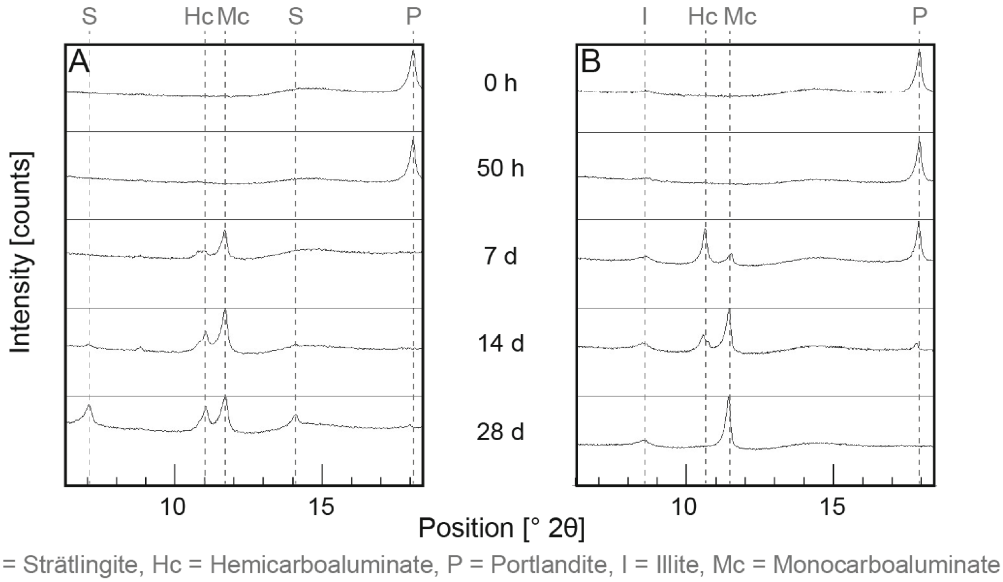

Fig. 5. XRD patterns of metakaolin (A) and metaillite (B) without anhydrite at 0 h, 50 h, 7 d, 14 d and 28 d

28 d. The formation of strätlingite can only be detected in the system with metakaolin after 14 d.

The reaction with metamuscovite shows a slight formation of AFm-Hc and AFm-Mc after 7 d, which does not change significantly until 28 d. Portlandite is still present after 28 d.

Metakaolin forms ettringite continuously in presence of anhydrite until 28 d. In addition AFm-Hc and AFm-Mc can be detected from 7 d on. For metaillite the formation of ettringite continues until 7 d and seems to stagnate until 28 d. The formation of kuzelite (hemisulfate) is visible after 7 d. Metamuscovite just shows small differences as compared to the in situ measurement after 28 d. It seems as if metamuscovite provides a small amount of water to form ettringite and lower the monosulfate content. In all measurements series undissolved portlandite is still present after 28 d.

In accordance with [7] strätlingite is formed in the absence of anhydrite in the system with metakaolin only. The Si/Al ratio of metaillite (1.86) and metamuscovite (1.55) is too high and offers insufficient aluminum to form strätlingite. If anhydrite is added, the formation of ettringite lowers the aluminum level in the pore solution and prevents the crystallization of strätlingite.

4 Conclusion

The investigation reveals the reaction kinetics of metakaolin, metaillite and metamuscovite in a clinker free alkaline solution:

- The reaction is slow in the absence of anhydrite and leads to the formation of crystalline reaction products (AFm-Hc, AFm-Mc) after 7 d.
- The addition of anhydrite leads to a first formation of ettringite with all phyllosilicates tested.
- The water absorption capacity of phyllosilicates does not correlate with the BET–specific surface area (Table 1). Especially for metamuscovite the high water absorption leads to a simultaneous formation of monosulfate and gypsum after 17 h.
- The contribution of phase mixtures like natural clay to pozzolanic reactivity cannot be reduced to its metakaolin content. Metaillite and metamuscovite contribute to the formation of hydrate phases even at early ages of the reaction as well even though on a much lower level than metakaolin.
- The content and kind of phyllosilicates deserve more attention due to their water absorption, their contribution to reaction kinetics and their consumption of portlandite when calcined clays are used as SCM.

References

1. Sabir, B.B., Wild, S., Bai, J.: Metakaolin and calcined clays as pozzolans for concrete: a review. Cement Concr. Compos. **23**, 441–454 (2001)
2. Tironi, A., Trezza, M.A., Scian, A.N., Irassar, E.F.: Kaolinitic calcined clays: Factors affecting its performance as pozzolans. Constr. Build. Mater. **28**, 276–281 (2012)

3. Antoni, M., Rossen, J., Martirena, F., Scrivener, K.: Cement substitution by a combination of metakaolin and limestone. Cem. Concr. Res. **42**, 1579–1589 (2012)
4. ISO 13320: Particle size analysis - Laser diffraction methods (2009)
5. DIN ISO 9277: Bestimmung der spezifischen Oberfläche von Feststoffen durch Gasadsorption nach dem BET-Verfahren (Determination of the specific surface area of solids by gas adsorption using the BET method), Beuth-Verlag (2003)
6. DIN 18132: Bestimmung des Wasseraufnahmevermögenes, Beuth-Verlag (2012)
7. De Silva, P.S., Glasser, F.P.: Hydration of cements based on metakaolin: thermochemistry. Adv. Cement Res. **3**, 167–177 (1990)

8.4 Reaction kinetics during early hydration of calcined phyllosilicates in clinker-free model systems

Reprint:
Published in the journal “Cement and Concrete Research”
Volume 143, May 2021, p. 106382; doi: 10.1016/j.cemconres.2021.106382

Authors: S. Scherb, M. Maier, N. Beuntner, K.-Ch. Thienel and J. Neubauer

Cement and Concrete Research 143 (2021) 106382

Contents lists available at ScienceDirect

Cement and Concrete Research

journal homepage: www.elsevier.com/locate/cemconres

Reaction kinetics during early hydration of calcined phyllosilicates in clinker-free model systems

Sebastian Scherb [a,*], Matthias Maier [a], Nancy Beuntner [a], Karl-Christian Thienel [a], Jürgen Neubauer [b]

[a] Institute for Construction Materials, University of the Bundeswehr Munich, Werner-Heisenberg-Weg 39, Neubiberg 85579, Germany
[b] Mineralogy GeoZentrum Nordbayern, Friedrich-Alexander University Erlangen-Nürnberg, Schloßgarten 5a, Erlangen 91054, Germany

ARTICLE INFO

Keywords:
Calcined clay
Supplementary cementitious material
Reaction kinetics
Calorimetry
In situ X-ray diffraction
Thermogravimetry

ABSTRACT

Investigations of nearly pure, calcined phyllosilicates ("meta-phyllosilicates") in clinker-free model systems were performed in presence and absence of sulfate. Calorimetric investigations show a pronounced reaction during the early reaction period only for metakaolin. Quantitative in situ X-ray diffraction reveals calcium silicate hydrate formation in the systems with metakaolin and metaillite, but not in those with metamuscovite. Ettringite crystallizes in all systems containing sulfate, where only the metakaolin system reaches the maximum ettringite content possible. The amount of aluminum ions released from 2:1 meta-phyllosilicates seems to be insufficient to reach the maximum content. Differences in portlandite dissolution and bound water indicate adsorption effects of calcium or calcium – sulfate ion pair complexes on surfaces of the calcined clay particles. Thus, the chemical as well as the physical influence of the meta-phyllosilicates must be considered to predict the reaction kinetics of calcined clays during early hydration.

1. Introduction

Calcined clays are currently the subject of numerous research projects. Highly reactive metakaolin (MK), the best known and most investigated calcined clay, is already used as a concrete additive with substitution rates of 5–10wt% of the cement and improves the properties of the concrete [1–4].

Due to its high costs and competition with other industries, MK is unsuitable as supplementary cementitious material (SCM) when aiming high replacement levels. Therefore, less reactive clays are of interest for the application as SCM to achieve the ambitious goal of reducing the clinker factor to 0.6 [4]. Currently, three different categories of clays are in focus: Clays with high kaolinite content (kaolinitic clay) and with a low kaolinite content (low grade kaolinitic clay) in the raw clay and, in addition, illitic clays, whose composition is dominated by the 2:1 phyllosilicate illite. Low grade kaolinitic and illitic clays have in common that they both contain other phyllosilicates and a larger proportion of accompanying minerals such as quartz and feldspars. These two categories offer the greatest potential to reduce CO_2 emissions caused by the cement industry [4] by permitting high replacement levels due to their worldwide and local availability.

Difficulties in the characterization of the clays result from very large chemical-mineralogical differences, even inside a single clay pit, and therefore a variety of compositions occurs in addition to the chemical-mineralogical complexity [5]. For this reason, it is rather impossible to characterize clays after calcination in a uniform framework.

The effect of calcined clays during early hydration can be divided into physical and chemical mechanisms. The filler effect as physical mechanism is achieved by the availability of additional surfaces, which serve as further nucleation sites of hydration products or for adsorption of ions from the pore solution. These additional surfaces are strongly related to the BET surface area of the calcined clays [6,7]. Zunino and Scrivener [8] describe an influence of the sulfate balance in blended cements by the surface area, whereas higher surface area leads to an increased sulfate requirement due to the adsorption of sulfate ions onto calcium silicate hydrate (C-S-H). Jansen et al. [9] show with their "complete mass balance approach" that understanding the mechanism of adsorbed ions provides a major contribution to the knowledge of hydration reactions.

The chemical mechanism is determined by the amount of released

* Corresponding author.
E-mail addresses: sebastian.scherb@unibw.de (S. Scherb), matthias.maier@unibw.de (M. Maier), nancy.beuntner@unibw.de (N. Beuntner), christian.thienel@unibw.de (K.-C. Thienel), juergen.neubauer@fau.de (J. Neubauer).

https://doi.org/10.1016/j.cemconres.2021.106382
Received 2 September 2020; Received in revised form 10 December 2020; Accepted 25 January 2021
Available online 12 February 2021

silicon and aluminum ions. According to the traditional definition of the pozzolanic reaction, silicon ions react to form strength-building C-S-H phases. For calcined clays, which provide a considerable amount of aluminum for the reaction, this traditional approach must be extended by the incorporation of aluminum into the C-S-H phases and an increased monophase (AFm) or ettringite (AFt) formation [10]. An influence on the sulfate balance by the additional amount of aluminum ions released from the SCM is conceivable. Furthermore, it is important to note that the composition of C-S-H can vary greatly [11,12]. The additional presence of aluminum originating from the SCM causes its incorporation into the C-S-H structure on the bridging sites and leads to the formation of C-A-S-H phases. The C-S-H and C-A-S-H phases generally show a tendency towards lower Ca/Si ratios when using SCM compared to C-S-H phases resulting from pure cement hydration [13–15].

According to the European cement standard DIN EN 197-1 it is common to quantify the amount of reactive silica to describe the reactivity of SCM [16,17]. For calcined clays, however, this only covers a part of the reactivity and does not consider the dissolved aluminum ions. Other test methods, such as the solubility of Si- and Al-ions in alkaline solution [18] or the cumulative heat release after the R^3 test [19] yield a better characterization of the reactivity for calcined clays. On one hand, a direct dependence of the reactivity on the kaolinite content of the clays [5,19] and on the other hand a gradation of the reactivity of individual calcined phyllosilicates ("meta-phyllosilicates") (metamica < metaillite < metamontmorillonite < metakaolin), which can be components in clay compositions [20–22], is shown in the literature.

All these investigations using the ion solubility or the R^3 test have in common that they focus exclusively on the reactivity of the SCM, which largely depends on the calcination temperature. Neißer-Deiters et al. [23] highlight that the optimal calcination temperature should not depend solely on the highest reactivity. Physical-hygroscopic properties must also be considered in order to achieve an optimum in the interaction between water demand, workability and reactivity.

The described reactivity tests do not give information on the influence of calcined clays on the hydration of cement clinker nor on changes of hydrate phase formation over time. These aspects, however, are important for predicting the influence on the reaction mechanisms of calcined clays during early hydration.

Various investigations on the reaction behavior of MK in clinker-free systems have already been published [24–28]. Murat [27] describes in the MK-CH-H_2O system a dependence of hydrate phase formation on the portlandite (CH) content and the time frame. In addition to calcium silicate hydrates (C-S-H), different calcium aluminate hydrates (C_4AH_{13} or C_3AH_6) or strätlingite (C_2ASH_8) are formed in the absence of sulfate carriers and calcite. Studies on various meta-phyllosilicates (metakaolinite, metaillite, metasmectite/metamontmorillonite, metamica) also prove the formation of C-S-H and C_4AH_X. Strätlingite or C_3AH_6 is only detected for Al-rich clays at 40 °C after 7 or 150 days respectively [29]. In further investigations with various meta-phyllosilicates in the clinker-free model system [30] and in the cementitious system [31], initial results indicate a varying pozzolanic contribution of the meta-phyllosilicates during early hydration. The availability of sulfate and carbonate ions in the pore solution leads to the formation of AFt or to sulfate or carbonate containing AFm phases [19]. Thermodynamic models in cementitious systems by Lothenbach and Zajak [32] show the formation of AFt and AFm phases in the presence of sulfate and carbonate. The thermodynamic stability of the forming aluminate hydrate phases (AFt, monosulfoaluminate (AFm-Ms), hemicarboaluminate (AFm-Hc) and monocarboaluminate (AFm-Mc)) depends significantly on the content of sulfate and carbonate [33].

In order to achieve reliable information about the reaction mechanisms during early hydration in the future, it is important to know the reaction contributions and mechanisms of the individual meta-phyllosilicates that occur in common clays. As mentioned above, the mineralogical complexity of clays currently makes it difficult to make general predictions about their influence on early hydration. This is the starting point of the present work, in which three individual meta-phyllosilicates (metakaolin, metaillite and metamuscovite) are investigated in clinker free model systems. For the first time, complete in situ XRD quantifications of clinker free systems including the reacting "metaphases" are performed during the first 50 h of in situ measurements. By using the PONKCS method, it is possible to quantify C-S-H and the X-ray amorphous "metaphases" of the meta-phyllosilicates [34]. The study intends to answer questions about differences of the reaction behavior between the meta-phyllosilicates used and the influence of the sulfate carrier on the reaction behavior and mechanism. This understanding of the contribution and influence on the reaction mechanisms can improve predictions based on the mineralogical composition of clays on the reaction mechanisms in the future.

2. Materials, test series and methods

2.1. Characterization of the meta-phyllosilicates

This investigation concentrates on the hydration behavior of three different, nearly pure phyllosilicates: A pure muscovite ($KAl_2[(OH)_2/AlSi_3O_{10}]$) without any detectable crystalline impurities, a kaolinite ($Al_4[(OH)_8/Si_4O_{10}]$) and an illite ($(K,H_3O)Al_2[(H_2O,OH)_2/(Si,Al)_4O_{10}]$) with a phase purity of more than 90% each. While the kaolinite (PowerPozz w, Temcom Solutions GmbH) was industrially calcined and ready for use, the illite and muscovite were calcined in a laboratory muffle oven in platinum crucibles. Based on the dehydroxylation temperatures determined from thermogravimetric analyses, the illite and muscovite were calcined at different temperatures [30]. The selection of the optimal calcination temperature was done on the basis of the ion solubility (silicon (Si), aluminum (Al)) in alkaline solution following the method of Kaps and Buchwald [18,35], which uses 1 g sample in 400 ml alkaline solution and shakes it for 20 h (see Section 2.3.1). The alkaline solution (mixed hydroxide solution (MOH), pH = 13.5) used consists of 100 mmol l^{-1} sodium hydroxide (NaOH) and 500 mmol l^{-1} potassium hydroxide (KOH) to simulate a cementitious pore solution [10,36]. The results of the ion solubility at different calcination temperatures are given in [30]. The Si- and Al-solubility of the selected calcination temperature (illite: 770 °C; muscovite: 800 °C) as well as the Si to Al ratio are shown in Table 1. Analogous to the designation metakaolin (MK) for calcined kaolinite, the calcined illite was named metaillite (MI) and the calcined muscovite metamuscovite (MM). Additionally the specific surface area (BET) [37], the particle density (PD) [38], the water absorption capacity (WAC) [39] and the d_{10}, d_{50} and d_{90} values of the particle size distribution [40] are given in Table 1.

The chemical and mineralogical compositions of the meta-phyllosilicates are provided in Table 2. The chemical composition was determined by inductively coupled plasma – optical emission spectroscopy (ICP-OES) according to [41,42]. The mineralogical composition was determined by quantitative powder X-ray diffraction (QPXRD) with external standard [43]. A polycrystalline silicon disc calibrated on

Table 1
Si- and Al-solubility of 1 g meta-phyllosilicate in 400 ml MOH solution, specific surface area, particle density, water absorption capacity and particle size distribution of meta-phyllosilicates investigated.

	MK	MI	MM
Si [mmol l^{-1}]	7.97	1.85	0.44
Al [mmol l^{-1}]	7.64	3.44	0.29
Si/Al [−]	1.07	1.86	1.55
BET [m^2 g^{-1}] [37]	14.1	82.4	10.9
PD [g cm^{-3}] [38]	2.42	2.76	2.70
WAC [%] [39]	77.0	76.4	154.5
d_{10} [µm]	3.0	3.2	9.4
d_{50} [µm]	14.8	15.0	19.6
d_{90} [µm]	76.2	83.8	51.4

Table 2
MAC, chemical and mineralogical composition of meta-phyllosilicates investigated.

Oxides (wt %)	MK	MI	MM	Phases (wt%)	MK	MI	MM
SiO_2	54.5	49.5	47.4	Quartz	5.0		
Al_2O_3	40.2	21.3	32.7	Anatase	0.6		
Fe_2O_3	1.8	6.6	5.1	Phengite	1.4		
CaO	<0.1	6.9	0.2	Illite		31.3	
MgO	0.2	2.9	<0.1	Calcite		3.6	
SO_3	<0.1	<0.1	<0.1	Lime		0.5	
Na_2O	0.3	0.3	0.6	Portlandite		1.5	
K_2O	0.3	6.3	12.0	Muscovite			76.3
TiO_2	1.4	0.7	0.9				
LOI	1.3	5.4	0.9	X-ray amorphous	93.0	63.1	23.7
MAC (cm^2 g^{-1})	36.8	57.2	54.6				

silicon powder was used as external standard to calibrate the factor G [44]. The mass attenuation coefficients (MAC, Table 2) were calculated from the chemical composition using the MACs of the single elements given in International Tables for Crystallography for Cu Kα radiation [45].

2.2. Test series

Two test series were examined. The first series contained one meta-phyllosilicate each, portlandite (CH) in powder form and MOH in the mass-related ratio of 1:1:2. The second measurement series were conducted with a substitution of 10 wt% of the solid material by anhydrite (C$). An overview of the composition of all systems studied is given in Table A1. For the production of C$, gypsum (Merck) was dehydrated for 16 h at 380 °C in a muffle furnace. While the C$ is free of crystalline secondary phases, CH (Alfa Aesar) contains 3.5 wt% calcite. The nomenclature for the systems without anhydrite is based on the corresponding meta-phyllosilicate (e.g. MK-CH) and in the systems with anhydrite on the corresponding meta-phyllosilicate with the addition C$ (e.g. MK-CH-C$). The MOH to solid ratio was one. For the experiments, the same MOH solution (Section 2.1) was used as for the determination of the Si- and Al-solubility. In order to investigate the hydration kinetics of the meta-phyllosilicates, Si- and Al-solubility in MOH, isothermal calorimetry, in situ X-ray diffraction, thermogravimetry and scanning electron microscopy were performed. For all investigations, the weighed-in solids and MOH were equilibrated overnight in a heating cabinet at measurement temperature (25 °C).

2.3. Methods

2.3.1. Ion solubility

The Si- and Al- solubilities were determined by ICP-OES with a Varian 720 ES spectrometer and evaluated with the software 1.1 supplied with the instrument. The measurements and their evaluation were conducted according to [41] using a multi-point calibration with an external standard. For the determination of Si- and Al-solubility, one gram of the corresponding meta-phyllosilicate (MK, MI, MM) was shaken each in 400 ml MOH solution (see Section 2.1) on an interval agitator. The solubilities were determined at three points in time after 6, 20 and 48 h. For each sample and each point in time, the samples were prepared individually and determined twice. Afterwards, the suspensions were filtered and the filtrates were acidified with concentrated HCl to a pH of 1 and filled up to 500 ml in a volumetric flask with distilled water.

2.3.2. Thermogravimetry

Thermogravimetric investigations were carried out with Netzsch STA 449 F3. The samples were stopped with acetone after 6 and 48 h of hydration. The exact process for sample preparation and the experimental procedure is explained in [46]. The bound water (H_{bound}) was calculated at the temperature interval from 20 to 400 °C and is referred to weight percent of the paste for direct comparability with the in situ XRD measurements. The mass loss up to 400 °C represents the sum of water released from the hydrate phases formed (C-S-H, ettringite (AFt) and monophases (AFm) [47–51]). The CH content was calculated from the mass loss in the temperature interval between 450 and 550 °C (H_{CH}) [48,49] using the tangent method according to Marsh and Day [52]. To calculate the bound water (H_{bound}, H_{CH}) in wt% referred to the paste, the content of unbound water ($H_{unbound}$ [wt%]) before stopping the sample was calculated from the difference between the total water content (H_{total} [wt%]) of the sample at the beginning of the experiment and the bound water in the complete temperature interval between 20 and 550 °C. Subsequently, the bound water (H_{bound} [wt%]) was calculated according to Eq. (1) where $\Delta m_{T1\text{-}T2}$ is the mass difference within the temperature interval and m_w is the weighed mass of the stopped sample (≈250 mg).

$$H[wt\%] = \Delta m_{T1-T2} \times \frac{100 - H_{unbound}}{m_w} \quad (1)$$

The CH content was calculated from the bound water within the corresponding temperature interval (H_{CH}) and the molar masses of water (M(H)) and CH (M(CH)) according to Eq. (2).

$$CH[wt\%] = H_{CH} \times \frac{M(CH)}{M(H)} \quad (2)$$

2.3.3. Isothermal calorimetry

Isothermal calorimetry experiments were performed with TA instruments TAM Air calorimeter at 25 °C for 50 h with 2 g of quartz sand in the reference chamber. The equilibrated sample was stirred manually with a spatula for 60 s and immediately transferred into a calorimeter crucible. The measured heat flow was normalized to 1 g of the paste. Data analysis was done with Origin 2018b.

2.3.4. In situ X-ray diffraction

Similar to the calorimetric measurements, the samples were mixed manually, transferred to a sample holder and covered with a Kapton film. In situ XRD measurements were performed with a PANalytical Empyrean diffractometer equipped with a primary Bragg–BrentanoHD monochromator and a PIXcel^{1D} linear detector. A diffractogram was taken in an interval of 15 min from 6 to 40° 2Θ at 40 kV and 40 mA with Cu Kα radiation for 50 h (200 scans). The sample holder of the diffractometer was connected to a temperature-controlling device that allowed in situ XRD measurements at the same temperature as the calorimetric measurements and thus ensuring good comparability between both methods. The measurements were analyzed with High Score 4.7 [53] using Rietveld refinement [54,55] with a combination of G-factor and PONKCS method [44,56] according to Bergold et al. [34]. Table 3 lists all structures used for Rietveld refinement. In contrast to determining the phase content of the meta-phyllosilicates (Section 2.1), the polycrystalline silicon disc was covered with Kapton film in order to calculate the factor G. For the application of the PONKCS method and for the sake of lacking structural data, hkl-phase models were developed (Kapton film) and calibrated (free water, MK, MI, MM, calcium-silicate-hydrate (C-S-H)) for non-crystalline components of the sample. The exact procedure is explained in [46] for creating the hkl-phase model of the Kapton film and for creating and calibrating the hkl-phase models of free water, MK and MM. The same procedure was applied to create and calibrate the hkl-phase model of MI.

The creation of the model for C-S-H requires a different approach, since the C-S-H is not available as a pure sample or as a sample with a known amount of C-S-H, as the idea of the PONKCS method prescribes. Thus, it is impossible to prepare and measure any powder samples nor to model the scattering contribution of the C-S-H and calibrate it in the

Table 3
Phases, authors and ICSD numbers used for Rietveld refinement.

Phase	Author	ICSD-No.
Silicon	[57]	52266
Zincite	[58]	57450
Alite	[59]	94742
Quartz	[60]	174
Anatase	[61]	9854
Phengite	[62]	92934
Illite	[63]	166963
Calcite	[64]	40107
Lime	[65]	60199
CH	[66]	34241
Muscovite	[67]	68548
C$	[68]	16382
Gypsum	[69]	92567
Tobermorite[a]	[70]	403090
AFt	[71]	155395
Kuzelite[b]	[72]	100138
Hydrotalcite	[73]	6296

[a] Structure information used for creating hkl-phase model for C-S-H.
[b] Structure information used to quantify Calcium Aluminum Sulfate Hydrate ($Ca_4Al_2O_6(SO_4) \times 14\ H_2O$ PDF-Nr: 42-0062 [74], abbreviation:$C_4A\$ \times H_{14}$).

conventional way. Bergold et al. [34] describe the development of the C-S-H model on a completely hydrated alite sample, in which only CH and unbound water are present in addition to C-S-H. The space group and lattice parameters of a 14 Å tobermorite [70] were used as a starting point and the C-S-H-model was created by using a Pawley fit [75]. This approach was adapted for the creation of the C-S-H model. Fig. 1 shows the measurements of the alite immediately after water addition, the completely hydrated alite sample and the contribution of the refined C-S-H phase in the completely hydrated alite sample. The prevention of overlapping of the alite with the resulting C-S-H phase is essential to create the C-S-H model [34]. The C-S-H model was calibrated by thermogravimetric analysis of a hydrated, dried alite sample. A composition of $C_{1.7}SH_{2.6}$ [76,77] was assumed to calculate the C-S-H quantity according to Eq. (3), where $M(H_2O)$ and $M(C_{1.7}SH_{2.6})$ are the molar masses of water and C-S-H respectively:

$$C-S-H[wt\%] = \frac{(M(C_{1.7}SH_{2.6}))}{2.6 \times M(H_2O)} \times water\ loss(< 300°C)[wt\%] \quad (3)$$

Due to the significant difference in dehydration temperatures between C-S-H and portlandite [48,49], the water loss below 300 °C (9.7 wt%) can be assigned to the C-S-H and allows its quantification and thus the calibration of the hkl – phase model.

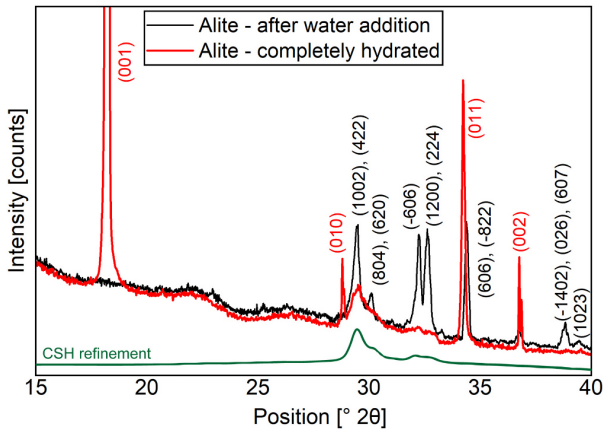

Fig. 1. Measurement of the alite sample immediately after water addition (black) and completely hydrated (red). The refined contribution of C-S-H (green), the (hkl) of alite (black) and CH (red) are given. (For interpretation of the references to color in this figure legend, the reader is referred to the web version of this article.)

In order to ensure a stable refinement over the measurement period of 200 scans, as few parameters as possible should be unlocked during Rietveld refinement, especially if the PONKCS method is used with several hkl-phase models. Fig. 2 illustrates the quantification procedure of the in situ XRD measurements. Apart from the hkl-phase model of the Kapton film, which remained fixed during refinement, the background was refined by a 1/2Θ first order polynomial. The lattice parameters of the crystalline phases in the starting material were refined on a powder sample and those of the resulting hydrate phases on the last scan of the in situ XRD measurement. Thus, only their scale factor required a refinement during the quantifications. For the calibrated hkl-phase models, also only the scaling factor was refined. There is no structure proposal for $C_4A\$ \times H_{14}$ in the ICSD database. For this reason, the lattice parameters of the kuzelite structure [72] were adapted to the PDF data sheet 42-0062 [74] and used for refinement. The differences in atomic number and position were neglected.

Since kaolinite is completely converted into an X-ray amorphous metaphase during calcination, only the scaling factor of the hkl-phase model was refined. Previous investigations of the authors [42] showed a congruent dissolution behavior of MK and thus the X-ray-amorphous metakaolin can be described with a single hkl-phase model. For MI and MM, the structural changes during dehydroxylation are much more complex and only a part of the crystalline raw material changes into disordered structures or X-ray amorphous phases. Therefore, both the scaling factor of the hkl-phase models and the crystalline structure were refined and presented as a sum.

2.3.5. SEM

The SEM investigations were performed on a Zeiss Evo LS 15 equipped with a secondary electron detector at 20 kV and a working distance of 8.5 mm. The samples were prepared analogously to the thermogravimetric measurements (Section 2.3.2, [46]) and stored in a heating cabinet at 25 °C for 48 h. Thereafter, a piece of the sample was placed on a sample holder with instant adhesive and coated with gold. The age of the samples ranged between 48 and 50 h, since the SEM examinations were performed on non-stopped samples and therefore it was impossible to achieve uniform times of examination for the samples.

3. Results

3.1. Time dependent solubility of Si- and Al-ions

Table 4 shows the Si- and Al-solubility as well as the Si/Al ratio after 6, 20 and 48 h. A precipitation of phases can be excluded due to the high water to solid value of 400 [35,42]. MK has a significantly higher ion solubility compared to MI and MM at every time investigated. After 48 h, the Si- or Al-solubility of MK is approximately 2.5 or 4 times compared to that of MI and 18 or 26 times higher than that of MM. The Si/Al ratio is about 1 for the 1:1 meta-phyllosilicate metakaolin, and between 1.5 and 2.0 for the 2:1 meta-phyllosilicates metaillite and metamuscovite, as already known from literature [78–80].

Considering the solution rate of Si and Al per hour [mmol l^{-1} h^{-1}] in the different time intervals (0–6; 6–20; 20–48; 0 - 48 h) (Table 5), the solution rate for MK is almost constant in the first two intervals up to 20 h and decreases significantly in the last interval between 20 and 48 h. MI and MM behave differently. The dissolution rates are halved already during the time interval between 6 and 20 h compared to the first time interval between 0 and 6 h. Between 20 and 48 h, both solution rates decrease significantly and in the same manner as for MK.

3.2. Meta-phyllosilicate – CH – MOH systems

Fig. 3 displays the results of the TG measurements after 6 and 48 h.

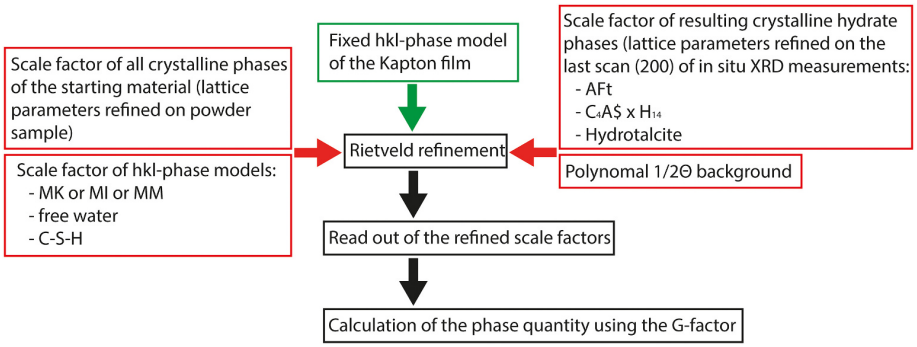

Fig. 2. Schematic illustration of the refinement routine during Rietveld refinement.

Table 4
Si- and Al-solubility [mmol l^{-1}] and Si/Al – ratio [molar] in MOH after 6, 20 and 48 h.

Time [h]	MK			MI			MM		
	Si	Al	Si/Al	Si	Al	Si/Al	Si	Al	Si/Al
6	2.34	2.09	1.12	1.48	0.75	1.97	0.21	0.11	1.90
20	7.97	7.64	1.04	3.44	1.85	1.85	0.45	0.29	1.55
48	10.36	9.78	1.06	3.82	2.40	1.59	0.56	0.37	1.51

Table 5
Si and Al dissolution rate [mmol l^{-1} h^{-1}].

Time interval	MK		MI		MM	
[h]	Si	Al	Si	Al	Si	Al
0–6	0.390	0.348	0.247	0.125	0.035	0.018
6–20	0.402	0.396	0.123	0.069	0.015	0.011
20–48	0.085	0.076	0.013	0.020	0.004	0.003
0–48	0.216	0.204	0.080	0.05	0.012	0.008

During the first 6 h, the dissolution of CH for MI-CH is highest (3.0 wt%), followed by MK-CH (2.2 wt%), while hardly any dissolution of CH takes place for MM-CH. Within the second time interval between 6 and 48 h, MK-CH achieves by far the highest dissolution of CH (8.4 wt%). For MI-CH and MM-CH, the dissolution of CH in the second time interval is 3.5 wt% and 0.7 wt%, respectively. Although the CH dissolution is the highest for MI-CH during the first 6 h, MK-CH contains more bound water during this interval. In all systems, the bound water increases between 6 and 48 h. The quantified bound water is 8.6 wt% for MK-CH, 5.1 wt% for MI-CH and 1.4 wt% for MM-CH after 48 h.

Fig. 4 shows the quantification of the in situ XRD measurements (left y-axis) and the heat flow (right y-axis) of MK-CH (A) and MI-CH (B) during the first 50 h. Some crystalline phases, which do not change during the 50 h within the error range or which content is very low, are left out. This concerns the phases anatase, phengite and quartz for MK as well as calcite and lime for MI. As described in Section 2.3.4, MI represents the sum of crystalline and X-ray amorphous components of metaillite. At the beginning of the reaction, the dissolutions of both MK and CH are accelerated, which correlate with the first maximum of the heat flow (Q^+1 after 2 h, Fig. 4A). Afterwards, the dissolution of MK continues at a relatively constant rate. The CH dissolution accelerates one more time between 15 and 25 h. The formation of C-S-H begins after 10 h and becomes very pronounced up to 30 h, until it slows down afterwards. Here, the formation of C-S-H correlates with the second maximum (Q^+2) observed by isothermal calorimetry after 30 h. The calorimetric curve of MI-CH reveals no further maximum apart from a broad initial heat flow. Comparable to MK-CH, CH and MI dissolve with the highest rate during the first hours. Subsequently, the two phases dissolve evenly over the entire period of investigation, with a lower rate

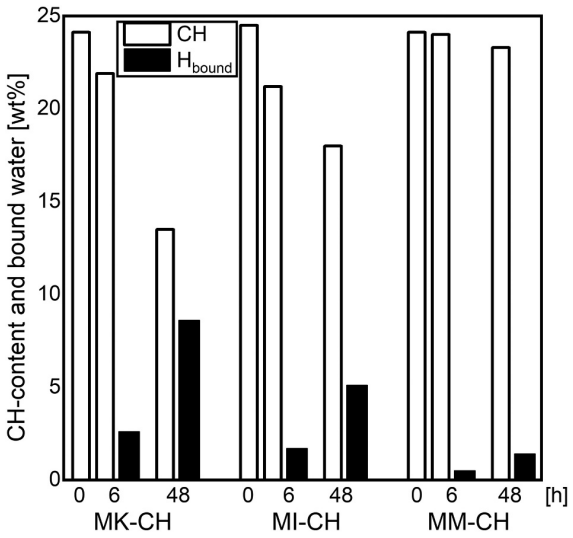

Fig. 3. CH content after 0, 6 and 48 h and bound water after 6 and 48 h of the meta-phyllosilicate – CH –MOH systems.

than observed for MK-CH. The formation of C-S-H starts after 28 h and increases constantly until the end of the measurement.

The presentation of MM-CH has been omitted, because apart from an initial heat flow (see [30]) and a low dissolution of CH (comparable to thermogravimetry (≈1 wt%)) no further effects can be observed. Neither a dissolution of the starting material nor a hydrate phase formation can be identified during the first 50 h.

Fig. 5 shows the SEM images of MK-CH (left) and MI-CH (right) after 48 to 50 h. Both images give a similar visual impression and display particles of the corresponding meta-phyllosilicate (MK, MI), CH crystals and poorly crystalline C-S-H. The C-S-H seems to grow out of the CH crystals (center of the right image) as well as on the surfaces of the meta-phyllosilicate particles (named C-S-H inside the images).

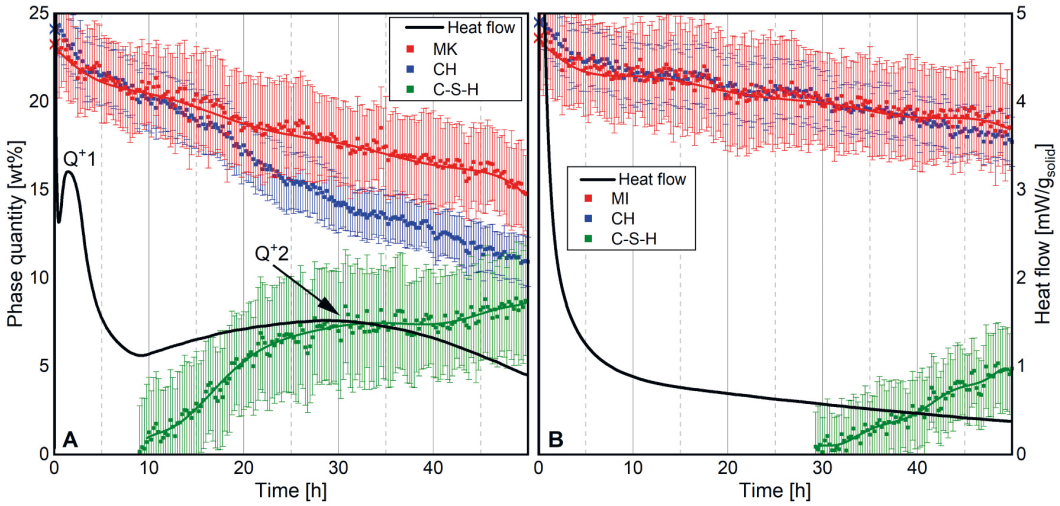

Fig. 4. XRD quantification (left y-axes) and heat flow (right y-axes) of MK-CH (A) and MI-CH (B). The start values of the initial phases are marked with a cross on the y-axis. The error bars are calculated by multiple determination of the systems.

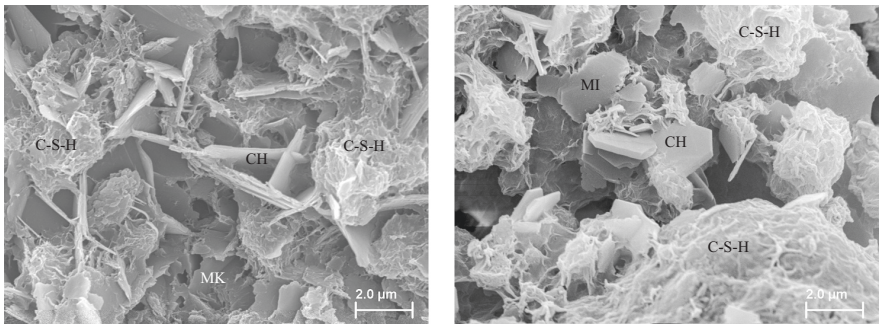

Fig. 5. SEM images of MK-CH (left) and MI-CH (right) after 48 to 50 h.

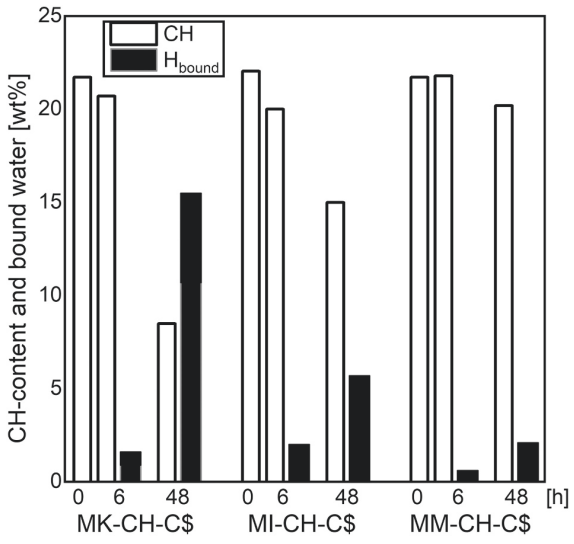

Fig. 6. CH content after 0, 6 and 48 h and bound water after 6 and 48 h of the meta-phyllosilicate – CH – C$– MOH systems.

3.3. Meta-phyllosilicate – CH – C$ – MOH systems

Fig. 6 gives the CH content and the bound water after 6 and 48 h of the meta-phyllosilicate – CH – C$ – MOH systems. 2.1 wt% CH dissolve during the first 6 h for MI-CH-C$ and 1.0 wt% for MK-CH-C$. For MM-CH-C$, the absolute CH content after 6 h is 21.8 wt%. Thus, there is no CH dissolution in the system with MM. In the time interval between 6 and 48 h, 12.2 wt% CH dissolve for MK-CH-C$, 5.0 wt% for MI-CH-C$ and 1.6 wt% for MM-CH-C$.

The bound water is 15.5 wt% for MK-CH-C$, 5.5 wt% for MI-CH-C$ and 2.1 wt% for MM-CH-C$ after 48 h. While after 6 h the content of bound water is still highest for MI-CH-C$ (2.0 wt%; MK-CH-C$: 1.6 wt%; MM-CH-C$: 0.6 wt%), the content of bound water after 48 h is highest for MK-CH-C$ due to a significant increase between 6 and 48 h (Δ10.6 wt%; MI-CH-C$: Δ3.5 wt%; MM-CH-C$: Δ1.5 wt%).

Fig. 7 shows the quantification of the in situ XRD measurements (left y-axis) and the heat flow (right y-axis) of MK-CH-C$ (A), MI-CH-C$ (B) and MI-CH-C$ (C) during the first 50 h. Other than for the quantification of the meta-phyllosilicate - CH - MOH systems (Section 3.2), all three systems are shown. Again, MI and MM represents the sum of the crystalline and the X-ray amorphous phase (see Section 2.3.4). A rapid dissolution of MK and CH is visible in the quantification of MK-CH-C$ (Fig. 7A) during the first 2 h of the reaction, which subsequently slows down until a further intense dissolution takes place between 15 and 25 h (MK) and 15 and 30 h (CH), respectively. Thereafter, both MK and CH

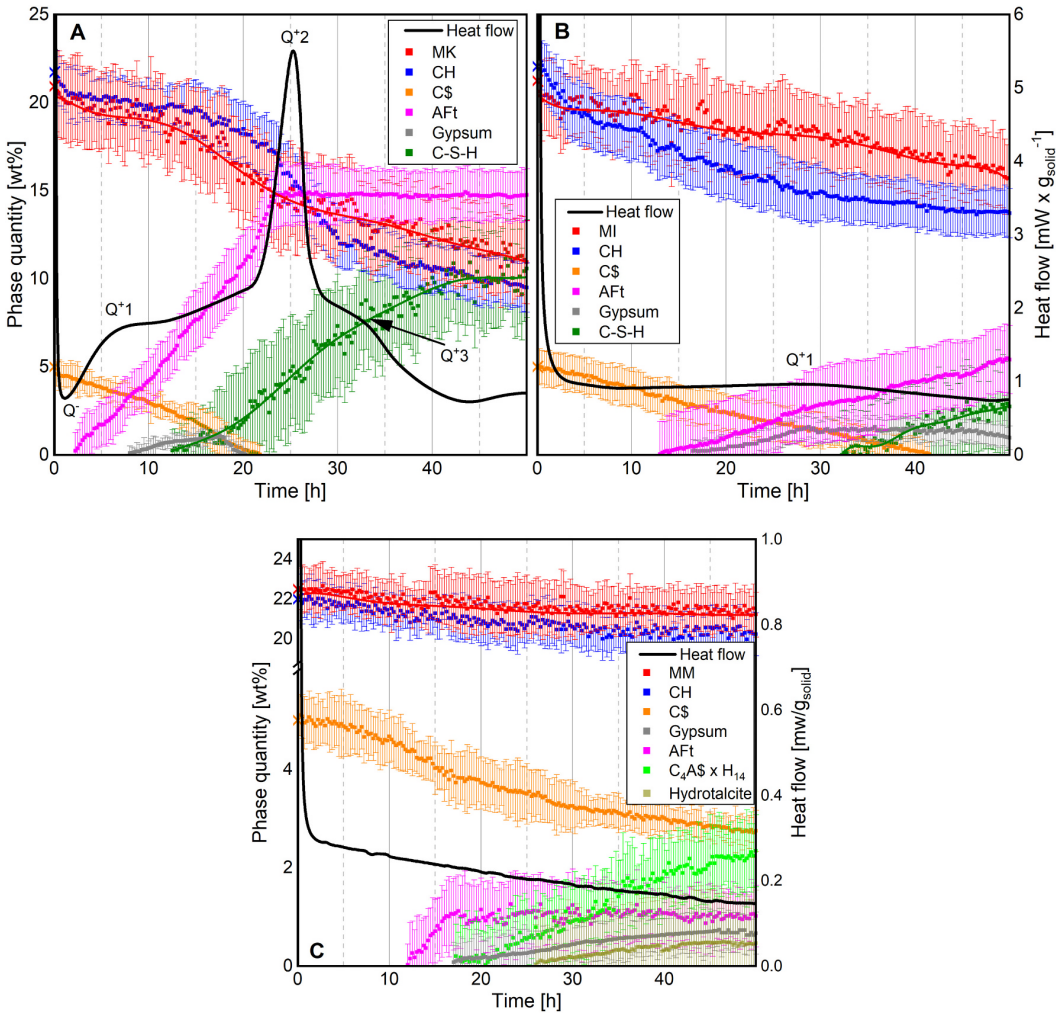

Fig. 7. XRD quantification (left y-axes) and heat flow (right y-axes) of MK-CH-C$ (A), MI-CH-C$ (B) and MM-CH-C$ (C). The start values of the initial phases are marked with a cross on the y-axis. The error bars are calculated by multiple determination of the systems.

dissolve continuously at a lower, but constant rate until the end of the measurement after 50 h.

Initially, C$ dissolves continuously up to about 15 h. Then, a slightly accelerated dissolution takes place until C$ is completely dissolved after 20 h. During the dissolution of C$, a small amount of gypsum precipitates after 8 h, which is also completely dissolved after 20 h. AFt initiates to form from 2 h after the start of the reaction. The content of AFt increases constantly until the sulfate carriers (gypsum and C$) are both completely dissolved after 20 h. This is followed by a briefly accelerated AFt formation. The quantity of AFt is 14.8 wt% after 26 h and remains constant until the end of the measurement after 50 h.

C-S-H begins to form after 12 h and is quantified with 10.6 wt% after 50 h. The formation is more pronounced up to about 40 h and slows down afterwards. Overall, a main reaction and a clear correlation between in situ XRD and calorimetry can be determined for MK-CH-C$ during the first 40 h. The end of the dormant period (Q^-) is accompanied by the beginning formation of AFt. The assignment of the maxima Q^+1 and Q^+3 is more difficult. Q^+1 seems to be related to the formation of ettringite and gypsum and Q^+3 corresponds with a change in dissolution rate of MK and CH and the initial formation of C-S-H. The pronounced maximum Q^+2 after 25 h can be attributed to an accelerated AFt formation following the complete dissolution of the sulfate carriers after 20 h. The effect of sulfate depletion thus occurs analogously to cementitious systems [81] in the clinker-free system with MK. The heat flow curve shows a slight time shift as compared to the XRD quantifications. This occurs despite the temperature control of the XRD measurements, because the XRD samples are temperature-controlled from below only, while ampoules in the heat flow calorimeter can compensate the heat of dissolution and hydration more directly.

The heat flow of MI-CH-C$ (Fig. 7B) exhibits no pronounced maximum during the first 50 h, except for the initial heat flow, and the heat flow remains rather constant at 1 mW × g_{solid}^{-1}. Only a slight maximum (Q^+) is detected after 28 h. The CH quantification of CH shows a strong dissolution at the beginning of the measurement, which gradually decreases during the course of the measurement. MI and C$ dissolve both constantly over the measurement period. C$ is completely dissolved after about 40 h. AFt formation starts after 13 h and increases linearly until the end of the measurement. Gypsum forms after 16 h and its amount present in the system rises until about 28 h. The maximum gypsum content correlates with the weak maximum Q^+ of the heat flow. Then, the gypsum content remains constant until it slowly begins to dissolve after 45 h. C-S-H is primarily detected after 32 h and increases constantly to about 3 wt% until the end of the measurement.

After the initial peak, the heat flow curve of MM-CH-C$ (Fig. 7C)

decreases constantly until the end of the measurement and shows no further maximum. CH and MM dissolve constantly but very slowly over the entire test period. For C$, an accelerated dissolution is observed in the time interval between 10 and 17 h. AFt formation begins after 12 h. After about 17 h, the AFt content is 1 wt% and remains constant until the end of the measurement. Instead of a further AFt formation, gypsum and $C_4A\$ \times H_{14}$ form simultaneously after 17 h. The amount of both phases increases continuously until the end of the measurement. Furthermore, the formation of small quantities of hydrotalcite can be determined after 27 h. An illustration of the first and last scan of in situ XRD measurement is given in Fig. A2. C-S-H cannot be detected during the entire measurement. The quantities of the phases, which are presented in Fig. 7 at the beginning of the measurement (t_0) and after 50 h, are summarized in Table 6. The significant deviation to 100 wt% results from free water and those phases, which are omitted in the table.

Fig. 8 shows the SEM images of MK-CH-C$ (left) and MM-CH-C$ (right) after 48 to 50 h. Partly idiomorphic and partly less idiomorphic grown AFt crystals dominate the optical impression of MK-CH-C$. The large number and size of the AFt crystals hinders the proper identification of the other phases. AFt crystals and poorly crystalline C-S-H cover most surfaces of the particles. Still, MK particles can be detected occasionally. For MM-CH-C$, the preparation after 48 h is critical because the sample is still very moist and has not hardened noticeably. The selected image section mainly shows muscovite and its amorphous content, which cannot be distinguished from each other in SEM. In the border area of the MM particles, however a multitude of small needles can be identified, which are characteristic for the sample in each image section. A more detailed examination of the needles is not possible due to their small size and it cannot be determined with certainty whether these needles are C-S-H or AFt needles.

Fig. 9 shows the SEM image of MI-CH-C$ after 48 to 50 h at two different magnifications. The right image is an enlarged detail of the section, which is marked in the left image. In the center of the images, idiomorphically grown, prismatic AFt crystals can be seen. In comparison to MK-CH-C$, their amount is significantly lower, which leads to a better visibility of the C-S-H on the particle surfaces as well as the MI particles themselves. It is noteworthy that at the edges of the clay particles comparable fine needle structures can be seen as in MM-CH-C$ (Fig. 9, right image inside the black circle).

4. Discussion

The experiments on Si and Al solubility revealed a decreasing solubility of MK to MI to MM. While the 1:1 meta-phyllosilicate MK has a molar Si/Al ratio of about 1, the 2:1 meta-phyllosilicates MI and MM have a molar Si/Al ratio between 1.5 and 2. The results are in line with the chemical formula of the phyllosilicates (Section 2.1) and the literature [29,78–80]. Fig. 10 shows the bound water (H_{bound}, Fig. 6) as a function of the sum of the dissolved ions (Si + Al, Table 4). The solubility and the bound water after 6 and 48 h are considered. MK, MI and MM without and with C$ are each combined to a measurement series. An increasing amount of dissolved Si and Al ions correlates linearly with an increase in bound water for the systems without C$. The correlation has a very high coefficient of determination R^2 [82]. Systems with C$ exhibit larger deviations. Compared to measurements without C$, they reveal both very water-rich AFt and C-S-H with significantly less bound water. Due to the different Si/Al ratio of the meta-phyllosilicates, no linear correlation between dissolved ions and bound water is to be expected in these systems. Nevertheless, the dissolution rate of the meta-phyllosilicates (Table 5) correlates in general well with the reaction behavior from the XRD quantifications (Fig. 7). Differences in the time dependent observations can be attributed to the chemical-mineralogical differences between the MOH solution and the reacting systems. While it is a straight dissolution process in highly aqueous MOH solution, reaction products are formed in the presence of CH and sulfate carrier and change thereby continuously the composition of the pore solution. Thus, it is possible to determine the relative reactivity of the individual meta-phyllosilicates based upon the time-resolved dissolution experiments, but is neither possible to predict any reaction mechanisms nor to derive time points of hydrate phase formation.

Considering the XRD and calorimeter data, only for the systems with MK a pronounced reaction within the first 50 h can be determined. For MI-CH-C$, the heat flow is relatively constant at 1 $mW \times g_{solid}^{-1}$ with a slight maximum after 28 h. In the other systems, only a continuously decreasing heat flow can be observed after the initial peak. When comparing the sulfate-free systems with the systems with C$, it is noticeable that the formation of C-S-H in the sulfate-free systems starts earlier in both MK and MI. Zunino and Scrivener [83] found an enhancement of C-S-H formation in a model cement system when sulfate is added resulting from an accelerated alite reaction. Bergold et al. [34] describe the formation of C-S-H during alite hydration in two steps. During the first hours, short-range ordered C-S-H originate from alite, which cannot be detected nor quantified using the hkl-phase model. Subsequently, both alite and short-range ordered C-S-H react to form long-range ordered C-S-H (C-S-H_{lro}), which can be quantified with the C-S-H model. Thus, it cannot be said with certainty that C-S-H generally forms earlier in systems without C$, but only C-S-$H_{lro}$. No statement can be made about the formation of short-range ordered C-S-H during the first hours of hydration, due to the lack of quantification. One reason for the earlier quantification of C-S-H_{lro} without C$ could be the incorporation of Al into C-S-H. The Al released from MK reacts with C$ to AFt, while no crystalline sulfate-free calcium aluminate hydrate is formed in absence of C$. Consequently, an increased incorporation of Al into C-S-H is to be expected. Another reason might be the Ca/Si ratio in the composition of the C-S-H as reported by Naber et al. [84]. Since the model for the quantification of the C-S-H is based on the hydration of alite, a lower Ca/Si ratio can be expected when the C-S-H forms from the meta-phyllosilicates. The formation of AFt additionally causes a consumption of Ca ions in the presence of C$, which are in consequence not available for the formation of C-S-H. Therefore, a higher Ca/Si ratio of C-S-H in the systems without C$, which is closer to the composition of the hkl model, could lead to an earlier quantification of C-S-H.

The XRD quantifications and TG measurements after 6 h of MI systems (Fig. 7B) show a strong CH dissolution during the first hours of reaction, while the content of bound water is comparatively lower. This could be explained by the significantly higher BET surface area of MI compared to MK and leads to the hypothesis that Ca^{2+} ions adsorb onto the negatively charged surfaces of the clays [85,86] and thus enable a further dissolution process, even if only small amounts of hydrate phases are formed in relation to the dissolved ions. The continuous dissolution process of the C$ does also support this hypothesis. Especially the measurements of the 2:1 meta-phyllosilicates show a significant amount

Table 6
Summary of the phases presented in Fig. 7 at the beginning of the measurement (t_0) and after 50 h in wt%. Phases that do not change during the first 50 h and the free water are omitted.

Phase [wt%]	MK-CH-C$	MI-CH-C$	MM-CH-C$
MK - t_0	20.9	–	–
MI - t_0	–	21.2	–
MM - t_0	–	–	22.5
CH - t_0	20.7	22.1	20.7
C$ - t_0	5.0	5.0	5.0
MK	10.9	–	–
MI	–	15.7	–
MM	–	–	21.2
CH	9.5	13.8	20.2
C$	0	0	2.8
AFt	14.8	5.4	1.0
C-S-H	10.6	2.9	<1.0
Gypsum	0	1.0	0.7
$C_4A\$ \times H_{14}$	<0.3	<0.3	2.3
Hydrotalcite	<0.3	<0.3	0.5

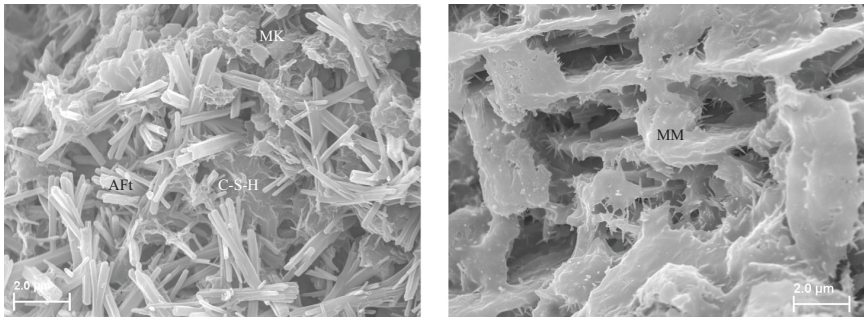

Fig. 8. SEM images of MK-CH-C$ (left) and MM-CH-C$ (right) after 48 to 50 h.

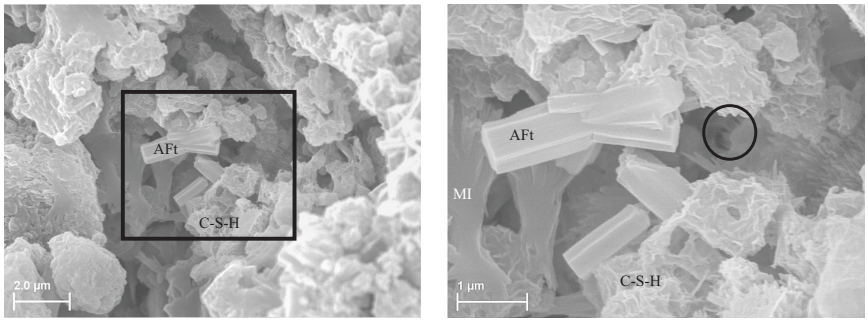

Fig. 9. SEM images of MI-CH-C$ after 48 to 50 h at two different magnifications. The right picture shows the enlarged black framed area.

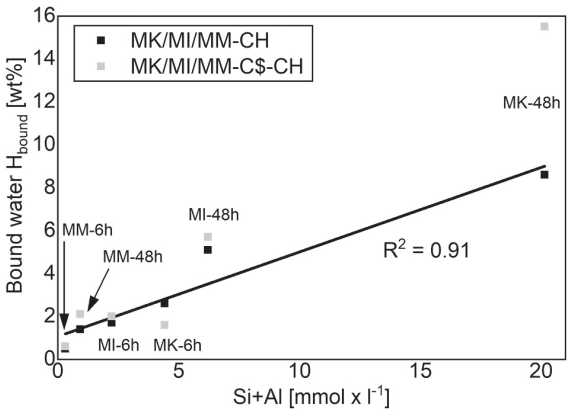

Fig. 10. Correlation of the ion solubility (Si + Al) and the bound water (H_{bound}). A linear regression is possible for the systems without C$ (MK/MI/MM-CH) only.

of dissolved C$ before AFt is formed. Myers et al. [87,88] describe the adsorption of calcium – sulfate ions pair complexes onto the negative surfaces of Al-rich leached layers of tricalcium aluminate. This complex formation could also occur on the negatively charged surfaces of the calcined clay and explain the continuous dissolution process of C$. Due to the small amount of C-S-H in clinker-free systems during early hydration, adsorption must take place on the clay surfaces [85] in addition to adsorption effects on the C-S-H surfaces, as observed by Zunino and Scrivener [8]. The comparatively low amount of bound water after 6 h in the MI compared to the MK systems can be attributed to the lower Si and Al ion solubility. MI provides an insufficient amount of Si and Al ions to form more hydration products.

When considering the total sulfate content of the systems with C$, the maximum AFt content (AFt_{max}) calculated according to Hesse et al. [62] is 15.4 wt%. With a deviation of 0.6 wt% between the quantified and theoretically calculated content, it is assumed that AFt_{max} is reached for MK-CH-C$. When reaching AFt_{max} after 20 h, neither AFm-Ms, nor AFm-Hc nor AFm-Mc are formed. This indicates an incorporation of the released Al into C-S-H following AFt_{max}. It is assumed that the rate of release and quantity of the released Al is not enough to form AFm-Ms at early ages of hydration. Another reason could be a low concentration of OH^-, which inhibits the formation of AFm-Ms as described in [33,89]. Matschei et al. [33,90] additionally describe a stabilization of ettringite by formation of Hc or Mc in the presence of calcite. Thermodynamic modelling of hydrated cements by Lothenbach and Zajac [32] confirm the occurrence of AFm-Hc or AFm-Mc depending on the calcite content already at early times of hydration. In the present study, AFm-Hc or AFm-Mc could not be detected during the first 50 h in any of the investigated systems. For the MK systems the calcite content (<1 wt%) seems to be insufficient to form AFm-Hc or AFm-Mc during early hydration. For the systems containing MI, AFt_{max} has not yet been reached and it can be assumed that sulfate in the pore solution prevents the formation of AFm-Hc or AFm-Mc despite higher contents of calcite. The availability of Al in MI-CH-C$ seems to be insufficient to form more AFt. It is assumed that the gypsum will continue to dissolve in the further course of the process and, after its complete dissolution, induce a slightly accelerated formation of AFt. This assumption is supported by the maximum heat flow after 65 h (Q^+2, Fig. A1). These results are consistent with the visual impression from SEM images, which show AFt as dominant phase in MK-CH-C$ (Fig. 8) only and can explain the high amount of bound water (Fig. 6). Previous studies by the authors show that HC and MC are present in clinker-free systems after 7 days of hydration [30]. Overall, a strong sulfate consumption can be observed for MK-CH-C$ already during early hydration, whereby the available sulfate carrier was bound completely into AFt after 22 h. Due to the slower and lower absolute solubility of Al from MI (about 25% of that of MK), sulfate consumption in MI-CH-C$ takes place much slower and to a

lower extent. Therefore it is crucial to distinguish between kaolinitic and illitic clays regarding the sulfate balance of a composite cement with calcined clays. The chemical influence of the meta-phyllosilicates must be considered.

Table 7 gives the CH dissolution and the bound water until 400 °C derived from TG measurements after 48 h as well as the C-S-H content for measurements without C$ and C-S-H + AFt for the measurements with C$ derived from XRD quantifications after 50 h. The content of MK was set at 100%. Since no C-S-H could be detected in the measurements with MM, there is no value for the XRD quantification of MM-CH and MM-CH-C$ represents AFt only. Altogether, the reactivity of MM can be regarded as very low, reaching between 3.9 and 16.3% of the values of MK. For cementitious systems it can therefore be assumed that the influence of the MM on the reaction mechanisms is less due to the chemical contribution than caused by physical hygroscopic properties, as already described by Neißer-Deiters et al. [23]. A more differentiated picture can be seen for MI. For MI-CH, all values are within a narrow range between 56.6 and 61.3% compared to MK-CH. For MI-CH-C$, the individual values are much more divergent. While the CH dissolution is 53% of the value of MK-CH-C$, the bound water up to 400 °C and C-S-H + AFt reach only 36.8% and 32.3%, respectively. The values of bound water and hydrate phase formation correlate very well with the Si- and Al-solubility (MI has 30.9% of the Si- and Al-solubility compared to MK according to Table 4 after 48 h). However, considerably less water is bound and hydrate phases are formed than the CH dissolution suggests in comparison to MK. This strongly indicates adsorption effects of calcium – sulfate ion pair complexes on the calcined clay surfaces as mentioned above. Since this effect can only be observed for the measurement MI-CH-C$, the sulfate in comparison to MI-CH and the BET surface area (82.4 for MI and 10.9 for MM) in comparison to the MM systems seem to play a decisive role in the adsorption behavior. Overall, it can be concluded that MI contributes not only physically but clearly also chemically to the early hydration in a clinker-free model system. Physical properties such as BET surface area appear to influence the composition of the pore solution by adsorption of ions or ions pair complexes additionally and thus the dissolution and reaction behavior.

Fig. 11 summarizes schematically the general results from the sulfate-free and sulfate-containing systems with MK and MI. An increased Si/Al ratio and a decreasing absolute amount of Si and Al ions from the left to the right side of the graph are reflected in the amount of bound water as well as in the composition and quantity of hydrate phases. While for sulfate-free systems is limited to the silicate reaction to C-(A)-S-H formation (lower, orange part of the graph), the entire graph must be considered for sulfate-containing systems (C-(A)-S-H + AFt).

Table 7
CH dissolution and bound water until 400 °C determined by TG and C-S-H + (AFt) determined by XRD after 48 h.

	CH dissolution (TG) [wt%]	[a]	Bound water until 400 °C (TG) [wt%]	[a]	C-S-H + (AFt) (XRD) [wt%]	[a]
MK-CH	10.6	100	8.6	100	8.7	100
MI-CH	6.5	61.3	5.1	59.3	4.9	56.6
MM-CH	0.8	7.5	1.4	16.3	–	–
MK-CH-C$	13.2	100	15.5	100	25.4	100
MI-CH-C$	7.0	53.0	5.7	36.8	8.3	32.6
MM-CH-C$	1.2	9.1	2.1	13.5	1.0	3.9

[a] Percentage from the preceding column normalized to the content of the measurements with MK in %.

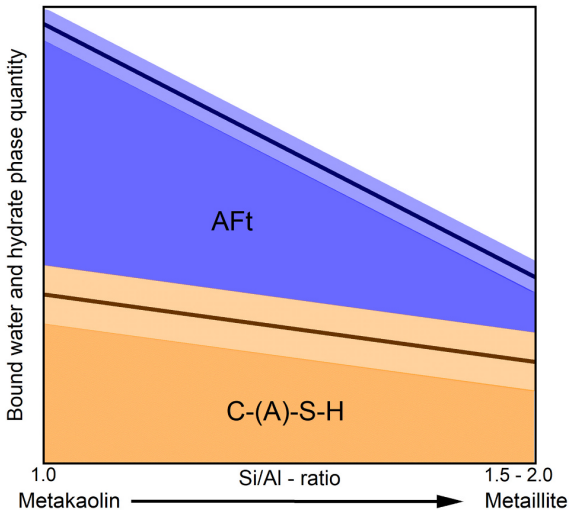

Fig. 11. Schematic model to predict reactivity and hydrate phase formation during early hydration after 48 h of kaolinitic and illitic clays.

The brighter orange and blue areas indicate differences of bound water and hydrate phase quantity, as well as they reflect uncertainties in quantification.

5. Conclusion

Three different meta-phyllosilicates-CH mixtures in alkaline solution with and without the addition of C$ were investigated. The combination of TG, calorimetry and in situ XRD quantifications lead to the following conclusions: All examined meta-phyllosilicates yield an autonomous formation of hydrate phases. While for MK and MI both silicate and aluminate hydrate phases can be verified by XRD, for MM only aluminate hydrate phases are detectable. However, TG measurements also indicate the formation of C-S-H in MM systems. A pronounced reaction can only be determined for the systems with MK. MI and MM systems are characterized by a continuous dissolution process in the clinker-free system during early hydration and show no intense maxima of the heat flow during main reaction. Only MK is able to form the maximum AFt content during early hydration, while the 2:1 meta-phyllosilicates do not release enough aluminum to reach the maximum AFt content. Moreover, dissolution processes of the reactants and formation of hydrate phases do not seem to be directly coupled, which is supported by differences between the CH dissolution and the amount of bound water. This could be explained by the adsorption of calcium and calcium – sulfate ion pair complexes on calcined clay surfaces. The BET surface area has a decisive influence on the adsorption behavior of the meta-phyllosilicates. Furthermore, the presence of sulfate as a reaction partner for the released ions from the meta-phyllosilicates leads to a higher CH dissolution and a stronger reaction. Thus, the chemical as well as the physical influence of the meta-phyllosilicates on the reaction behavior during early hydration must be considered. The sulfate balance in the systems and thus the correct sulfation plays an important role and requires more detailed investigations. The influence of MM on the hydration kinetics stems less from the chemical contribution than rather from its physical-hygroscopic properties.

CRediT authorship contribution statement

Sebastian Scherb: Conceptualization, Methodology, Investigation, Validation, Data curation, Writing – original draft. **Matthias Maier:** Data curation, Methodology, Writing – review & editing. **Nancy Beuntner:** Funding acquisition, Conceptualization, Writing – review &

editing. **Karl-Christian Thienel:** Supervision, Writing – review & editing. **Jürgen Neubauer:** Writing – review & editing.

Declaration of competing interest

The authors declare that they have no known competing financial interests or personal relationships that could have appeared to influence the work reported in this paper.

Acknowledgement

The authors like to thank Deutsche Forschungsgemeinschaft (DFG, Germany) for the financial support of the research project "Efficiency and influence of calcined phyllosilicates during the early hydration of cement" (BE 7038/2-1).

Appendix A

Table A1
Mineralogical composition and MAC of all systems examined.

Phases (wt%)	MK-CH	MI-CH	MM-CH	MK-CH-CS;$^{-}$	MI-CH-CS;$^{-}$	MM-CH-CS;$^{-}$
Quartz	1.25					
Anatase	0.15					
Phengite	0.35					
Illite		7.83			7.04	
Calcite	0.88	1.78	0.88	0.79	1.60	0.79
Lime		0.13			0.12	
Muscovite			19.1			17.17
CH	24.13	24.5	24.13	21.72	22.05	21.72
C$				5	5	5
MOH-solution	50	50	50	50	50	50
X-ray amorphous	23.25	15.78	5.93	20.93	14.20	5.33
MAC ($cm^2\ g^{-1}$)	36.92	42.02	41.38	37.61	42.20	41.62

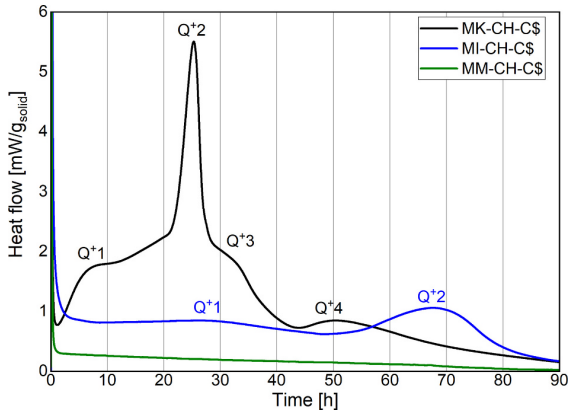

Fig. A1. Heat flow curves of the systems containing C$ until 90 h of hydration.

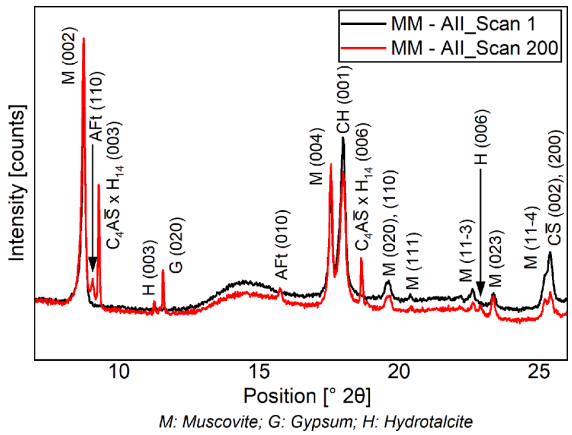

M: Muscovite; G: Gypsum; H: Hydrotalcite

Fig. A2. Comparison of the first (Scan 1) and last (Scan 200) scan of MM-CH-C$.

References

[1] M.H. Zhang, V.M. Malhotra, Characteristics of a thermally activated alumino-silicate pozzolanic material and its use in concrete, Cem. Concr. Res. 25 (1995) 1713–1725, https://doi.org/10.1016/0008-8846(95)00167-0.
[2] R. San Nicolas, M. Cyr, G. Escadeillas, Performance-based approach to durability of concrete containing flash-calcined metakaolin as cement replacement, Constr. Build. Mater. 55 (2014) 313–322, https://doi.org/10.1016/j.conbuildmat.2014.01.063.
[3] A.A. Ramezanianpour, H. Bahrami Jovein, Influence of metakaolin as supplementary cementing material on strength and durability of concretes, Constr. Build. Mater. 30 (2012) 470–479, https://doi.org/10.1016/j.conbuildmat.2011.12.050.
[4] K.L. Scrivener, V.M. John, E.M. Gartner, Eco-efficient cements: potential economically viable solutions for a low-CO2 cement-based materials industry, Cem. Concr. Res. 114 (2018) 2–26, https://doi.org/10.1016/j.cemconres.2018.03.015.
[5] M. Maier, N. Beuntner, and K.-C. Thienel, *An approach for the evaluation of local raw material potential for calcined clay as SCM, based on geological and mineralogical data: Examples from German clay deposits*, in *Calcined Clays for Sustainable Concrete*, S. Bishnoi, Editor. 2020, Springer: Singapore. p. 37–47. doi: https://doi.org/10.1007/978-981-15-2806-4_5.
[6] B. Lothenbach, K. Scrivener, R.D. Hooton, Supplementary cementitious materials, Cem. Concr. Res. 41 (2011) 1244–1256, https://doi.org/10.1016/j.cemconres.2010.12.001.
[7] E.H. Kadri, S. Aggoun, G. De Schutter, K. Ezziane, Combined effect of chemical nature and fineness of mineral powders on Portland cement hydration, Mater. Struct. 43 (2010) 665–673, https://doi.org/10.1617/s11527-009-9519-6.
[8] F. Zunino, K. Scrivener, The influence of the filler effect on the sulfate requirement of blended cements, Cem. Concr. Res. 126 (2019) 105918, https://doi.org/10.1016/j.cemconres.2019.105918.
[9] D. Jansen, C. Naber, D. Ectors, Z. Lu, X.M. Kong, F. Goetz-Neunhoeffer, J. Neubauer, The early hydration of OPC investigated by in-situ XRD, heat flow calorimetry, pore water analysis and 1H NMR: learning about adsorbed ions from a complete mass balance approach, Cem. Concr. Res. 109 (2018) 230–242, https://doi.org/10.1016/j.cemconres.2018.04.017.
[10] N. Beuntner and K.-C. Thienel, *Solubility and kinetics of calcined clay: study of interaction by pore solution*, in *2nd International Conference on the Chemistry of Construction Materials (ICCCM 2016)*, J. Plank, L. Lei, and T. Echt, Editors. (2016), Gesellschaft Deutscher Chemiker e.V.: Munich, Germany. p. 157–160.
[11] I.G. Richardson, The nature of C-S-H in hardened cements, Cem. Concr. Res. 29 (1999) 1131–1147, https://doi.org/10.1016/S0008-8846(99)00168-4.
[12] I.G. Richardson, The calcium silicate hydrates, Cem. Concr. Res. 38 (2008) 137–158, https://doi.org/10.1016/j.cemconres.2007.11.005.
[13] C.A. Love, I.G. Richardson, A.R. Brough, Composition and structure of C–S–H in white Portland cement–20% metakaolin pastes hydrated at 25 °C, Cem. Concr. Res. 37 (2007) 109–117, https://doi.org/10.1016/j.cemconres.2006.11.012.
[14] F. Avet, E. Boehm-Courjault, K. Scrivener, Investigation of C-A-S-H composition, morphology and density in Limestone Calcined Clay Cement (LC3), Cem. Concr. Res. 115 (2019) 70–79, https://doi.org/10.1016/j.cemconres.2018.10.011.
[15] J. E. Rossen, *Composition and morphology of C-A-S-H in pastes of alite and cement blended with supplementary cementitious materials*, in *Faculté des Sciences et Techniques de l'Ingénieur, Laboratoire des Matériaux de Construction*. (2014), École Polytechnique Fédérale de Lausanne: Lausanne. p. 154.DOI: doi: https://doi.org/10.5075/epfl-thesis-6294.
[16] N.K. Katyal, J.M. Sharma, A.K. Dhawan, M.M. Ali, K. Mohan, Development of rapid method for the estimation of reactive silica in fly ash, Cem. Concr. Res. 38 (2008) 104–106, https://doi.org/10.1016/j.cemconres.2007.08.020.
[17] DIN EN 197-1, Zement - Teil 1: Zusammensetzung, Anforderungen und Konformitätskriterien von Normalzement (Cement - Part 1: Composition, specifications and conformity criteria for common cements), (2011), Beuth-Verlag, p. 8.
[18] A. Buchwald, R. Kriegel, C. Kaps, and H.-D. Zellmann. *Untersuchung zur Reaktivität von Metakaolinen für die Verwendung in Bindemittelsystemen*. in *Gesellschaft Deutscher Chemiker e.V -Jahrestagung*. 2003. Munich, Germany.
[19] F. Avet, R. Snellings, A. Alujas Diaz, M. Ben Haha, K. Scrivener, Development of a new rapid, relevant and reliable (R^3) test method to evaluate the pozzolanic reactivity of calcined kaolinitic clays, Cem. Concr. Res. 85 (2016) 1–11, https://doi.org/10.1016/j.cemconres.2016.02.015.
[20] J. Ambroise, M. Murat, J. Pera, Hydration reaction and hardening of calcined clays and related minerals. IV. Experimental conditions for strength improvement on metakaolinite minicylinders, Cem. Concr. Res. 15 (1985) 83–88, https://doi.org/10.1016/0008-8846(85)90011-0.
[21] R. Fernandez, F. Martirena, K.L. Scrivener, The origin of the pozzolanic activity of calcined clay minerals: a comparison between kaolinite, illite and montmorillonite, Cem. Concr. Res. 41 (2011) 113–122, https://doi.org/10.1016/j.cemconres.2010.09.013.
[22] S. Hollanders, R. Adriaens, J. Skibsted, Ö. Cizer, J. Elsen, Pozzolanic reactivity of pure calcined clays, Appl. Clay Sci. 132–133 (2016) 552–560, https://doi.org/10.1016/j.clay.2016.08.003.
[23] A. Neißer-Deiters, S. Scherb, N. Beuntner, K.-C. Thienel, Influence of the calcination temperature on the properties of a mica mineral as a suitability study for the use as SCM, Appl. Clay Sci. 179 (2019) 105168, https://doi.org/10.1016/j.clay.2019.105168.
[24] J. Cabrera, M.F. Rojas, Mechanism of hydration of the metakaolin–lime–water system, Cem. Concr. Res. 31 (2001) 177–182, https://doi.org/10.1016/S0008-8846(00)00456-7.
[25] P.S. De Silva, F.P. Glasser, Phase relations in the system CaO•Al2O3•SiO2•H2O relevant to metakaolin - calcium hydroxide hydration, Cem. Concr. Res. 23 (1993) 627–639, https://doi.org/10.1016/0008-8846(93)90014-Z.
[26] M. Frías and J. Cabrera, *Influence of MK on the reaction kinetics in MK/lime and MK-blended cement systems at 20°C.* Cement and Concrete Research. 31 (2001) 519–527. doi: https://doi.org/10.1016/s0008-8846(00)00465-8.
[27] M. Murat, Hydration reaction and hardening of calcined clays and related minerals: I. Preliminary investigation on metakaolinite, Cem. Concr. Res. 13 (1983) 259–266, https://doi.org/10.1016/0008-8846(83)90109-6.
[28] M.F. Rojas, M.I. Sánchez de Rojas, The effect of high curing temperature on the reaction kinetics in MK/lime and MK-blended cement matrices at 60 °C, Cem. Concr. Res. 33 (2003) 643–649, https://doi.org/10.1016/s0008-8846(02)01040-2.
[29] C. He, B. Osbæck, E. Makovicky, Pozzolanic reactions of six principal clay minerals: activation, reactivity assessments and technological effects, Cem. Concr. Res. 25 (1995) 1691–1702, https://doi.org/10.1016/0008-8846(95)00165-4.
[30] S. Scherb, N. Beuntner, and K.-C. Thienel, *Reaction kinetics of the basic clays present in natural mixed clays*, in *Calcined Clays for Sustainable Concrete - Proceedings of the 2nd International Conference on Calcined Clays for Sustainable Concrete*, F. Martirena, A. Favier, and K. Scrivener, Editors. (2018), Springer Nature: La Havanna, Cuba. p. 427-433.DOI: doi: https://doi.org/10.1007/978-94-024-1207-9_69.
[31] S. Scherb, N. Beuntner, M. Köberl, and K.-C. Thienel, *The early hydration of cement with the addition of calcined clay - From single phyllosilicate to clay mixture*, in *20. Internationale Baustofftagung ibausil*, H.-B. Fischer and A. Volke, Editors. (2018), F. A. Finger-Institut für Baustoffkunde, Prof. Dr.-Ing. H.-M. Ludwig: Weimar, Germany. p. 658–666.
[32] B. Lothenbach, M. Zajac, Application of thermodynamic modelling to hydrated cements, Cem. Concr. Res. 123 (2019) 105779, https://doi.org/10.1016/j.cemconres.2019.105779.
[33] T. Matschei, B. Lothenbach, F.P. Glasser, The AFm phase in Portland cement, Cem. Concr. Res. 37 (2007) 118–130, https://doi.org/10.1016/j.cemconres.2006.10.010.
[34] S.T. Bergold, F. Goetz-Neunhoeffer, J. Neubauer, Quantitative analysis of C–S–H in hydrating alite pastes by in-situ XRD, Cem. Concr. Res. 53 (2013) 119–126, https://doi.org/10.1016/j.cemconres.2013.06.001.
[35] C. Kaps and A. Buchwald. *Property controlling influences on the generation of geopolymeric binders based on clay*. in *Geopolymer* 2002 *3rd International Conference*. 2002. Melbourne, Australia.
[36] A. Vollpracht, B. Lothenbach, R. Snellings, J. Haufe, The pore solution of blended cements: a review, Mater. Struct. (2015) 1–27, https://doi.org/10.1617/s11527-015-0724-1.
[37] DIN ISO 9277, Determination of the specific surface area of solids by gas adsorption - BET method, (2003), Beuth-Verlag, p. 19.
[38] DIN EN ISO 17892-3, Geotechnical investigation and testing - Laboratory testing of soil - Part 3: Determination of particle density, (2015), Beuth-Verlag, p. 21.
[39] DIN 18132, Soil, testing procedures and testing equipment - Determination of water absorption, (2012), Beuth-Verlag, p. 14.
[40] ISO 13320, Particle size analysis - Laser diffraction methods, (2009), p. 51.
[41] DIN EN ISO 11885, Water quality - Determination of selected elements by inductively coupled plasma optical emission spectrometry (ICP-OES), (2009), Beuth-Verlag, p. 37.
[42] S. Scherb, M. Köberl, N. Beuntner, K.-C. Thienel, J. Neubauer, Reactivity of metakaolin in alkaline environment: correlation of results from dissolution experiments with XRD quantifications, Materials. 13 (2020) 18, https://doi.org/10.3390/ma13102214.
[43] B. H. O'Connor and M. D. Raven, *Application of the Rietveld refinement procedure in assaying powdered mixtures.* Powder Diffraction. 3 (1988) 2–6. doi: https://doi.org/10.1017/S0885715600013026.
[44] D. Jansen, F. Goetz-Neunhoeffer, C. Stabler, J. Neubauer, A remastered external standard method applied to the quantification of early OPC hydration, Cem. Concr. Res. 41 (2011) 602–608, https://doi.org/10.1016/j.cemconres.2011.03.004.
[45] U. W. Arndt, D. C. Creagh, R. D. Deslattes, J. H. Hubbel, P. Indelicato, E. G. Kessler JR, and E. Lindroth, *Production and Properties of Radiation, Table 4.2.4.3. Mass attenuation coefficients (cm^2g^{-1})*. International Tables of Crystallography. Vol. C, Chapter 4. 2006: Springer Verlag.
[46] S. Scherb, N. Beuntner, K.-C. Thienel, J. Neubauer, Quantitative X-ray diffraction of free, not chemically bound water with the PONKCS method, J. Appl. Crystallogr. 51 (2018) 1535–1543, https://doi.org/10.1107/S1600576718012888.
[47] J. Ambroise, M. Murat, J. Péra, Hydration reaction and hardening of calcined clays and related minerals V. Extension of the research and general conclusions, Cem. Concr. Res. 15 (1985) 261–268, https://doi.org/10.1016/0008-8846(85)90037-7.
[48] P.S. De Silva, F.P. Glasser, Hydration of cements based on metakaolin: thermochemistry, Adv. Cem. Res. 3 (1990) 167–177, https://doi.org/10.1680/adcr.1990.3.12.167.
[49] V.S. Ramachandran, R.M. Paroli, J.J. Beaudoin, A.H. Delgado, Handbook of Thermal Analysis of Construction Materials, Elsevier Science, Norwich, NY, 2002.
[50] L. Baquerizo, T. Matschei, and K. Scrivener, *Impact of water activity on the water content of cement hydrates*, in *18th Internationale Baustofftagung, ibausil*, J. Stark, Editor. (2012), F. A. Finger Institut: Weimar, Germany. p. 1/0249–1/0260.
[51] B. Lothenbach, G. Le Saout, E. Gallucci, K. Scrivener, Influence of limestone on the hydration of Portland cements, Cem. Concr. Res. 38 (2008) 848–860, https://doi.org/10.1016/j.cemconres.2008.01.002.

[52] B.K. Marsh, R.L. Day, Pozzolanic and cementitious reactions of fly ash in blended cement pastes, Cem. Concr. Res. 18 (1988) 301–310, https://doi.org/10.1016/0008-8846(88)90014-2.
[53] T. Degen, M. Sadki, E. Bron, U. König, G. Nénert, The HighScore suite, Powder Diffract. 29 (2014) S13–S18, https://doi.org/10.1017/S0885715614000840.
[54] H.M. Rietveld, Line profiles of neutron powder-diffraction peaks for structure refinement, Acta Crystallogr. 22 (1967) 151–152, https://doi.org/10.1107/S0365110X67000234.
[55] H. M. Rietveld, *An Algol Program for the Refinement of Nuclear and Magnetic Structures by the Profile Method*, in *RCN*. (1969), Reactor Centrum Nederland.
[56] N.V.Y. Scarlett, I.C. Madsen, Quantification of phases with partial or no known crystal structures, Powder Diffract. 21 (2006) 278–284, https://doi.org/10.1154/1.2362855.
[57] M. C. Neuburger, *Präzisionsmessung der Gitterkonstante von Silicium*, in *Zeitschrift für Kristallographie - Crystalline Materials*. (1935). p. 313.DOI: doi: https://doi.org/10.1524/zkri.1935.92.1.313.
[58] K. Kihara, G. Donnay, Anharmonic thermal vibrations in ZnO, Can. Mineral. 23 (1985) 647–654.
[59] Á.G. De La Torre, S. Bruque, J. Campo, M.A.G. Aranda, The superstructure of C3S from synchrotron and neutron powder diffraction and its role in quantitative phase analyses, Cem. Concr. Res. 32 (2002) 1347–1356, https://doi.org/10.1016/S0008-8846(02)00796-2.
[60] Y. Le Page, G. Donnay, Refinement of the crystal structure of low-quartz, Acta Crystallogr. Sect. B: Struct. Sci. 32 (1976) 2456–2459, https://doi.org/10.1107/S0567740876007966.
[61] M. Horn, C.F. Schwerdtfeger, E.P. Meagher, Refinement of the structure of anatase at several temperatures, Z. Kristallogr. Krist. 136 (1972) 273–281, https://doi.org/10.1524/zkri.1972.136.3-4.273.
[62] G. Ivaldi, G. Ferraris, N. Curetti, R. Compagnoni, Coexisting 3T and 2M1 polytypes of phengite from Cima Pal (Val Savenca, western Alps): chemical and polytypic zoning and structural characterisation, Eur. J. Mineral. 13 (2001) 1025–1034, https://doi.org/10.1127/0935-1221/2001/0013-1025.
[63] V.A. Drits, B.B. Zviagina, D.K. McCarty, A.L. Salyn, Factors responsible for crystal-chemical variations in the solid solutions from illite to aluminoceladonite and from glauconite to celadonite, Am. Mineral. 95 (2010) 348–361, https://doi.org/10.2138/am.2010.3300.
[64] S.A. Markgraf, R.J. Reeder, High-temperature structure refinements of calcite and magnesite, Am. Mineral. 70 (1985) 590–600.
[65] I. Oftedal, The lattice constants of CaO, CaSe, CaS, CaTe, Z. Phys. Chem. 128 (1927) 154–158.
[66] W.R. Busing, H.A. Levy, Neutron diffraction study of calcium hydroxide, J. Chem. Phys. 26 (1957) 563–568, https://doi.org/10.1063/1.1743345.
[67] M. Catti, G. Ferraris, G. Ivaldi, Thermal strain analysis in the crystal structure of muscovite at 700 °C, Eur. J. Mineral. 1 (1989) 625–632, https://doi.org/10.1127/ejm/1/5/0625.
[68] A. Kirfel, G. Will, Charge density in anhydrite, CaSO4, from X-ray and neutron diffraction measurements, Acta Crystallogr. B 36 (1980) 2881–2890, https://doi.org/10.1107/S0567740880010461.
[69] P.F. Schofield, C.C. Wilson, K.S. Knight, I.C. Stretton, Temperature related structural variation of the hydrous components in gypsum, Z. Kristallogr. Krist. 215 (2000) 707, https://doi.org/10.1524/zkri.2000.215.12.707.
[70] C. Hoffmann and T. Armbruster, *Clinotobermorite, Ca5[Si3O8(OH)]2 · 4 H2O - Ca5 [Si6O17] · 5 H2O, a natural C-S-H(I) type cement mineral: determination of the substructure*, in *Zeitschrift für Kristallographie - Crystalline Materials*. (1997). p. 864. DOI: doi: https://doi.org/10.1524/zkri.1997.212.12.864.
[71] F. Goetz-Neunhoeffer, J. Neubauer, Refined ettringite (Ca6Al2(SO4)3(OH)12·26H2O) structure for quantitative X-ray diffraction analysis, Powder Diffract. 21 (2005) 4–11, https://doi.org/10.1154/1.2146207.
[72] R. Allmann, Refinement of the hybrid layer structure [Ca2Al(OH)6]+ [1/2SO4 3H2O]⁻, Neu. Jb. Mineral 3 (1977) 136–144.
[73] H.P. Jepsen, R. Allmann, Die Struktur des Hydrotalkit, Neues Jahrbuch für Mineralogie, Monatshefte, 1969, pp. 544–551.
[74] H. Pöllmann and J. Kuzel H., *PDF data sheet: 42–0062, Calcium Aluminum Sulfate Hydrate*. (1990): Mineralogical Institute of University Erlangen, ICDD Grant-in-Aid.
[75] G. Pawley, Unit-cell refinement from powder diffraction scans, J. Appl. Crystallogr. 14 (1981) 357–361, https://doi.org/10.1107/S0021889881009618.
[76] A. T. Allen, J. J.; Jennings, H. M. , *Composition and density of nanoscale calcium-silcate-hydrate in cement.* Nature Materials. Vol. 6 Nr. 4 (2007) 311–316. doi: https://doi.org/10.1038/nmat1871.
[77] D. Jansen, S.T. Bergold, F. Goetz-Neunhoeffer, J. Neubauer, The hydration of alite: a time-resolved quantitative X-ray diffraction approach using the G-factor method compared with heat release, J. Appl. Crystallogr. 44 (2011) 895–901, https://doi.org/10.1107/S0021889811025933.
[78] C. He, E. Makovicky, B. Osbæck, Thermal stability and pozzolanic activity of calcined kaolin, Appl. Clay Sci. 9 (1994) 165–187, https://doi.org/10.1016/0169-1317(94)90018-3.
[79] C. He, E. Makovicky, B. Osbæck, Thermal stability and pozzolanic activity of calcined illite, Appl. Clay Sci. 9 (1995) 337–354, https://doi.org/10.1016/0169-1317(94)00033-M.
[80] C. He, E. Makovicky, B. Osbæck, Thermal stability and pozzolanic activity of raw and calcined mixed-layer mica/smectite, Appl. Clay Sci. 17 (2000) 141–161, https://doi.org/10.1016/S0169-1317(00)00011-9.
[81] C. Hesse, F. Goetz-Neunhoeffer, J. Neubauer, A new approach in quantitative in-situ XRD of cement pastes: correlation of heat flow curves with early hydration reactions, Cem. Concr. Res. 41 (2011) 123–128, https://doi.org/10.1016/j.cemconres.2010.09.014.
[82] G. Kundt, H. Krentz, and Ä. Glass, *Epidemiologie und Medizinische Biometrie (Epidemiology and Medical Biometry)*. Berichte aus der Statistik. 2011, Aachen: Shaker Verlag. 246.
[83] F. Zunino, K. Scrivener, Factors influencing the sulfate balance in pure phase C3S/C3A systems, Cem. Concr. Res. 133 (2020) 106085, https://doi.org/10.1016/j.cemconres.2020.106085.
[84] C. Naber, S. Stegmeyer, D. Jansen, F. Goetz-Neunhoeffer, J. Neubauer, The PONKCS method applied for time resolved XRD quantification of supplementary cementitious material reactivity in hydrating mixtures with ordinary Portland cement, Constr. Build. Mater. 214 (2019) 449–457, https://doi.org/10.1016/j.conbuildmat.2019.04.157.
[85] L. Lei, J. Plank, A study on the impact of different clay minerals on the dispersing force of conventional and modified vinyl ether based polycarboxylate superplasticizers, Cem. Concr. Res. 60 (2014) 1–10, https://doi.org/10.1016/j.cemconres.2014.02.009.
[86] R. Sposito, N. Beuntner, and K.-C. Thienel, *Characteristics of components in calcined clays and their influence on the efficiency of superplasticizers.* Cement and Concrete Composites. 110 (2020). doi: https://doi.org/10.1016/j.cemconcomp.2020.103594.
[87] R.J. Myers, G. Geng, E.D. Rodriguez, P. da Rosa, A.P. Kirchheim, P.J.M. Monteiro, Solution chemistry of cubic and orthorhombic tricalcium aluminate hydration, Cem. Concr. Res. 100 (2017) 176–185, https://doi.org/10.1016/j.cemconres.2017.06.008.
[88] R.J. Myers, G. Geng, J. Li, E.D. Rodríguez, J. Ha, P. Kidkhunthod, G. Sposito, L. N. Lammers, A.P. Kirchheim, P.J.M. Monteiro, Role of adsorption phenomena in cubic tricalcium aluminate dissolution, Langmuir. 33 (2017) 45–55, https://doi.org/10.1021/acs.langmuir.6b03474.
[89] M. Antoni, J. Rossen, F. Martirena, K. Scrivener, Cement substitution by a combination of metakaolin and limestone, Cem. Concr. Res. 42 (2012) 1579–1589, https://doi.org/10.1016/j.cemconres.2012.09.006.
[90] T. Matschei, B. Lothenbach, F.P. Glasser, The role of calcium carbonate in cement hydration, Cem. Concr. Res. 37 (2007) 551–558, https://doi.org/10.1016/j.cemconres.2006.10.013.

8.5 The early hydration of cement with the addition of calcined clay – From single phyllosilicate to clay mixture

Reprint

Published in Proceedings of the 20th International Conference on Building Materials 2018, Weimar, Germany, ISBN: 978-3-00-059950-7

Authors: S. Scherb, N. Beuntner, M. Köberl, K.-Ch. Thienel

Authors: Scherb, S.; Beuntner, N., Köberl, M.; Thienel, K.-Ch.

The early hydration of cement with the addition of calcined clay From single phyllosilicate to clay mixture

1. Introducti

High-performance supplementary cementitious materials (SCM) will be required in the future for the optimization of cements with regard to their ecological and technological properties and in order to satisfy the predicted worldwide increase in cement demand. In addition to established binders, calcined clays are an attractive alternative to existing additives due to their worldwide availability and they are also considered to be an energy-efficient material. Calcined mixed layer clays contain, in addition to kaolinite, other phyllosilicates and secondary components and are particularly interesting for the cement industry. Due to possible higher substitution rates they are considered particularly promising for the future [1]. The influence of calcined clays on cement hydration results from chemical-pozzolanic reaction and physical effects. Investigations on the early hydration of cementitious systems with the addition of calcined clays [2, 3] indicate an interaction between pozzolanic reaction and cement hydration already within the first hours, which exceeds the often described filler and nucleation effect [4, 5]. The pozzolanic reaction kinetics of calcined clays in the clinker-free model system was first described by Beuntner [6] and Scherb et al. [7]. In addition to the content and type of the phyllosilicates and the solubility behavior of their silicon and aluminum ions, the authors showed that the formation of first reaction products in early hydration is controlled by the content of sulfate ions in the model pore solution. In this paper, the interaction of pozzolanic reaction of different calcined phyllosilicates and a calcined mixed layer clay with early cement hydration is examined. It is shown to what extent calcined clays influence hydration kinetics and provide a pozzolanic contribution during the early hydration.

2. Materials and methods

2.1. Characterization of calcined materials

For the test series three different preferably pure phyllosilicates (kaolinite, illite and muscovite) and one mixed layer clay (CT) were used. The procedures for determining the calcination temperatures and performing the calcination are described in [7]. The industrial calcination process of the mixed layer clay in a rotary kiln is described in detail in [8]. BET specific surface area [9], particle density, optimum water demand [10] and water absorption capacity [11] of the calcined clays were measured (Tab. 1). Further their particle size distribution [12] (Fig. 1) was determined.

Tab. 1: Characterization of metakaolin (MK), metaillite (MI), metamuscovite (MM) and calcined mixed layer clay (CT)

	MK	MI	MM	CT
BET [m^2/g]	14.1	82.4	10.9	5.3
Particle density [g/cm^3]	2.42	2.76	2.70	2.63
Optimum water demand [%]	43.4	38.6	55.4	30.0
Water absorption capacity [%]	77.0	76.4	154.5	73.7

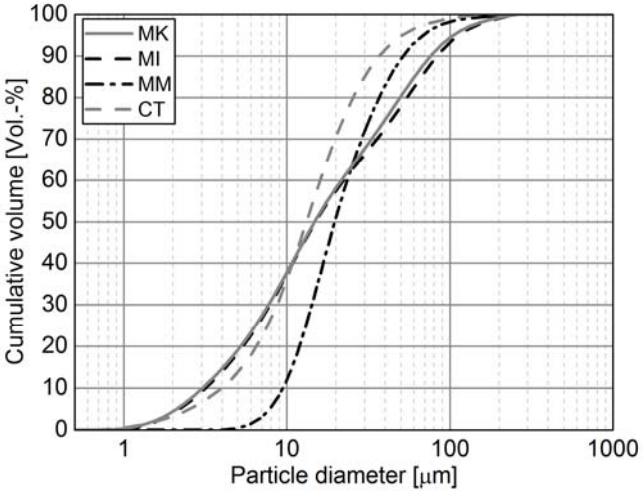

Fig. 1: Particle size distribution of the calcined materials

The mineralogical composition (Tab. 2) of the calcined materials was determined on powder samples using X-ray diffraction (XRD). Zincite was used as internal standard to quantify the x-ray amorphous content of the samples.

Tab. 2: Mineralogical composition of the calcined materials

Phases (wt. %)	MK	MI	MM	CT
Quartz	-	-	-	18.3
Kaolinite	2.5	-	-	-
Anatase	1.1	-	-	-
Phengite	3.3	-	-	-
Carbonate	-	3.6	-	0.4
Illite	-	31.3	-	4.4
Lime	-	0.5	-	-
Portlandite	-	1.5	-	-
Feldspar	-	-	-	7.9
Muscovite (Mica)	-	-	76.3	(3.8)
Sulfate	-	-	-	1.1
Secondary silicates	-	-	-	0.6
Ore	-	-	-	1.8
X-ray amorphous	93.1	63.1	23.7	59.3

2.2. Experimental program

The test series concentrate on the role of the calcined materials during early hydration. Therefore an ordinary Portland cement CEM I 42.5 R was used at a water-binder-ratio (w/b) of 0.6 as reference system. The measurements including the calcined materials were carried out with a substitution rate of 20 % by mass.

In situ XRD and isothermal calorimetry ran up to 48 h while thermogravimetric (TG) measurements after 6 h and 48 h were performed to investigate the reaction kinetics of the early hydration. Equipment and procedure of in situ XRD and isothermal calorimetry are described in [7]. The heat flow of calorimetric measurements was normalized to 1 g of cement. From the calorimeter data, the minimum heat flow Q_{min} and time t_{min} of the minimum during the dormant period were determined. Furthermore, the heat flow and times of the two maxima of the main reaction (Q_{1max}, t_{1max}; Q_{2max}, t_{2max}) were obtained. The analysis of the in situ XRD was done qualitatively by creating level plots with the software HighScore Plus 4.6. In addition, the times of dissolution of the sulfate carriers gypsum and anhydrite, the maximum ettringite content and the first formation of the hydrate phases portlandite (CH) and hemicarboaluminate (AFm-Hc) were identified from the diffractograms.

Thermogravimetric (TG) measurements were performed with Netzsch STA 449 F3 Jupiter with a heating rate of 2 K/min on samples stopped with acetone after 6 respectively 48 h [3]. The binding water was evaluated in two temperature steps from 20 to 140 °C (H_I) and 140 – 400 °C (H_{II}) according to equation 1 where $\Delta m_{T1\text{-}T2}$ is the mass difference of the temperature stage and m_w is the weighted mass of the stopped sample [3].

$$H\ [wt\%] = \frac{\Delta m_{T1-T2}}{m_w} \times 100 \qquad (1)$$

The dehydration reaction of portlandite in the temperature range between 450 °C and 530 °C was evaluated using the tangent method according to Marsh and Day [13]. The calculation of the CH content in g/100 g cement is done according to equation 2 from the mass loss Δm_{CH} in the temperature range, the cement content in the sample f_c, the sample weight m_w and the molar mass of CH (M_{CH}) and water (M_H).

$$CH\ \left[\frac{g}{100g}\,cement\right] = \frac{\frac{M_{CH}}{M_H} \times \Delta m_{CH}}{f_c \times m_w} \times 100 \qquad (2)$$

3. Experimental results and discussion

3.1. Isothermal calorimetry up to 48 h

Fig. 2 shows the heat flow and the hydration heat of the systems investigated. The phyllosilicates MK, MI and MM have a significant influence on the heat flow of the cement during early hydration. Both, the dormant period and the main reaction are affected. While MM shortens the dormant period and the minimum occurs already after 2 h, the measurement with MK shows no change in the time. For MI, the end of the dormant period is postponed by one hour. It is noticeable that for all three phyllosilicates the minimum heat flow during the rest period is clearly higher than that of the reference. Here MI shows the highest heat flow. Conversely, the measurement with CT shows hardly any difference during the dormant period compared to the reference.

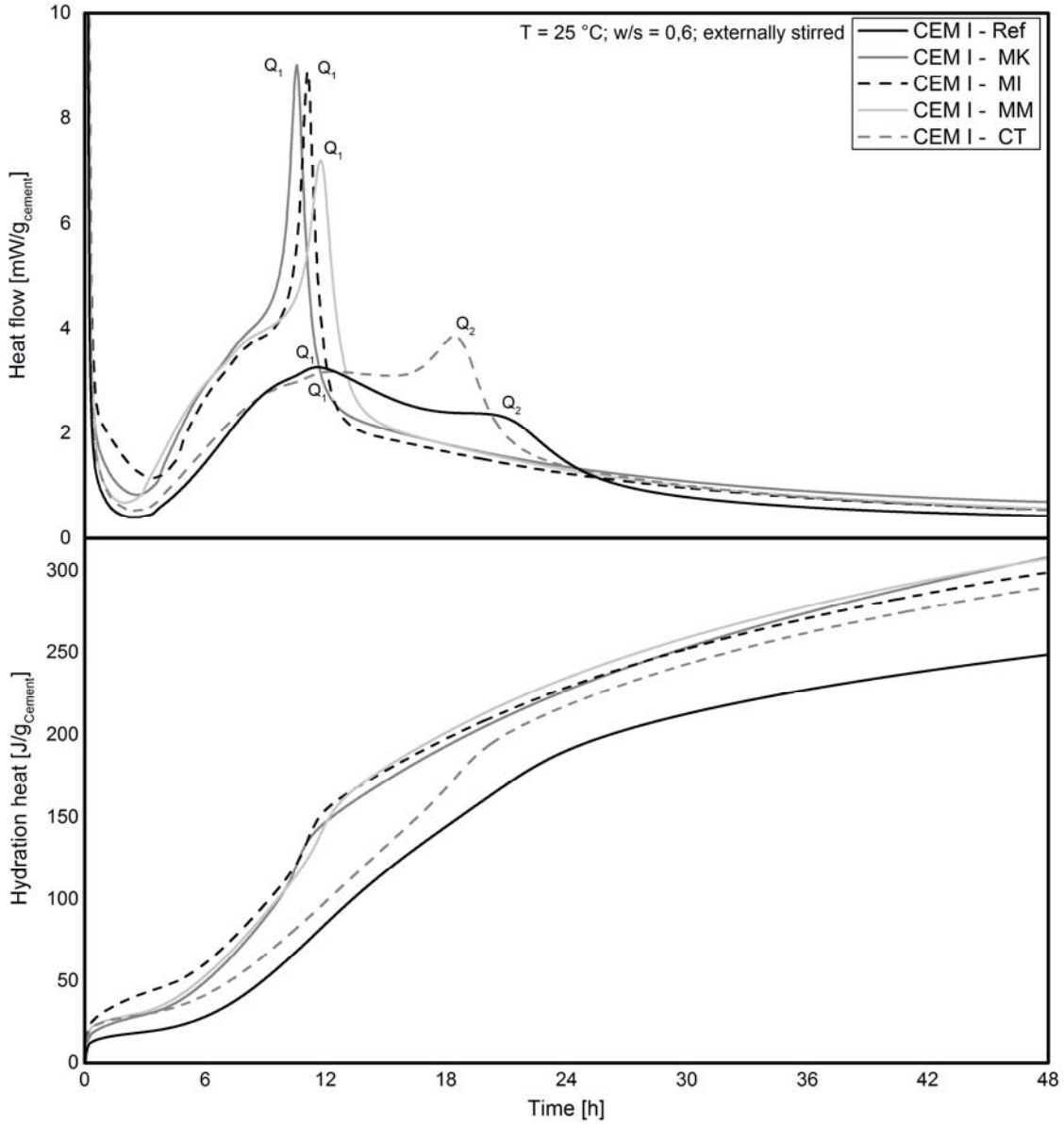

Fig. 2: Heat flow and hydration heat of systems investigated over 48 h

Tab. 3: Heat flow minima or maxima (Q [mW/g$_{cement}$]) with the corresponding time (t [h])

	Q_{min}	t_{min}	Q_{1max}	t_{1max}	Q_{2max}	t_{2max}
Ref	0.4	2.5	3.3	11.6	2.3	20.5
MK	0.8	2.6	9.0	10.6	-	-
MI	1.2	3.4	8.9	11.1	-	-
MM	0.7	2.0	7.2	11.8	-	-
CT	0.5	2.5	3.2	12.3	3.9	18.4

An accelerated reaction is observed for the calcined phyllosilicates MK, MI and MM after the dormant period, which changes over to a strongly pronounced heat flow peak after 10.6 to 11.8 h (Q_{1max}). According to Beuntner [3], this dominant heat peak results from

an overlapping of the silicate and aluminate clinker reaction. The heat flow at the beginning of the acceleration period is not only attributed to the alite dissolution and portlandite formation [14], but results also from a continuous ettringite formation. A separation of the two heat flow maxima during the main period is therefore not possible for the calcined phyllosilicates. The significant decrease of the heat flow after the maximum is conspicuous, as already observed by Antoni [15] for metakaolin-blended systems. In the CT system, the heat flow maximum Q_{1max} is only marginally affected. In the further reaction progress, a clear second peak occurs after 18.4 h. In case of CT, this second maximum is caused by an increased formation of aluminate hydrate phases (ettringite and AFm-phases) and by inhibited crystallization of portlandite [3]. The aluminate reaction plays a decisive role in the interaction with calcined clays and is examined in detail by using in situ XRD.

3.2.In situ XRD

Fig. 3 shows the level plot of the investigated systems from 8.5 to 18.5 °2θ. The time of the dissolution of the gypsum (G) and the formation of hemicarboaluminate (AFm-Hc) are shown in this figure. The other reflexes were designated with the respective phase and the corresponding hkl. The in situ XRD investigations confirm the acceleration of the aluminate reaction due to the addition of calcined clays. The dissolution of the gypsum accelerates from 12.5 h for the reference to about 7 h for MK and CT and 5 h for MI and MM. The solution of anhydrite is also accelerated (Tab. 4). While in the reference only a slight formation of AFm-Hc occurs after 42 h, its formation arises significantly earlier (after 12 to 14 h) with the addition of the calcined phyllosilicates (MK, MI, MM). With CT the AFm-Hc formation takes place after 22 h. The time of maximum ettringite formation correlates well with the maximum heat flow Q_{1max} for the phyllosilicates and Q_{2max} for CT. The clinker phase C_3A is dissolved completely at that time for all calcined clays, while undissolved C_3A is still present in the reference system at the time of maximum ettringite formation (30 h) and also at the end of the measurement after 48 h.

The influence on the silicate reaction is more difficult to determine from the in situ XRD measurements. Although the calorimetry measurements reveal an acceleration of the silicate reaction, this cannot be confirmed by the qualitative analysis of the XRD measurements. An acceleration of the silicate reaction cannot be detected from the formation of CH, which takes place between 4 and 7 h for all measurements. A summary of the times of dissolution of the sulfate carriers and the formation of the hydrate phases is given in Tab. 4.

According to Beuntner [3, 6], the formation of aluminate hydrate phases (ettringite and AFm-phases) is favored with binding of CH when calcined clays are added. This relationship can be proven in clinker-free systems as a pozzolanic contribution of calcined clays during early hydration. Scherb et al. [7] point out the special role of the sulfate carrier.

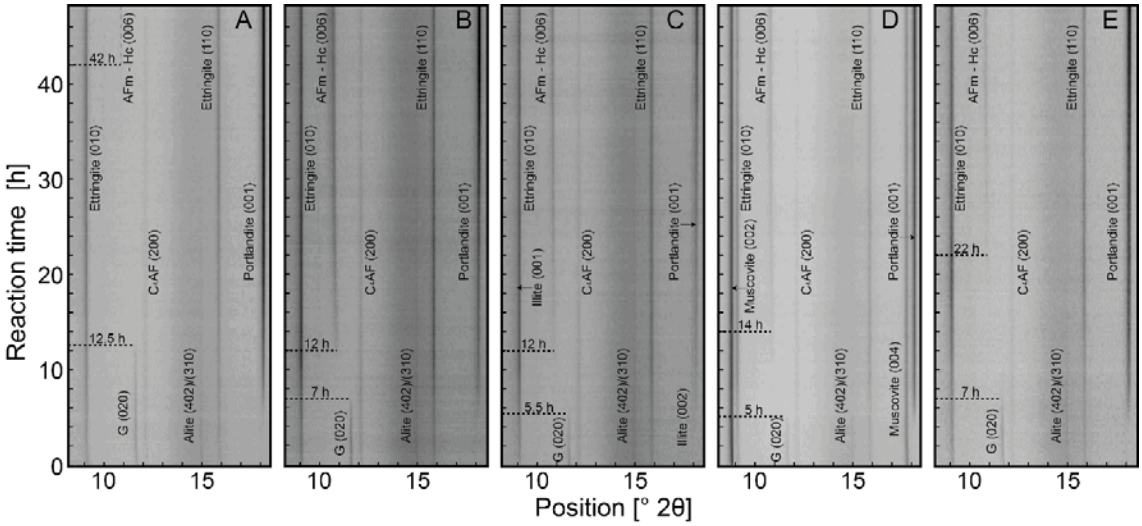

Fig. 3: Levelplots from 8.5 to 18.5 °2Θ for 48 h of the Ref (A), MK (B), MI (C), MM (D) and CT (E)

Tab. 4: Summary of the times [h] of gypsum and anhydrite dissolution, maximum ettringite content, as well as the first CH and AFm-Hc formation

	Gypsum	Anhydrite	CH	AFm-Hc	Ettringite
Ref	12.5	14.5	5	42	30
MK	7	10	5	12	10.5
MI	5.5	10	7	12	11
MM	5	8	4	14	11.5
CT	7	11	5	22	18.5

3.3. Thermogravimetric measurements after 6 and 48 h

Thermogravimetric (TG) investigations allow an evaluation of the reaction progress via the water binding of the hydrate phases and the formation of strength-building CSH phases from the cement reaction via the release of portlandite.

The bound water of the investigated systems ranges between 3.1 and 4.4 wt% after 6 h. Unexpectedly, MI shows the highest amount of bound water, which correlates with the highest hydration heat after 6 h (Fig. 2) and a fast sulfate carrier dissolution. The higher degree of reaction after the first 6 h of the system with MI compared to MK can be explained by higher BET surface area (Tab. 1) with approximately the same particle size distribution (Fig. 1). An independent pozzolanic contribution can be excluded for MI at this time. The ion solubility and thus the chemical-pozzolanic contribution of MI is significantly lower than that of MK [7]. In total, the bound water of the investigated systems is in the range of the bound water of the Ref after 6 h. Thus, regardless of their chemical-mineralogical compositions or granulometric properties, the calcined clays significantly influence the solution equilibrium of cementitious systems and the early hydration kinetics within the first hours. The fraction of aluminate hydrate phases (H_{II}(140-400 °C)) increases with higher Al-solubility of the phyllosilicates. While for MI (Si/Al = 1.86 [7]) a water binding in stage II of 4.5 wt% was determined, it is 5.0 wt% for MK (Si/Al = 1.07 [7]). In accordance with the heat flow calorimetry, the CH content after

6 h for MK, MI and MM is clearly above the CH content of the reference mixture. This confirms an accelerated C_3S reaction for these systems. In the further reaction progress up to 48 h the differences become less obvious and the bound water is between 10.0 and 11.2 wt%. For Ref, MI and MK an approximately equal content of bound water can be detected, while for MM and CT it is 1 wt% lower. The CH content is significantly higher only for MK than in Ref. For MM and CT the CH contents are in the range of Ref, for MI it is even slightly lower. The evaluation of the pozzolanic reaction contribution in early hydration via the determined CH content seems difficult, since physical influences on the C_3S reaction overlap with the chemical-pozzolanic effects.

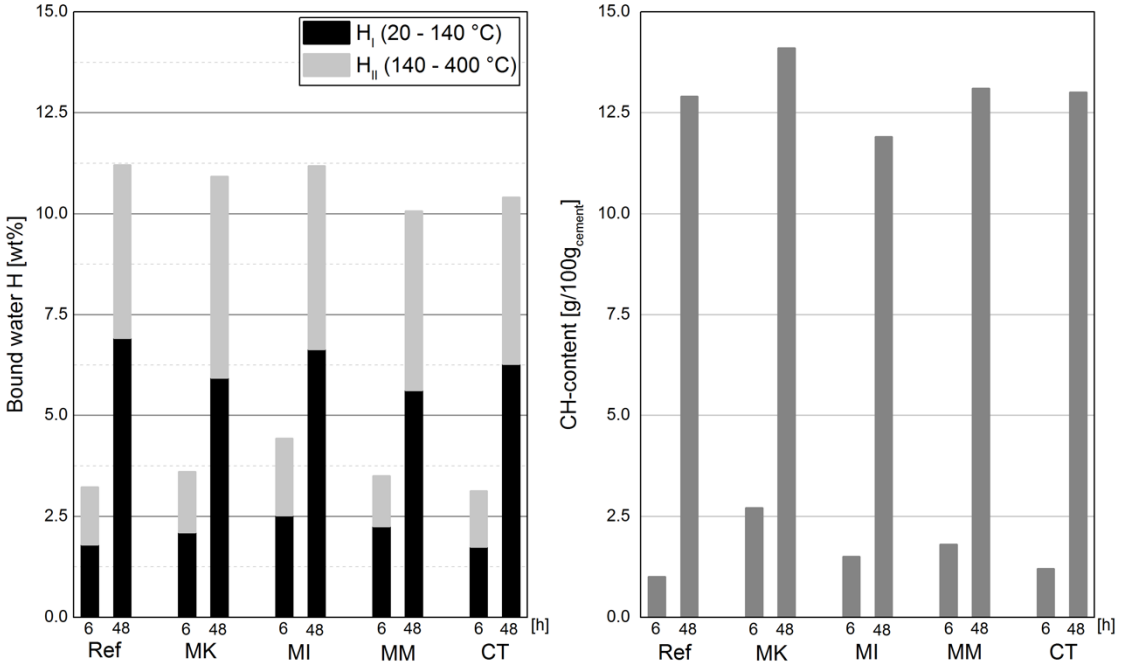

Fig. 4: Amount of bound water H (left) and the CH content (right) of the systems investigated after 6 and 48 h

4. Discussi

The investigations indicate for cements with addition of calcined clays that the early hydration in the first 48 h is chemically controlled by the available ions and the surface chemistry of the respective phyllosilicates. The physical influence seems to be caused less due to the particle size distribution of the calcined clays but more due of the outer and inner surfaces. Also for calcined clays with lower ion solubility (MM) high heat flow rates and hydration heat (comparable to those of highly reactive metakaolin) can be determined. The chemical-mineralogical influence of the calcined clays investigated can be represented via the measured bound water in H_I and H_{II}. After 48 h, there was a tendency for a higher amount of bound water in H_{II} due to preferred ettringite formation. The AFm-Hc formation occurs for the phyllosilicates MK, MI, MM already after 12 to 14 h and thus significantly earlier than in the Ref (42 h). Differences between the individual phyllosilicates cannot be figured out with the selected methods. The investigations shown here do not allow a separate consideration of the effects of chemical-pozzolanic reaction and physical effects. Rather, it can be stated that the described effect and influence on early hydration by the granulometry of SCM must be extended by

considering the very special surface properties of phyllosilicates and by taking into account a chemical contribution from the aluminate reaction. A special role is attributed to metamuscovite, which has a clear influence on the heat flow and the dissolution of the sulfate carrier despite its low ion solubility, coarse particle size distribution and low BET surface area. These initial results indicate that effects of water adsorption behavior should be considered in addition.

5. Referen

1. Thienel, K.-C. and N. Beuntner, *Calcinierte Tone und ihr Potenzial für die moderne Betontechnologie*, in *14. Symposium Baustoffe und Bauwerkserhaltung KIT - Betone der Zukunft - Herausforderungen und Chancen*, U. Nolting, et al., Editors. 2018, KIT Scientific Publishing: Karlsruhe. p. 37-48.
2. Danner, T., T. Ostnor, and H. Justnes, *Calcined Marl as a Pozzolan for Sustainable Development of the Cement and Concrete Industry*, in *ACI SP 289 - 12th International Conference on Recent Advances in Concrete Technology and Sustainability Issues*, T.C. Holland, P.R. Gupta, and V.M. Malhotra, Editors. 2012, Sheridan Books: Prag. p. 357-368.
3. Beuntner, N., *Zur Eignung und Wirkungsweise calcinierter Tone als reaktive Bindemittelkomponente in Zement*, in *Fakultät für Bauingenieurwesen und Umweltwissenschaften*. 2017, Universität der Bundeswehr München: Neubiberg.
4. Lothenbach, B., K. Scrivener, and R.D. Hooton, *Supplementary cementitious materials.* Cement and Concrete Research, 2011. **41**(12): p. 1244-1256.
5. Cyr, M., P. Lawrence, and E. Ringot, *Efficiency of mineral admixtures in mortars: Quantification of the physical and chemical effects of fine admixtures in relation with compressive strength.* Cement and Concrete Research, 2006. **36**(2): p. 264-277.
6. Beuntner, N. and K.-C. Thienel, *Solubility and kinetics of calcined clay: study of interaction by pore solution*, in *2nd International Conference on the Chemistry of Construction Materials (ICCCM 2016)*, J. Plank, L. Lei, and T. Echt, Editors. 2016, Gesellschaft Deutscher Chemiker e.V.: Munich, Germany. p. 157-160.
7. Scherb, S., N. Beuntner, and K.-C. Thienel, *Reaction kinetics of the basic clays present in natural mixed clays*, in *Calcined Clays for Sustainable Concrete - Proccedings of the 2nd International Conference on Calcined Clays for Sustainable Concrete*, F. Martirena, A. Favier, and K. Scrivener, Editors. 2018, Springer Nature: La Havanna, Cuba. p. 427-433.
8. Beuntner, N., *Leistungsfähigkeit großtechnisch calcinierter Tone und deren Wirksamkeit in zementären Systemen*, in *Innovationen in Beton - 1. DAfStb-Jahrestagung mit 54. Forschungskolloquium*, R. Breitenbücher and P. Mark, Editors. 2013, Deutscher Ausschuss für Stahlbeton: Bochum. p. 239-244.
9. DIN ISO 9277, *Bestimmung der spezifischen Oberfläche von Feststoffen durch Gasadsorption nach dem BET-Verfahren (Determination of the specific surface area of solids by gas adsorption using the BET method)*. 2003, Beuth-Verlag: Berlin. p. 19.
10. DIN EN 196-3, *Prüfverfahren für Zement - Teil 3: Bestimmung der Erstarrungszeiten und der Raumbeständigkeit*. 2009.
11. DIN 18132, *Bestimmung des Wasseraufnahmevermögenes*. 2012, Beuth-Verlag.

12. ISO 13320, *Particle size analysis - Laser diffraction methods*. 2009. p. 51.

13. Marsh, B.K. and R.L. Day, *Pozzolanic and cementitious reactions of fly ash in blended cement pastes.* Cement and Concrete Research, 1988. **18**(2): p. 301-310.

14. Hesse, C., F. Goetz-Neunhoeffer, and J. Neubauer, *A new approach in quantitative in-situ XRD of cement pastes: Correlation of heat flow curves with early hydration reactions.* Cement and Concrete Research, 2011. **41**(1): p. 123-128.

15. Antoni, M., et al., *Cement substitution by a combination of metakaolin and limestone.* Cement and Concrete Research, 2012. **42**(12): p. 1579-1589.

Authors

Dipl. Min. Sebastian Scherb
Bundeswehr University Munich
Institute for Construction Materials
Werner-Heisenberg-Weg 39
85579 Neubiberg, Germany
sebastian.scherb@unibw.de

Dr.-Ing. Nancy Beuntner
Bundeswehr University Munich
Institute for Construction Materials
Werner-Heisenberg-Weg 39
85579 Neubiberg, Germany
nancy.beuntner@unibw.de

Dr. rer. nat. Mathias Köberl
Bundeswehr University Munich
Institute for Construction Materials
Werner-Heisenberg-Weg 39
85579 Neubiberg, Germany
mathias.koeberl@unibw.de

Univ.-Prof. Dr.-Ing. Karl-Christian Thienel
Bundeswehr University Munich,
Institute for Construction Materials
Werner-Heisenberg-Weg 39
85579 Neubiberg, Germany
christian.thienel@unibw.de

9 Appendix

A list of all publications prepared during the doctorate:

2021:

Peer-reviewed Journals:

- S. Scherb, M. Köberl, N. Beuntner, K.-C. Thienel, J. Neubauer, Reaction kinetics during early hydration of calcined phylloslictes in clinker-free model systems. Cement and Concrete Research 2021, 143, 106382, doi: 10.1016/j.cemconres.2021.106382
- Maier, M.; Scherb, S.; Neißer-Deiters, A.; Beuntner, N.; Thienel, K.-C. Hydration of cubic tricalcium aluminate in the presence of calcined clays. *J Am Ceram Soc* **2021**, *104*, 1-13, doi:https://doi.org/10.1111/jace.17745

2020:

Peer-reviewed Journals:

- S. Scherb, M. Köberl, N. Beuntner, K.-C. Thienel, J. Neubauer, Reactivity of metakaolin in alkaline environment: Correlation of results from dissolution experiments with XRD quantifications. *Materials* **2020**, *13-102214*, doi: 10.3390/ma13102214
- C. Oullet-Plamondon, S. Scherb, M. Köberl, K-Ch. Thienel, Acceleration of cement blended with calcined clays. Construction and Building Materials. 245 (2020) 118439, doi: 10.1016/j.conbuildmat.2020.118439

2019:

Peer-reviewed Journals:

- A. Neißer-Deiters, S. Scherb, N. Beuntner, K.-Ch. Thienel, Influence oft he calcination temperature on the properties of a mica mineral as a suitability study for the use as SCM. Applied clay Science. 179 (2019) 105168. doi: 10.1016/j.clay.2019.105168

Conference Proceedings:

- R. Sposito, M. Schmid, N. Beuntner, S. Scherb, J. Plank, K.-Ch. Thienel, Early hydration behavior of blended cementitious systems containing calcined clays and superplasticizer. in: 15th International congress on the Chemistry of Cement, J. Gemrich (Ed.), Research Institute of binding materials Prague, (2019), paper no 57, p.10

2018:

Peer-reviewed Journals:

- S. Scherb, N. Beuntner, K.-C. Thienel, and J. Neubauer, Quantitative X-ray diffraction of free, not chemically bound water with the PONKCS method. Journal of Applied Crystallography. 51 (2018) 1535-1543. doi: 10.1107/S1600576718012888

Other Journals

- K.-C. Thienel, N. Beuntner, C. Chucholowski, S. Scherb, Эффективность использования кальцинированных глин в составе строительных материалов (Efficiency of using calcined clays in building materials), Цемент и его применение (Cement and its Application) (6) (2018) 76-81

Conference Proceedings:

- K.-C. Thienel, N. Beuntner, C. Chucholowski, S. Scherb, Performance of calcined clays in mineral construction materials. in 20. Internationale Baustofftagung ibausil, H.-B. Fischer and A. Volke (Ed.). F.A. Finger-Institut für Baustoffkunde, Prof. Dr.-Ing. H.-M. Ludwig, Weimar. Tagungsband Vol 1 (2018) p. 175-192

- S. Scherb, M. Köberl, N. Beuntner, K.-C. Thienel, The early hydration of cement with the addition of calcined clay – From single phyllosilicate to clay mixture. in: 20. Internationale Baustofftagung ibausil, H.-B. Fischer and A. Volke (Ed.). F.A. Finger-Institut für Baustoffkunde, Prof. Dr.-Ing. H.-M. Ludwig, Weimar. Tagungsband Vol 1 (2018) p. 658-666
- S. Scherb, N. Beuntner, and K.-C. Thienel, Reaction kinetics of the basic clays present in natural mixed clays, in Calcined Clays for Sustainable Concrete - Proceedings of the 2nd International Conference on Calcined Clays for Sustainable Concrete, F. Martirena, A. Favier, and K. Scrivener, Editors. 2018, Springer Nature: La Havanna, Cuba. p. 427-433. doi: 10.1007/978-94-024-1207-9_69

2015:

Technical Report:

- W. Eden, S. Scherb, K.-C. Thienel, W. Burtscher, S. Wolfram, Einsatz von calciniertem Ton als Bindemittelkomponente zur Verbesserung der CO2-Bilanz bei gleichzeitiger Optimierung der Kalksandsteinqualität – Gemeinsamer Schlussbericht zum Kooperationsprojekt KF3029502 KI2. (2015), Arbeitsgemeinschaft industrieller Forschungsvereinigungen „Otto von Guericke“ e.V. (AiF).